# Summary

Cultured adult cardiac myocytes represent an important approach to study the failing heart on the cellular level. I have developed a long-term culture of adult rat ventricular myocytes based on serum-free medium and substrates coated by extracellular matrix proteins allowing the sustained adenovirus-mediated expression of the $Ca^{2+}$ sensor inverse pericam. I used this single-cell model to investigate the effects of chronic neuroendocrine $G_q$-coupled stimulation on cellular and subcellular $Ca^{2+}$ signalling. I assessed the loading state of internal $Ca^{2+}$ stores and the activity of transport systems in fura-2 loaded myocytes following caffeine applications (10 mM), while spatially resolved $Ca^{2+}$ imaging (realtime confocal microscopy) was undertaken to characterise the spatio-temporal features of $Ca^{2+}$ sparks and waves. The control cells displayed a 6-fold augmentation of the wave frequency from day 6 *in vitro* onwards. Also on day 6, the spark distribution changed from a cytoplasmic spread into a sub-plasma membrane ring. Interestingly I could measure a 24% and 33% increase of the size of the spark spread on day 1 and day 6 respectively compared to freshly isolated cells. Furthermore, on days *in vitro* 3 and 6, I observed decreased amplitudes of caffeine-induced $Ca^{2+}$ transients. The latter ones displayed two distinct decay time constants: a slow one due to $Na^+/Ca^{2+}$ exchangers and a rapid one to a large extent influenced by sarcoplasmic reticulum (SR)-$Ca^{2+}$ ATPases (SERCA), the precise role of which in the failing heart is still under controversy. After one week of culture, I could measure a 2-fold increase of the rapid decay time constant. Chronic stimulation of the $G_q$-coupled pathways with phenylephrine (100 µM) or endothelin-1 (100 nM) led to a rapid (3 days) dedifferentiation of the myocytes into so called myoballs, which formed spreading complexes from day 6 onwards, the spontaneous activity of which was predominantly waves. In the one week old chronically stimulated cells, the decreased amplitudes of caffeine responses were abolished and $Ca^{2+}$ spark amplitude was augmented. In addition, the rapid decay time constant was increased by 50% compared to control cells at the same stage. I conclude that chronic neuroendocrine stimulation leads to a remodelling of the cellular $Ca^{2+}$ handling, especially in terms of spontaneous activity, elementary events, SR loading and activity of the SERCA pumps, which could be a key target for the hormones tested. Moreover, neuroendocrine stimulation of adult myocytes might thus be an

important part of cardiac remodelling *in vivo* that can be mimicked and studied in an *in vitro* model of adult myocytes.

# Zusammenfassung

## CHARAKTERISIERUNG EINES EINZELZELL-MODELS VON ADULTEN KARDIOMYOZYTEN

Die Kultivierung adulter Kardiomyozyten ist eine wichtige Methode um ihre physiologische wie pathophysiologische Funktion auf zellulärer Ebene zu studieren. Primäres Ziel meiner Studien war es, ein neuartiges Kultivierungssystem für adulte ventrikuläre Myozyten der Ratte zu untersuchen, das mit unterdrückter Dedifferenzierung einhergeht und die intensive experimentelle Manipulation der Zellen erlaubt. Darüber hinaus sollte ich in der Lage sein, mithilfe eines solchen Systems exogene und endogene Proteine zu exprimieren. Hierfür wurden eine ganze Reihe verschiedener Kulturbedingungen, wie z. B. Mediumzusammensetzung, Substratbeschichtung und elektrische Stimulation, untersucht. Untersuchungsparameter hierbei waren (i) Überlebensrate, (ii) Morphologie, (iii) Frequenzabhängigkeit von elektrisch induzierten Kontraktionen, (iv) Frequenzabhängigkeit von elektrisch induzierten $Ca^{2+}$-Transienten und (v) Verträglichkeit einer viralen Expression der $Ca^{2+}$-Sonde Inverse-Pericam. Isolierte Myozyten, die in Medium ohne Zusätze oder in serumhaltigen Medien kultiviert werden, zeigen sowohl morphologische wie auch physiologische Dedifferenzierung in kürzester Zeit (weniger als 3 Tage). Innerhalb von wenigen Tagen bauen sich die vormals quergestreiften und backsteinförmigen Zellen in flache, fibroblastenähnliche Myoblasten um. Demgegenüber konnte eine Supplementierung des Mediums mit einem Insulin/Transferrin/Selen-(ITS-)Gemisch diesen Vorgang der Dedifferenzierung deutlich verlangsamen. Selbst am Tag 6 nach der Isolation war ein Großteil der Zellen klar quergestreift und langgestreckt. Dies wurde durch eine Beschichtung des Zellsubstrats mit einem Gemisch aus Proteinen der extrazellulären Matrix (EZM) noch weiter unterstützt. Unter diesen Bedingungen konnten wir ebenfalls eine wesentlich verbesserte Anhaftung der Zellen an das Substrat (Plastik und Glas) feststellen. Ich habe außerdem das physiologische Verhalten der Zelle

unter diesen optimierten Kulturbedingungen getestet und stellte fest, dass nicht nur die Morphologie konserviert worden war, sondern auch die Physiologie der Zellen. Hierzu habe ich das stimulationsfrequenzabhängige Verhalten von Kontraktionen und elektrisch induzierten Kalziumtransienten untersucht. Unter Bedingungen der ITS-Supplementierung und der EZM-Beschichtung konnte ich eine optimierte Konservierung dieser physiologischen Parameter der isolierten Myozyten feststellen. Darüber hinaus habe ich einen Adenovirus untersucht, der es erlaubt, „Inverse-Pericam“ in enddifferenzierten, nicht proliverativen Zellen, wie adulten Herzmuskelzellen, zu exprimieren. Diese Expression schädigte die Myozyten nicht und ihre Überlebensrate war durch die Infektion nicht vermindert. In Myozyten, die die Inverse-Pericam exprimieren, konnte ich mittels Hochgeschwindigkeits-Videomikroskopie über mehrere Stunden hinweg stabile elektrisch induzierte Kalziumtransienten aufzeichnen, ein Unterfangen, das mit herkömmlichen Kalziumindikatoren wie Fura2 oder Indo1 kaum möglich gewesen wäre. Dieses Einzelzellmodel mit massiv reduzierter Dedifferenzierung der Myozyten stellt daher einen wesentlichen Fortschritt auf dem Weg zu einem High-Content-Screening-System für adulte Ventrikelmyozyten dar.

Nach der Etablierung des Zellmodells untersuchte ich die Wirkung von chronischer neuroendokriner Stimulation auf die zellulären und subzellulären Kalziumsignale der Myozyten. Hierzu bestimmte ich den Kalzium-Beladungszustand des internen Speichers (sarkoplasmatisches Retikulum, SR) mithilfe von Koffein-Pulsen (10 mM, 15-20s Dauer) unter diesen Bedingungen. Mittels hochauflösender Echtzeitkonfokalmikroskopie charakterisierte ich mögliche Veränderungen von subzellulären Kalziumsignalen, die Kalziumsparks und Kalziumwellen.

Während dieser langen Koffeinpulse zeigte der zelluläre Kalziumtransient eine Abnahme der Kalziumkonzentration mit zwei charakteristischen Phasen: (i) einer langsamen Phase während der Koffeinapplikation, die im Wesentlichen auf die Aktivität des $Na^+/Ca^{2+}$-Austauschers zurückzuführen war und (ii) eine schnelle Phase nach Auswaschen des Koffeins, die auf die zusätzliche Aktivität der SR-Kalziumpumpen (SERCA-Pumpen) zurückzuführen war. Die Amplitude der koffeininduzierten Kalziumtransienten gibt ein relatives Maß für den SR-Kalzium Beladungszustand. Ohne neuroendokrine Stimulation zeigte sich eine deutliche

Verlangsamung der SERCA-abhängigen Kalziumabnahme, während die vom $Na^+/Ca^{2+}$-Austauscher vermittelte Reduktion nicht verändert war. Die Amplitude dieser Kalziumtransienten unterlag nach 3 Tagen einer kontinuierlichen Verkleinerung bis zum Tag 6 nach Kultivierung. Im gleichen Zeitraum konnte ich eine 6-fache Erhöhung der Frequenz von spontanen Kalziumwellen ermitteln, die einherging mit einer Umverteilung der Lokalisation von Kalziumspark-Stellen. Diese war initial homogen über die Zelle verteilt, während sie sich später wie in einem Ring unter die Zellmembran legten, im Zellinneren konnte zu diesem Zeitpunkt nur eine residuelle Sparkaktivität gefunden werden. Interessanterweise veränderte sich ebenfalls die Charakteristik der individuellen elementaren Kalziumsignale, der Kalziumsparks. Schon ab Tag 1 nach Isolation unterlagen die Sparks einer Vergrößerung ihrer subzellulären lateralen Ausbreitung.

Chronische Stimulierung mit Phenylephrine (100 µM) oder Endothelin-1 (100 nM) führt zu einer schnellen (3 Tagen) Dedifferenzierung der Myozyten: initial zu runden „Myoballs“, später dann auch zu fibroblastenähnlichen Zellen. Ihre hauptsächliche subzelluläre Art der spontanen Kalziumfreisetzung war die Erzeugung sich schnell ausbreitender Kalziumwellen. Bemerkenswerterweise wurde der in Kontrollzellen gefundene Verlust der Koffein-Antworten im Kalziumsignal (d. h. abnehmende Amplitude) durch die neuroendokrine Stimulation der Zellen praktisch vollständig unterdrückt. Während die $Na^+/Ca^{2+}$-Austauscher-bestimmte langsame Komponente der Koffein-Antworten nur unter Phenylephrine-Bedingungen sich veränderte, stellte ich eine weitere Verlangsamung der SERCA-Pumpen vermittelten schnellen Komponente fest (weitere 50% Verlangsamung). Aus diesen Ergebnissen schließe ich, dass die chronische neuroendokrine Stimulation der Myozyten zu einem charakteristischen Remodelling der Kalziumhomöostase führt, hier vor allem in Bezug auf SR-Kalziumgehalt und die Aktivität der SERCA-Pumpen. Ein ähnliches Remodelling wird ebenfalls *in vivo* in erkrankten Herzen von Tiermodellen und Menschen gefunden.

Zusammenfassend kann gesagt werden, dass die neuroendokrininduzierte Stimulation von isolierten Herzmuskelzellen zu einem charakteristischen Remodelling der Kalziumhomöostase führt, die unter Umständen ein gutes Modell für *in vivo*- Remodelling sein könnte.

# Introduction

## 1. Function and structure of the heart

Every single cell of the body needs to be supplied with oxygen in its vicinity. Blood provides the support of the oxygen transport through a complex network of vessels and cavities called circulatory system. The motor of the movement of blood is the heart. Because of its rhythmic contractions, every cell receives the necessary oxygen and nutrients to ensure its metabolism while the products of the catabolism (such as carbon dioxide) are removed.

### *1.1. The morphology of the heart*

The heart is the pump of the body and therefore essentially characterised by the presence of muscle tissue. The heart consists of 4 chambers (Fig. 1): the left and right atria (the upper chambers) and the left and right ventricles (the lower chambers). A muscular wall called the septum separates the left and right atria (also called the atrium syncytium) and the left and right ventricles (or ventricular syncytium). Fibrous tissue divides these 2 syncytia and encircles the valves that regulate the direction of the blood flow between the atria and the ventricles. The largest and strongest chambers of the heart are the ventricles because they have to push blood through the aortic valves and further into the body or the lungs. Both ventricles and atria are mainly composed of the very same elements: endothelial and fibroblastic cells, muscle cells, capillaries, arteries, arterioles, veins, veinules, and nerves.

The heart is located between the lungs in the middle of the chest and surrounded by a sac – a double-layered membrane called the pericardium. The wall of the heart consists of several layers (from outside to inside):

**Epicardium**: the inner layer of the pericardium, a conical sac of fibrous tissue that surrounds the heart and the roots of the large blood vessels.

**Meso- or myocardium**: actually the “proper” heart muscle. It consists of single cells, which are electrically connected to each other through gap junctions. They are not

innervated by motoneurones but are autonomically active. There are 2 types of heart muscle: the working myocardium and the system of excitation generation and propagation. During the postnatal stage, proliferation of cardiac muscle cells is ceased, and the heart grows by increasing the size of its myocytes (also called developmental hypertrophy) as well as raising the number of non-myocytes (or hyperplasy).

**Endocardium**: smooth internal layer with reduced friction resistance which consists of platy endothelial cells.

The other components of the heart are:

**Autonomic nervous system in the heart**: it consists of slow unmyelinated fibres, which are surrounded by a laminar coat. Fibroblastic cells and collagen usually separate myocytes from the nerve cells. Parasympathetic (cholinergic) and sympathetic (adrenergic) fibers innervate the cardiac muscle and regulate the heart rate.

**Vessels and capillaries**: blood vessels are usually composed of three layers: the tunica intima, the tunica media and the tunica adventitia. The first one consists of a layer of endothelial cells lining the lumen of the vessel as well as a subendothelial layer made up of mostly loose connective tissue. Often, the internal elastic lamina separates the tunica intima from the tunica media. The tunica media of the vessels is mainly composed of circumferentially arranged smooth muscle cells. Again, the external elastic lamina often separates the tunica media from the tunica adventitia. Finally, the tunica adventitia is primarily composed of loose connective tissue made up of fibroblasts and associated collagen fibers. In contrast to vessels, capillaries are extremely thin and only composed of one epithelial cell thick. They connect the two types of vessels, arteries (they allow the transport of blood out of the heart) and veins (responsible for the transport back to the heart), and enable for instance the exchange of oxygen and carbone dioxide between red blood cells and tissues.

**Extracellular Matrix (ECM)**: the cardiac ECM is a network serving as a structural, mechanical and chemical support for the cells of the myocardium. It is involved in cardiac physiology as well as in pathological phenomena. The ECM is composed of: structural proteins, among them collagen types I and III and elastin; laminin, fibronectin, collagen types IV and VI responsible for the adhesion; anti-adhesive proteins such as thrombospondin, osteopontin and tenascin; negatively charged

proteoglycans and enzymes, among them metalloproteinases, which are involved in processes of degradation but can also process several bioactive molecules. ECM proteins are ligands for integrins at the cell surface, the latter ones playing an important role in cell signalling.

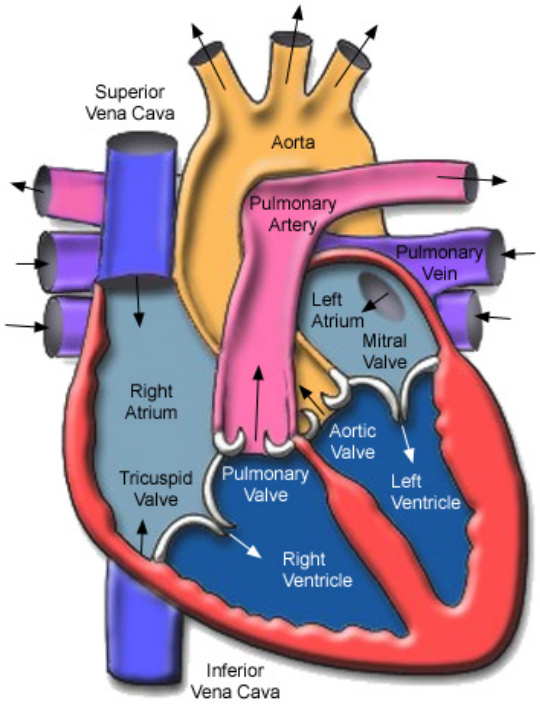


**Fig. 1. Anatomy of the heart.**
**The illustration exhibits a schematic sagittal cross section of the heart showing the four chambers (atria and ventricles), vessels as well as the valves that control the blood flow (indicated by arrows) through the heart.**
**(From Texas Heart Institute, 2007)**

## *1.2. Electrical activity of the heart*

The rhythmic contractions of the heart cells are triggered by the so called pacemaker cells that comprise a cluster of electrically active, specialised muscle cells localised in the so called sinus node situated in the upper part of the wall of the right atrium. The sinus node is also called sinoatrial node or, for short, SA node, and is the primary pacemaker of the heart.

The entire conduction system and all myocytes possess the fundamental ability of generating spontaneous activity, albeit with varying frequencies. This system

comprises a strict hierarchy with the SA nodal cells representing the top layer (Fig. 2). The latter displays the highest spontaneous frequency that is imposed downstream onto the rest of the heart. By way of such a system losses of higher level pacemaking can be compensated for by the spontaneous activity of the next pacemaking level. Nevertheless this goes hand in hand with lower pacing frequencies – leading to a reduced cardiac performance.

Starting from the SA node the electric impulse initially excites both atria. The propagation of the excitation onto the ventricles is suppressed by a specialised layer of non-excitable cells between the atria and the ventricles functionally insulating both types of tissue. Under physiological conditions, excitation is transmitted into the ventricles by a specialised structure, the atrioventricular (AV) node. With its slowly rising depolarisation (see Fig. 5) it delays impulse propagation into the ventricles and thus supports proper refilling of the ventricles with blood (supported by atrial contraction). After having passed through the AV-node, the Bundles of His and the left and right bundle branches, the electrical wave is distributed into the ventricular tissue by specialised muscle cells, the Purkinje cells. This ensures homogenous excitation and contraction of both ventricles.

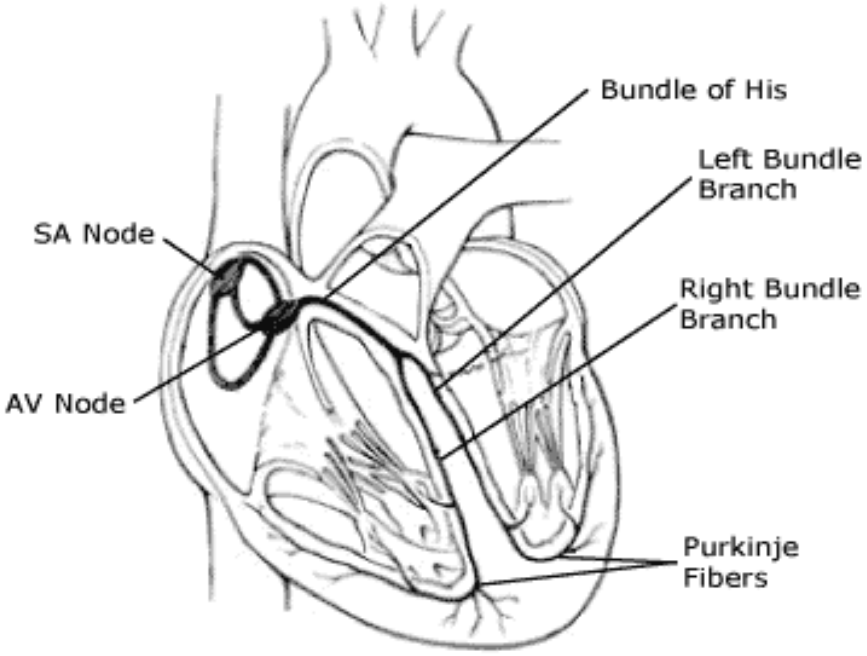

**Fig. 2. Conduction system of the heart.**
**The different levels of the morphological structure that sustains the propagation of the electrical excitation are represented in this cartoon. The impulse starts in the SA node and terminates in the Purkinje fibers.**
**(From St. Jude Medical, 2007)**

When the electrical impulse finally reaches the myocardial cells, it stimulates the cell so that the negative membrane potential ($E_m$) at rest is slowly depolarised and reaches a threshold value that induces the opening of voltage-gated ion channels and an influx of positively charged ions (cations) into the cell. Upon reaching the threshold, an action potential (AP) is triggered, which is usually separated into 5 phases (Fig. 3). Phase 0 is the upstroke or rapid depolarisation, phase 1 is the early rapid repolarisation, followed by the plateau-phase or phase 2, phase 3 is the final rapid repolarisation, phase 4 is the resting $E_m$ and diastolic depolarisation. In phase 0 of the cardiac AP, activation follows $Na^+$ channel opening. This leads to a rapid depolarisation (200 V/s). The $E_m$ usually peaks at +35 to +50 mV. The depolarisation is sustained by the phenomenon of regenerative activation of the $Na^+$ current $I_{Na}$ that allows the activation of additional $Na^+$ channels until inward $I_{Na}$ is stronger than outward $I_{K}^+$ and shuts off some inward currents such as the inwardly rectifying $I_{Ki}$. As $Na^+$ channels inactivate, slowly activating $Ca^{2+}$ channels and a few fast $K^+$ channels open. The equilibrium between the outward ionic flow (carried by delayed rectifier $K^+$ currents) and the inward ionic flow (carried by the current of the L-type $Ca^{2+}$ channel $I_{Ca,L}$ ) generates the plateau of the AP that is of variable duration (~200 ms in ventricular cells). It is noteworthy that in rat and mouse ventricular myocytes there is almost no plateau phase because early repolarisation, which takes place right after the AP peak, is so dominant. Early repolarisation is mainly due to the contribution of $Ca^{2+}$ release from internal stores that activates the $Cl^-$ current $I_{Cl(Ca)}$ and inactivates $I_{Ca,L}$, but also to the activation of the transient outward $K^+$ $I_{to}$ which is predominant in rat and mouse ventricular myocytes. The termination of the plateau and the repolarisation are due to the deferred opening of supplementary $Ca^{2+}$-activated $K^+$ channels ($Ca^{2+}$ increases in the cytoplasm) together with the closing of the $Ca^{2+}$ channels. During this phase, a positive feedback takes place, leading to an acceleration of the repolarisation. Indeed, the inwardly rectifier $K^+$ currents, the delayed $I_{Kr}$ and the resting $I_{K1}$ (the latter being responsible for the maintenance of the resting potential towards -80 mV) reactivate and increase respectively as the membrane potential drops. Remarkably, $I_{K1}$ is low or absent in pacemaker cells,

enabling the induction of spontaneous APs. In addition, the usual mode ($Ca^{2+}$ is extruded) of $Na^{+}/Ca^{2+}$ exchangers in the plasma membrane facilitates the balance in favour of an increase of the outward currents during phase 3 (for a detailed review about currents during AP, see Bers, 2001). The duration of the muscle twitch is nearly the same as the duration of the AP (Fig. 4) but usually delayed by several milliseconds. Since there is quite a long refractory period in cardiac muscle, tetanic stimulation does not induce tetanic contractions such as those found in the skeletal muscle.

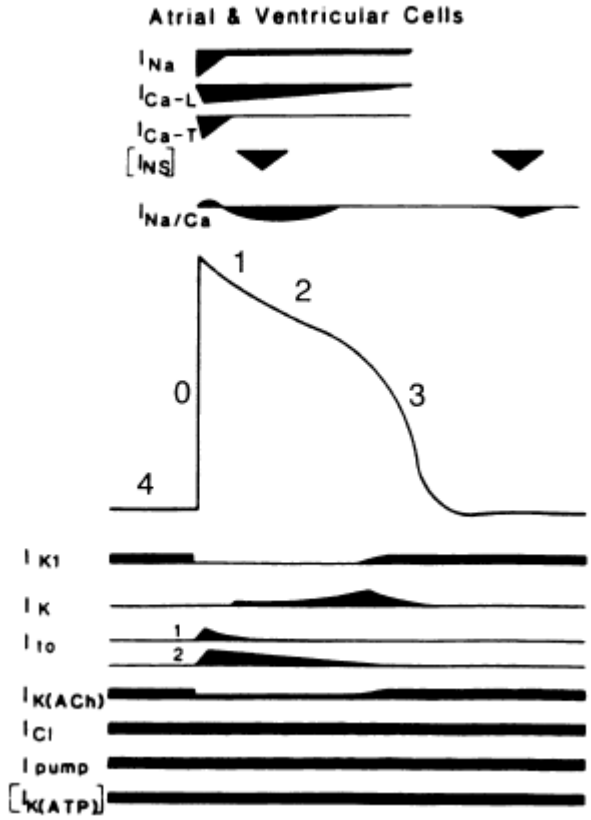


**Fig. 3. Ionic currents underlying the cardiac AP.**
**This cartoon describes the shape of a cardiac AP ($E_m$ versus time) and the involvement of the indicated ionic currents. The black bars illustrate the channel activation: outward currents are above the line, inward currents below the line. The square brackets indicate that these channels are only involved in pathological conditions. (From Shih, 1994).**

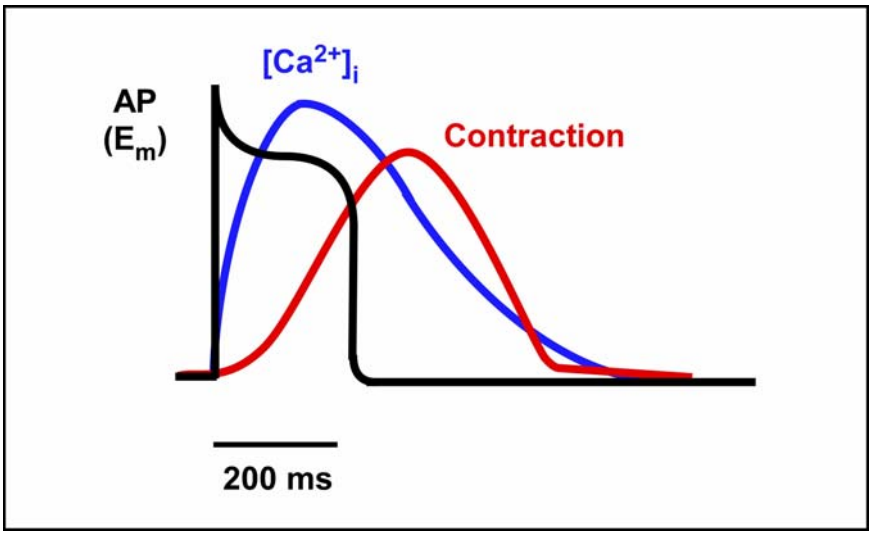


**Fig. 4. Time course of a cardiac AP, $Ca^{2+}$ transient and contraction.**
**This figure depicts the changes of the $E_m$ over time during an AP in a cardiac myocyte together with the concordant increase of the intracellular $Ca^{2+}$ concentration $[Ca^{2+}]_i$ and the twitch force. The units for $Ca^{2+}$ transient and contraction are arbitrary. (Adapted from Bers, 2002).**

The APs are heterogenous in the heart. Indeed, their parameters differ from one tissue to another, from one cell type to another (Fig. 5). This can be explained by the different distribution of the various channels, pumps, exchangers, and regulatory proteins, responsible for the properties of the AP.

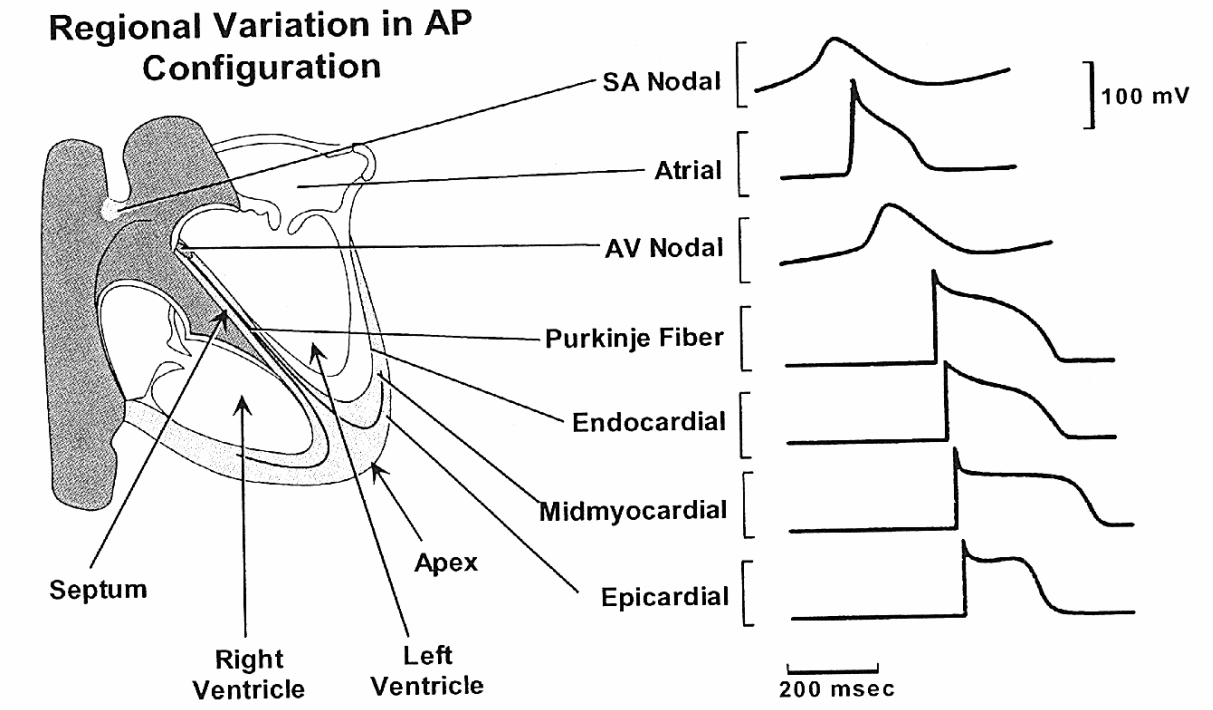

**Fig. 5. Heterogeneity of the AP.**
**The cardiac AP is not the same within the heart tissues. Its amplitude, duration, upstroke and decay vary among the different types of cardiac cells.**
**(From Bers, 2001).**

# 2. Long-term primary culture of adult cardiac myocytes

## *2.1. History of heart cell culturing*

The earliest attempts of heart tissue culture were described by Burrows over 90 years ago on embryonic chick hearts (Burrows, 1912). The initial dissociation and maintenance of heart tissue as *single cells* in culture was performed by Cavanough who also worked on chick embryo myocytes (Cavanough, 1955). The pioneers in isolating and culturing neonatal rat heart cells were Harary and Farley (Harary & Farley, 1960). After years of improvement, a detailed technique for the isolation of viable adult ventricular myocytes was published in 1976 (Powell & Twist, 1976), followed by the first culturing of adult cells in 1977 (Jacobson, 1977). Usually, long-term culturing of cardiac myocytes was only undertaken on embryonic or neonatal myocytes (e.g. Simpson *et al*., 1982). Nevertheless, as most of the cardiac physiological and pathological studies concern the adult myocardium, it seems rather difficult to transfer effects observed in the developing heart and function to end-differentiated cells since the patterns of gene expression are very different in both cases. The initial reviews about adult myocytes in culture were published about 20 years ago (e. g. Jacobson & Piper, 1986). Less than 10 years later, the first progresses in the conservation of the phenotype of adult cardiac myocytes in culture were achieved (Berger *et al*., 1994; Schackow *et al*., 1995). Mitcheson and his colleagues reported the advances in terms of adult cardiac myocytes culturing in a detailed and comprehensive review (Mitcheson *et al*., 1998), where they summarised different methods of long-term cultivating of rabbit and rat muscle cells. Recently, the Alliance for Cell Signalling released an interesting study on adult mouse myocytes in short-term culture (Sambrano *et al*., 2002). They described a model of culturing based on serum-free supplemented medium that allowed a preservation of the myocytes for up to 72 hours. Despite the lack of a basic characterisation of the morphology and the functionality of these cells, they were able to show a conservation of the responses to important hormonal stimulus.

## *2.2. The purposes of using cell culture*

Cultured myocytes are a complementary approach to whole animal or intact heart preparations, especially with regard to long-term investigations. Myocyte cultures enable the investigator to work with a homogenous population of cells (devoid of non-myocytes, such as fibroblasts and endothelial cells), which are both easy to visualise and manipulate. Moreover, the environment of the myocytes is tightly controllable. As enzymatic isolation is an insult for the cells, it has been shown that culturing improves the recovery of the native myocytes after such a procedure, especially re-expression of damaged receptors and ion channels at the cell membrane (Borg *et al.*, 1990; Terracio *et al.*, 1990). Cultured adult myocytes can remain viable for days or even up to one week, depending on the culture conditions used (Decker *et al*., 1991), and are thus feasible for long term studies. Cell culture implies the possibility to control the environment in which cells are maintained and to manipulate protein expression in single myocytes using molecular biological techniques. These techniques require that the myocytes preserve their viability when the protein expression changes (Shubeita *et al*., 1992). Furthermore culturing heart cells leads to a reduction of the number of animals having to be sacrificed and at the same time to reduced investment of time and money spent for isolating cells.

Myocytes in culture usually undergo a drastic “dedifferentiation” (i. e. a loss of the adult phenotype) while adapting to the culture environment, and therefore they do not represent a stable model system under these conditions. Indeed the adaptation from a three-dimensional, *in vivo* substrate to the two-dimensional substrate in culture leads to a reorganisation of the cytoskeleton (Decker *et al*., 1990, 1991). The expression of β-myosin heavy chains (βMHCs are absent in adult, but present in immature myocardium), which have been used as markers of fetal phenotype together with dedifferentiation, remains stable in some cultures (Ellingsen *et al*., 1993) but increases in others (Nag & Cheng, 1986). It is not entirely clear whether the majority of the *in vivo* properties of adult heart muscle are still observed in cultured myocytes whatever conditions tested. Interestingly, some of these properties appeared to remain conserved even in the most morphologically altered states during culturing (Bugaisky & Zak, 1989).

## *2.3. Culture of adult ventricular myocytes*

Initially Jacobson and Piper (1986) have introduced two fundamental methods for culturing adult ventricular myocytes. The first (or conventional) one uses myocytes in a serum-supplemented medium. In this case myocytes round up into so-called myoballs, losing their rod shaped morphology they exhibit *in vivo*. After 2 to 4 days they start to "spread", sending out pseudopodia-like extensions all over the substrate. During the spreading phase, the highly differentiated structure undergoes massive changes, which is named "dedifferentiation" (Jacobson & Piper, 1986). The myocytes re-express proteins for the transverse (T) tubule system, sarcoplasmic reticulum (SR) and mitochondria (Ikeda *et al*., 1990), as well as for gap junctions (Eppenberger & Zuppinger, 1999). Under these conditions, myocyte cultures tend to become spontaneously active over time (Claycomb & Lanson, 1984). If neighbouring cells form contacts with one another, synchronous contraction of all cells occurs, indicating that functional gap junctions have been re-expressed (Polontchouk, 2002).

One advantage of the "dedifferentiated" culture model is that myocytes can be maintained for weeks or even months (Jacobson *et al*., 1985). However, the myocytes are morphologically and functionally different from *in vivo* myocardium; they indeed often display a higher frequency of spontaneous beating (Bugaisky & Zak, 1989). These contractions are characteristically different to those often associated with high SR $Ca^{2+}$ content (Allen *et al*., 1984) or loss of $Ca^{2+}$ tolerance after the isolation procedure, which is close to the well-known phenomenon of the $Ca^{2+}$ paradox (Xu *et al*., 2006). The mechanisms of spontaneous contractions observed in dedifferentiated cultures may be similar to the contractile activity of fetal cells and result from catecholamines as well as other positively inotropic agents contained in serum (Mitcheson *et al*., 1998). Actually, the dedifferentiation method implies to supplement the medium with serum, which contains substantial concentrations of unknown exogenous signalling molecules such as growth factors and hormones, most likely leading to unquantifiable effects on myocytes, especially on gene expression. Therefore, it may be preferable to omit the serum and to cultivate cells in a defined environment.

The second and novel culture technique aims to preserve the morphology of the adult myocytes during culturing. Using this technique, the rabbit muscle cells retained their rod-shaped and striated appearance of acutely isolated myocytes for 1 to 2 weeks (Mitcheson *et al*., 1996). Indeed, myocytes cultured using the "serum-free" method display very few spontaneous contractions and may remain viable for up to 14 days (Piper *et al*., 1988; Volz *et al*., 1991). Moreover, serum-free conditions suppress the proliferation of non-myocyte cells such as fibroblasts, and thus anti-mitotic agents are not needed. Nowadays, the issue to address is finding and establishing techniques and methods which improve the viability, the morphology and the functionality of the myocytes in serum-free conditions, leading to optimised long term *in vitro* models of adult myocytes.

## *2.4. Continuous electrical stimulation of cell populations*

The establishment of the serum-free method for cultured myocytes results in the absence of regular depolarisations as they occur *in vivo*, and this could play a role in the loss of physiological properties. Indeed, repetitive depolarisations leading to an increase of the cytosolic $Ca^{2+}$ concentration and contraction may be important for the functionality of the cell, particularly for the expression of contractile proteins and membrane ion channels (Davidoff *et al*., 1997).

The question to address is then whether continuous repetitive electrical stimulations of adult cardiomyocytes in primary culture have any effect on the morphology and protein expression. Berger and co-workers (1994) reported an attractive method to stimulate rat myocytes at frequencies of 0.1 to 5 Hz in short-term culture (Berger *et al*., 1994). Myocytes were seeded onto laminin pre-treated culture flasks and preserved in serum-free medium. Contraction was induced by brief voltage-pulses (5 ms duration) through graphite electrodes. Contractile properties displayed an initial decrease after 6 hours, which was then maintained over the next 36 hours. Thereafter, contractility showed an increase. In contrast, the amplitude of contraction, velocities of shortening and relaxation remained stable in paced cultured myocytes after 72 hours. The current density for L-type $Ca^{2+}$ channels was increased in stimulated compared to non-stimulated cells. Unfortunately no direct comparisons were undertaken with freshly isolated myocytes. AP parameters, thought to be

connected to modifications in contractility, were not considered either (Mitcheson *et al*., 1998). In conclusion, the authors suggested that continuous electrical pacing may help to prevent the deterioration of contractile properties found in unstimulated myocytes (Ellingsen *et al*., 1993). Paced rat myocytes remained quiescent when verapamil (L-type $Ca^{2+}$ channels blocker) was included to the medium. This led to a reduction of contractility when the cells were electrically stimulated after verapamil removal (Berger *et al*., 1994). Thus, it seems that mechanical activity may preserve contractility, but electrical stimuli alone appeared not to be sufficient. Paced myocytes (frequency 3 Hz) displayed substantially higher protein content and rates of protein synthesis in comparison to unstimulated cells (Kaye *et al*., 1996), consistent with data from adult feline cardiomyocytes (Kato *et al*., 1995). In the latter study, the protein content of quiescent rod-shaped myocytes diminished by 14% between days 1 and 4 of culture and then remained constant up to day 7. Interestingly, protein content of continually paced myocytes (frequency 1 Hz) remained constant between days 1 and 4 and increased from day 4 onwards. It was supposed that an acceleration of the rate of protein synthesis (and not catabolism) was partially responsible for that.

Taken together, these studies propose that adaptive hypertrophy might have occurred in the paced cells cultured in a serum-supplemented medium because of an increase in work load, without any supplementary exogenous growth factors or hormones. The importance of repetitive depolarisations in cardiac myocytes during culturing underlines the central role played by the phenomenon of excitation-contraction coupling (ECC) in cardiomyocyte function, which will be discussed in the next section.

# 3. $Ca^{2+}$ signalling in cardiac cells

$Ca^{2+}$ is the most ubiquitous second messenger in the living cells. The regulation of the intracellular $Ca^{2+}$ concentration represents a fine-tuned process, regulating development, growth, maturation, remodelling and survival or death of cells. Intracellular $Ca^{2+}$ changes modulate a plethora of processes in cells, from gene expression to phosphorylation events.

## *3.1. Excitation-contraction coupling*

As described above, an electrical impulse leading to an AP initiates the systole of the heart (basically the rhythmic contraction of the myocytes in the myocardium, especially in the ventricles, by which blood is driven through the aorta and pulmonary artery after each dilatation or diastole). The link between the depolarisation of the AP and the contraction is a release of $Ca^{2+}$ from the internal stores, referred to as ECC.

In ventricular cells, ECC is characterised by morphological structures called T-tubules. These are tube-shaped invaginations of the sarcolemma (cardiac muscle plasma membrane) that pertrude deep into the muscle cell and thus conduct the AP into the inner part of the myocyte. The lumen of the T-tubule is continuous with the extracellular space, and membrane depolarisations during APs occur across the entire T-tubular membrane. Interestingly, atrial myocytes do not possess T-tubules. Nevertheless, many of these cells might possess an irregular tubular system identified as transverse-axial tubular system or TATS (Kirk *et al*., 2003).

How does depolarisation in the T-tubule membrane open a $Ca^{2+}$ channel in the SR membrane? A voltage sensor in the T-tubule membrane (this voltage-sensitive protein is the L-type $Ca^{2+}$ channel or LCC, also called dihydropyridine receptors or DHPR) changes its conformation in response to the depolarisation of the AP. This conformational change induces the opening of the DHPR and thus leads to a $Ca^{2+}$ influx that is transmitted to the head of the SR $Ca^{2+}$ channel, the so called ryanodine receptor RyR2 (sensitive to the plant alkaloid ryanodine and to caffeine), causing it to open and enabling $Ca^{2+}$ release in the dyadic cleft space of roughly 12 nm (see Fig. 6 in Section 4). This phenomenon is termed $Ca^{2+}$-induced $Ca^{2+}$ release (CICR). The involvement of the latter can be studied in high $Ca^{2+}$ buffering conditions in order to minimise it and separate it from the $Ca^{2+}$ transient (named "$Ca^{2+}$ spike") solely due to the activation of the couplon LCC/RyRs embedded in the dyadic cleft (Song *et al*., 2006). It is noteworthy that this indirect interaction between the T-tubule voltage sensor and the SR $Ca^{2+}$ channel is specific to ECC in cardiac muscle and is called electrical coupling, whereas skeletal muscle cells display a direct interaction between DHPR and RyR1, underlying a mechanical or conformational coupling (Bers, 2001; Paolini, 2007).

$Ca^{2+}$ release from the SR induces an elevation of the intracellular $Ca^{2+}$ concentration from 100 nM to ~1 μM (Bers, 2002), which is sensed by the myofibril complex. The free $Ca^{2+}$ binds to troponin-C inducing a conformational change so that troponin-I exposes a site on the actin molecule that is able to bind to the myosin head and activate its ATPase activity. This results in ATP hydrolysis that supplies energy for a conformational change to occur in the actin-myosin complex. Finally a movement ("ratcheting") between the myosin heads and the actin takes place, causing the actin and myosin filaments to slide along one another, and thereby the single contractile unit (sarcomere) length is shortened (Klabunde, 2005).

The $Ca^{2+}$ cycling underlying ECC is terminated by two predominant mechanisms: (i) sarcoplasmic/endoplasmic reticulum $Ca^{2+}$ ATPase (SERCA, the cardiac isoform being SERCA2a) pump-mediated $Ca^{2+}$ reuptake into the SR and (ii) $Na^{+}/Ca^{2+}$ exchanger (NCX)-mediated extrusion of $Ca^{2+}$ from the myocyte (see Fig. 6 in Section 4). While the former process accounts for approximately 92%, the exchanger removes roughly 7% of the cytosolic $Ca^{2+}$ in rat and mouse ventricular myocytes. In rabbit, ferret, dog, cat, guinea-pig and human ventricle, the balance is 70% for SERCA, 28% for NCX (Bers, 2002). Minimal amounts of removal (1% in rat and 2% in rabbit) are undertaken by slow systems: the sarcolemmal $Ca^{2+}$ pump (PMCA) and the mitochondria $Ca^{2+}$ uniporter (Bers, 2001; Pott and Goldhaber, 2006). The relaxation phase thus depends on the coordination of these different $Ca^{2+}$ transport systems.

## *3.2 Classification of $Ca^{2+}$ events in cardiac muscle*

**Sparklet:** As described above, the initiation of ECC is mediated by the opening of LCCs. When a single LCC channel opens, this leads to $Ca^{2+}$ influx (Mejia-Alvarez, 1999), resulting in increase of the total amount of $Ca^{2+}$ in the cleft between the LCC in the plasma membrane and the opposing cluster of ryanodine receptors (RyRs) in the SR membrane. The increases can be recorded as $Ca^{2+}$ signals named $Ca^{2+}$-sparklets (Wang *et al*., 2001).

**Spark:** The cluster of RyRs, which faces the sparklet, senses the $Ca^{2+}$ ions, leading to synchronous opening of the entire cluster of RyRs and to a highly localised release of $Ca^{2+}$ out of the SR (see Fig. 6 in Section 4) into the membrane cleft

(Cheng *et al.*, 1993). These elementary signals, each issuing from ~10 RyRs (Mejia-Alvarez, 1999), are thought to sum up to underlie global $Ca^{2+}$ transients. The synchronised triggering of numerous (~10 000) $Ca^{2+}$ sparks upon membrane depolarisation results in an increase in $[Ca^{2+}]_i$ averaging from 100 nM to ~1 µM. These $Ca^{2+}$ ions then bind to myofilaments to initiate contraction (Sobie *et al*., 2005). $Ca^{2+}$ sparks are usually characterised by: amplitude of the $Ca^{2+}$ signal (corresponding to an elevation of the intracellular $Ca^{2+}$ concentration of 100 - 300 nM); duration (~150 ms); rise time (~10 ms); spatial spread as full width at half maximum (FWHM, ~2 µm); frequency of the spark site or of the sparks in one cell (Niggli & Shirokova, 2007). The measured opening rate of the RyRs (0,0001 $s^{-1}$) suggests that about 100 sparks per second occur in the whole cell at rest (Cheng *et al*., 1993), but this value depends on numerous parameters, such as SR $Ca^{2+}$ load or phospholamban phosphorylation (the protein that regulates the activity of SERCA pumps) for instance.

Each $Ca^{2+}$ spark represents a local positive feedback event in which $Ca^{2+}$ passing through a single RyR can activate neighbouring channels in the cluster. In theory, then, $Ca^{2+}$ sparks could continue indefinitely; however, their upstroke lasts roughly 10 ms under normal conditions. This brevity emphasizes the strength of the mechanism that overcomes the intrinsic positive feedback of CICR to terminate $Ca^{2+}$ sparks.

There are three putative mechanisms that underlie $Ca^{2+}$ spark termination: inactivation, refractoriness and adaptation. Sparks terminate due to a shift in RyR gating properties (e.g. RyR inactivation, the luminal side of the RyR complex is indeed said to have $Ca^{2+}$ activation and inactivation sites (Ching *et al*., 2000)). Then an interval has to elapse before sparks can again be triggered. In other words, at the moment of termination the cluster of RyRs is refractory to the $Ca^{2+}$ stimulus that had been keeping the channels open. Local refilling of SR stores is an important factor for the time necessary for the recovery phase, and this process is called restitution (Sobie *et al*., 2005). Besides inactivation and refractoriness, DelPrincipe and collaborators described the phenomenon of adaptation (DelPrincipe *et al*., 1999). An inactivated $Ca^{2+}$ spark site can be triggered again if the intensity of the stimulus is increased.

**Quarks:** By using two-photon photolytic activation of localized $Ca^{2+}$ release in cardiac myocytes, it has been shown that one single $Ca^{2+}$ spark actually consists of the summation of unitary $Ca^{2+}$ events characterised by a tiny amplitude of ~30 nM, a very short lifetime (rise time of ~5 s) and higher spatial confinement (~1 µm). Hence, each single RyR could give rise to $Ca^{2+}$ releases in the dyadic cleft called $Ca^{2+}$ quarks (Lipp & Niggli, 1998).

**Puffs:** While a $Ca^{2+}$ spark refers to the local release from a RyR cluster, $Ca^{2+}$ puff describes the local $Ca^{2+}$ increase as a result of the opening of a cluster of inositol 1,4,5-trisphosphate receptors ($InsP_3Rs$) localised in the endoplasmic reticulum (ER) or SR membrane (Lipp *et al.*, 1997). $Ca^{2+}$ puffs display a longer lifetime in comparison to $Ca^{2+}$ sparks (300 ms), an amplitude of 100 – 200 nM and a wider spread (~5 µm). Each $Ca^{2+}$ puff would be composed of elementary events named **$Ca^{2+}$ blips** (Parker & Yao, 1996). It still remains unclear whether these events are also present in excitable cells such as cardiac myocytes. However, there are pieces of evidence indicating that smooth muscle cells also display elementary $Ca^{2+}$ events, which are $InsP_3R$-dependent in the murine colon (Bayguinov *et al*., 2000), and such events were also characterised in neurones (Koizumi *et al.*, 1999).

**Scraps:** Attempts for the monitoring of $Ca^{2+}$ movements within the SR lumen led to the observation of local depletions of the $[Ca^{2+}]_i$, mirrors of $Ca^{2+}$ transients that could be recorded in the cytosol. These events were called $Ca^{2+}$ scraps (Shannon *et al*., 2003). Likewise, **$Ca^{2+}$ blinks** mean the confined SR depletions from single $Ca^{2+}$ sparks (Brochet *et al*., 2005).

**Marks:** An increasing amount of studies provide evidences that mitochondria can also act as short-term $Ca^{2+}$ buffering organelles, especially in the heart (Duchen, 1999). In the cardiac cell line H9C2 it has been shown that subsequent to $Ca^{2+}$ spark events rapid increases in $Ca^{2+}$ in neighbouring mitochondria can occur (Pacher, 2002). It was proposed that $Ca^{2+}$ marks were triggered by RyRs through a process involving the travel of $Ca^{2+}$ from spark sites into mitochondria.

**Waves:** $Ca^{2+}$ waves are global $[Ca^{2+}]_i$ increases from the SR or ER that propagate throughout the cardiac myocyte sustained by the phenomenon of CICR (see Fig. 6 in Section 4). These events have a longer lifetime and a bigger amplitude than the elementary events previously described. They adopt several appearances (spirals, U and V-shapes, circular waves). The analysis of wavefront kinetics, velocity and wave termination gives indications on how $Ca^{2+}$ is regulated in the cell, especially on the

level of sensitization of RyRs and the activity of proteins involved in buffering systems such as SERCA pumps (Keller *et al*., 2007).

### *3.3. Nuclear $Ca^{2+}$ signals*

Recently it has been shown that the nucleus can also be involved in the occurrence of $Ca^{2+}$ events, independently of what occurs to cytosolic $Ca^{2+}$ buffers or to other organelles. Lipp and collaborators described elementary $Ca^{2+}$ events in the ER membrane connected to the nuclear envelope in non-excitable cells. These events were most likely due to "perinuclear" $InsP_3Rs$ and resembled $Ca^{2+}$ puffs that propagate across the entire nucleus (Lipp *et al*., 1997). Moreover Bers and collaborators have reported nuclear $Ca^{2+}$ transients after Endothelin-1 treatment and depolarisation (Wu *et al*., 2006) exhibiting an apparent higher amplitude compared to transients in the cytosol and probably sustained by $InsP_3Rs$ type 2 present in the internal membrane of the nuclear envelope or in the perinuclear SR membrane (Berridge, 2006). It is noteworthy that some transcriptional processes depend on nuclear $Ca^{2+}$ signals that set off signalling events such as the phosphorylation of histone deacetylase 5 (HDAC5) through the activation of CAMKII, which leads to a nuclear export of HDAC5 and therefore to a derepression of the transcription. More strikingly, it appears that cytosolic and nucleoplasmic $Ca^{2+}$ signals activate distinct pathways that control gene expression in a differential manner (Hardingham *et al*., 1997).

# 4. Neurohormones and $G_q$-coupled pathways

Cardiac hypertrophy is an adaptative response of the heart that is characterised by the increase of the size of the myocytes due to the addition of new sarcomeres. There are two types of hypertrophies: compensatory hypertrophy represents a reversible physiological adaptation, whereas non-compensatory hypertrophy corresponds to a pathophysiological adaptation which is "not" reversible and leads to heart failure (cardiac cells become much less effective in terms of contraction) if the cardiac muscle is not able to recover its native functionality. This in turn may cause myocardial infarction and sudden death. Furthermore, these pathological states are

often accompanied by several forms of arrhythmias (i.e. disturbance of the rhythmic response of the myocytes to the imposed initial electrical stimulation).

An increasing amount of important studies reports the involvement of particular hormones at different stages of these pathologies, especially acting through G-protein-coupled receptors. The action of G-protein type S ($G_s$)-coupled receptors signalling is well known, especially the role of ß-adrenergic stimulation (through ß1 and ß2 receptors) on the induction of cardiac hypertrophy and failure via the proteine kinase A-induced phosphorylation of LCCs, RyRs and contractile proteins (Marx *et al*., 2000; Scoote & Williams, 2004). Besides $G_s$ proteins, it is now assumed that agonists of the 7-transmembrane (7TM) spanning proteins coupled to $G_q$ also play a major role in the regulation of cardiac function, particularly in terms of $Ca^{2+}$ handling and rhythmic activity. Nevertheless the precise molecular mechanisms leading to hypertrophy and arrhythmia remain poorly understood.

## *4.1. Cellular pathways coupled to $G_q$-proteins*

$G_q$-proteins are heterotrimeric GTPases composed of α, β, and γ subunits that are coupled to various signalling cascades. The hormonal activation of $G_q$-coupled receptors triggers the detachment of the subunit $G\alpha_q$ that stimulates phospholipase PLC-β to produce the intracellular messengers inositol trisphosphate ($InsP_3$) and di-acyl-glycerol (DAG) from phosphoinositol-4,5-biphosphate (PIP2). $InsP_3$ diffuses into the cytosol and elicits the release of $Ca^{2+}$ from intracellular stores through $InsP_3Rs$ leading to elementary $Ca^{2+}$ signals, as discussed above, and to global $Ca^{2+}$ oscillations which mainly rely on positive and negative feedback of the cytosolic $Ca^{2+}$ concentration $[Ca^{2+}]_c$ on $InsP_3Rs$ (Hajnoczky & Thomas, 1997). In addition DAG recruits and activates diverse isoforms of protein kinase C (PKC) to the membrane (Newton, 1997). PKCs, in turn, mediate a wide range of phosphorylation events that regulate fast phenomena such as ionic channel activity, but also long-term events such as gene expression for instance by the activation of the mitogen-activated protein kinase (MAPK) cascades (see Fig. 6A).

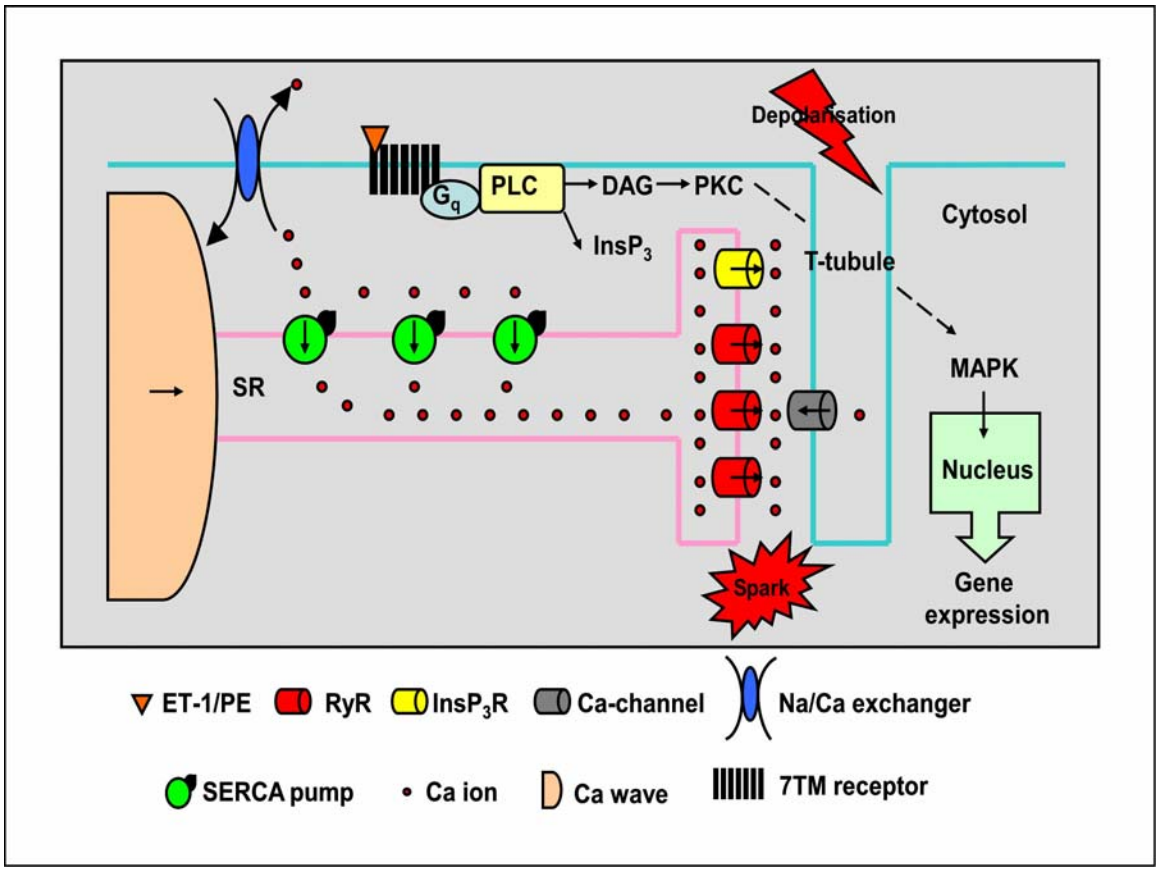


**Fig. 6A. Influence of $G_q$ signalling on $Ca^{2+}$ handling.**
**$G_q$ pathway is illustrated in this scheme with a particular emphasise of its involvement on $Ca^{2+}$ release during excitation-contraction coupling. The examples of endothelin-1 (ET-1) and phenylephrine (PE) are here represented. (Adapted from Keller *et al*., 2007).**

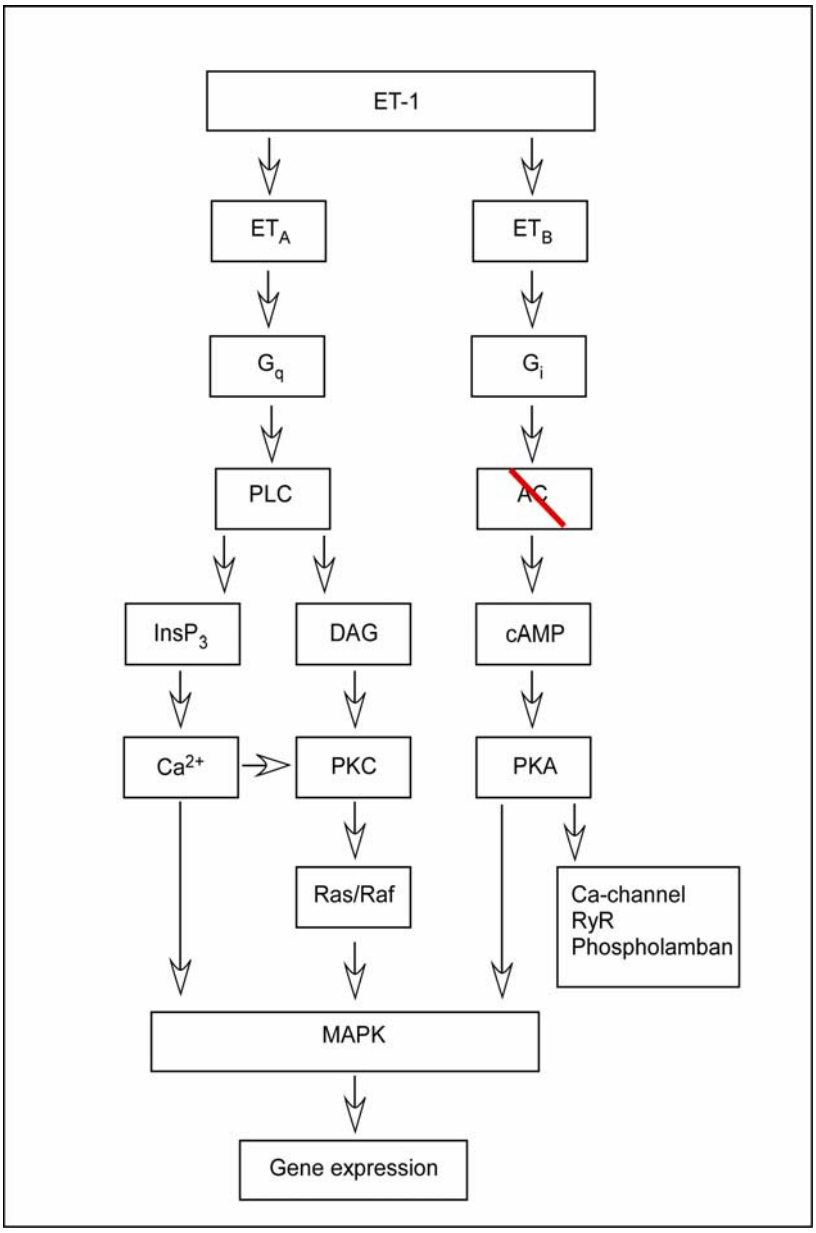


**Fig. 6B. Transduction mechanisms of endothelin-1.**
**Endothelin-1 (ET-1) can either activate its receptor subtype A ($ET_A$) or subtype B ($ET_B$). While $ET_A$ stimulates $G_q$-coupled pathways especially leading to the phosphorylation of the small GTPases Raf and Ras, ($ET_B$) modulates another type of G-protein ($G_i$) that inhibits the adenylate cyclase (AC) activity, thus impairing the production of cyclic AMP (cAMP) that triggers the action of the protein kinase A (PKA).**

## *4.2. Neurohormones and cardiac pathologies: examples*

The term “neurohormones” is based on the fact that these hormones are also produced in neuronal structures, such as dorsal root ganglia (Giaid *et al*., 1989), and

can be released from post-ganglionic sympathetic neurones for instance (Damon, 1999).

Endothelin-1 (ET-1) is a 21-residue vasoconstrictor/vasopressor peptide released from vascular endothelial cells, but has also been found to be a growth factor in a variety of mammalian cells including vascular smooth muscle cells and fibroblasts. It has been demonstrated that 100 nM of ET-1 induces hypertrophy of neonatal cardiomyocytes *in vitro*, associated with the stimulation of muscle specific genes (myosin light chain 2, α actin and troponin I) and a protooncogene (c-*fos*) (Ito *et al*., 1991). ET-1 can also be produced by a multiplicity of non-endothelial cells. It has been reported that preproET-1 mRNA is detected in a range of rat tissues including the heart (Sakurai, 1991). Furthermore Ito and his colleagues provided data that ET-1 is produced by cardiomyocytes and acts on them in an autocrine/paracrine manner (Ito *et al*., 1993).

Alternatively, numerous studies revealed the major role of ET-1 played in the induction of cellular arrhythmias in the model of atrial myocytes. Mackenzie and colleagues demonstrated the arrhythmogenicity of ET-1 (100 nM) in terms of the occurrence of extra $Ca^{2+}$ transients and spontaneous APs due to the recruitment of $Ca^{2+}$ sparks by $InsP_3Rs$ (Mackenzie *et al*., 2002). In an $InsP_3R$ type 2 knockout mouse model ET-1-induced arrhythmogenicity was suppressed (Li *et al*., 2005).

Besides the role of ET-1 in pathological states, it is noteworthy that ET-1 is also important both in the growth and in the development of cardiomyocytes. At a concentration of 100 nM it regulates nerve growth factor expression and thus controls the sympathetic innervation of the heart (Ieda *et al*., 2004).
Surprisingly, the great majority of the *in vitro* studies report the use of ET-1 at a concentration of 100 nM while the *in vitro* $K_d$ of ET-1 for endothelin receptor type A (coupled to $G_q$) ($ET_A$, see Fig. 6B) in intact cells should be at the nanomolar level (Desmarets *et al*., 1996). Actually the $K_d$ value of ET-1/$ET_A$ receptor complexes was estimated to be around 20 pM in membrane preparations (Desmarets *et al*., 1996). In contrast, computational simulations indicated that nanomolar rather than picomolar concentrations of ET-1 are required to occupy a significant part of picomolar sites under time-restricted circumstances (15 min, which corresponds to the time at which

the production of inositol phosphates was measured), still according to Desmarets' work. Hence, bovine $ET_A$ receptors have a single affinity site for ET-1 ($K_d$ = 20 pM) which might allow for nanomolar actions of ET-1 in intact cells (Desmarets *et al*., 1996). Interestingly, Dulce and his colleagues recently observed that 5 nM ET-1 was sufficient to induce hypertrophy in neonatal rat cardiomyocytes (Dulce *et al*., 2006).

In addition, the previously described autocrine/paracrine mode of ET-1 seems to be involved in the induction of hypertrophy by another neurohormone, namely angiotensin II (ANGII, 1 µM) (Ito *et al*., 1993).

Just like ET-1, locally produced ANGII is implicated in the hypertrophic response to hemodynamic overload (Sadoshima, 1993). It also sets off a multifaceted intracellular signalling leading to the re-expression of fetal genes and increase in protein synthesis, which represent reliable landmarks of cardiac hypertrophy (Dulce *et al*., 2006). ANGII as a potent vasoconstrictor hormone is also said to be hypertrophic *in vivo* (Goldspink *et al.*, 2001).

Though it is accepted that $AT_1$ (i. e. ANGII $G_q$-coupled receptors) membrane preparations exhibit a $K_d$ of 0.36 nM for [$^{125}$I]-ANGII (Martin *et al.*, 2001), the existing patho-physiological studies, which were mostly performed on neonatal cardiac myocytes, employed concentrations well above this value up to the micromolar range (Kim & Iwao, 2000). Nevertheless a recent report indicated the induction of hypertrophy in normal and postinfarcted adult ventricular cardiac myocytes by application of 1 nM ANGII for one week in culture (Liu *et al*., 1998).

A last compelling $G_q$ activator is phenylephrine (PE), which is an $\alpha_1$-adrenoceptor agonist. Usually this substance is used at a concentration of 10 – 100 µM to elicit hypertrophic responses mainly in neonatal cardiac cells (Barron *et al.*, 2003; Siddiqui *et al.*, 2004), but also in adult cells with a short-term stimulation (Anwar *et al*., 2005). In the latter experiment PE induced an increase of SERCA2 expression independently of PKC signal transduction. It is most likely that the typical PE-induced $Ca^{2+}$ oscillations (Lee *et al*., 2001) observed during acute hormonal stimulation are directly or indirectly linked to the changes of gene expression in cardiac myocytes during chronic hormonal stimulation.

Recently, interesting studies attempted to characterise the hypertrophic behaviour in mice deficient for $G\alpha_q/G\alpha_{11}$ (this is the G-protein heterotrimeric complex that mediates the intracellular signalling of the $AT_1$, $ET_A$, and α-adrenergic receptors). Since cardiomyocyte-specific overexpression of $AT_1$ or α-adrenergic receptors resulted in myocardial hypertrophy (Milano *et al.*, 1994; Hein *et al.*, 1997), the first investigation dealt with the creation of mice deficient for $G\alpha_q/G\alpha_{11}$ exclusively in cardiomyocytes. These animals failed to develop myocardial hypertrophy in response to pressure overload (Wettschureck *et al*., 2001). Surprisingly, overexpression of an $AT_1$ receptor lacking the $G\alpha_q$-coupling intracellular loop led to a greater atrial and ventricular growth than when the native receptor was expressed in the heart (Zhai *et al*., 2005).

These results indicate that the $G_q$ signalling pathways leading to cardiac remodeling are complex and imply interactions with a variety of parallel pathways involving growth factors and a plethora of various kinases.

# Objectives of the study

The acute isolation of adult cardiac myocytes was established decades ago (Powell & Twist, 1976) to investigate their physiological behaviour. In contrast, studies requiring extended culture periods, e.g. for protein expression or knock-down, have always been limited to a couple of days in culture due to extensive morphological and physiological alterations of the adult myocytes occurring shortly after isolation (Bugaisky & Zak, 1989). This restriction could not be compensated for adequately by the creation of cardiac cell lines since they do not represent cardiac myocyte physiology well enough (Kageyama *et al*., 2002). Currently, neonatal myocytes serve as a limited model for the adult cell. It has to be noted that in comparison to adult myocytes neonatal cells display a different phenotype and genotype. Nevertheless, long-term culturing of these cells even in larger quantities is routine.

In conventional culture, isolated adult rat cardiomyocytes rapidly change from a “brick-like” structure towards a more stellated, neonatal-like shape. Moreover, their size increases considerably (Poindexter *et al*., 2001). In serum-free culture medium,

adult cardiac myocytes from guinea-pigs, rats, rabbits and mice are usually quiescent and retain their viability, unique rod-shaped morphology for at least a couple of days (Mitcheson *et al*., 1998; Sambrano *et al*., 2002; Volz *et al*., 1991). These cells maintain highly organised membrane and myofibrillar structures that support contractions induced by electrical stimulation. Thus, they appear suitable to short-term (1-3 days) virus-mediated expression of exogenous proteins (Zhou *et al*., 2000). For future studies requiring long-term expression of exogenous proteins or vector-based RNA interference (RNAi) to knock-down protein expression it appears essential to employ longer culture periods without a loss of morphology and physiology of the freshly isolated cells. Moreover, experimental manoeuvres inducing "slow-onset" cellular responses will also entail long-term culturing of the myocytes. Additionally, molecular biology techniques such as Western blotting demand large amounts of proteins from homogeneous cell populations. Thus, culturing set-ups are needed that offer the possibility to electrically stimulate large homogeneous populations of cells simultaneously. A decade ago, an adult rat ventricular myocytes culture system was developed (Berger *et al*., 1994) with conditions that allow short-term (3 days) culture together with the ability to impose arbitrary electrical pulse protocols.

The goal of the first part of my thesis was to use that basic approach and refine it to a long-term culture system (7 days) with diminished cellular dedifferentiation. I tested the suitability of my system in multiple ways including morphology, survival rate, contractile behaviour, $Ca^{2+}$ signalling and success for adenoviral mediated expression of an exogenous protein (inverse pericam, a fluorescence calcium indicator based on calmodulin (Nagai *et al*., 2001)).

The aim of the second part of this study was to use the long-term culture system for adult ventricular myocytes allowing extended manipulation of these cells with minimised dedifferentiation in order to investigate – for the first time – cardiac $Ca^{2+}$ remodelling in adult ventricular myocytes *in vitro* with a more "physiological" onset (8 days) and especially the effects of chronic stimulation of $G_q$-coupled pathways on $Ca^{2+}$ handling in the ventricular myocytes of the rat.

# Materials and Methods

## 1. Isolation and primary culture of adult rat ventricular cardiomyocytes

I adopted a protocol for cell isolation based on established procedures in rabbit and mouse (Mitcheson *et al*., 1996; Hilal-Dandan *et al*., 2000) for the rat heart. Adult male Wistar rats (6 to 12 weeks old, 200-400 g) were handled and sacrificed in accordance with the *Guide for the Care and Use of Laboratory Animals* published by the US National Institutes of Health (NIH Publication No. 85-23, revised 1996). Animals were anaesthetised by an intraperitoneal injection (i.p.) of pentobarbital sodium, 160 mg/kg body weight (Narcoren; Merial, Germany). Directly afterwards, I injected (i.p.) 0.5-1 ml (according to the body weight) of a citrate (40 mM) solution for the prevention of blood clot formation. Ten minutes later, the animal was killed by decapitation. The heart was flushed with 10 ml of ice-cold $Ca^{2+}$-free solution (CFS) containing (in mM): NaCl 134, Glucose 11, KCl 4, $MgSO_4$ 1.2, $Na_2HPO_4$ 1.2, HEPES (Merck, Germany) 10 (pH adjusted to 7.35 with NaOH). After that, the heart was removed, attached to a Langendorff apparatus and perfused retrogradly with $O_2$ saturated CFS containing 200 µM EGTA at a rate of 4 ml/min for 5 min. The perfusate was then changed to $O_2$ saturated CFS containing either collagenase type I (Worthington, New Jersey, USA) at a final concentration of 1 mg/ml or Liberase Blendzyme type 4 (Roche, Germany) which is a defined mixture of neutral proteases and purified collagenase; this mixture was used at a final concentration of 0.3 mg/ml (duration in either case: 25 min).

The ventricles were removed, minced and placed in $O_2$ saturated CFS containing 1 mg/ml collagenase or 0.3 mg/ml Liberase Blendzyme (at 37°C in a water bath for 2 min). After sedimentation, the resulting supernatant was discarded and the pellet was mixed and resuspended in 20-25 ml of $O_2$ saturated CFS and incubated as above. The supernatant was discarded again and the pellet was mixed and resuspended in 20-25 ml of $O_2$ saturated low-$Ca^{2+}$ solution (LCS) containing 50% of CFS and 50% of high-$Ca^{2+}$ solution (HCS) and incubated as above. HCS is composed of CFS supplemented with 0.09% of DNAse and 200 µM of $CaCl_2$. Furthermore, the supernatant was discarded, the pellet was resuspended in 20-25 ml of $O_2$ saturated

HCS and incubated as above. Now rat ventricular myocytes were released from the soft tissue by gentle trituration. The cell suspension was plated into “peel-off” culture flasks (Techno Plastic Products AG, Switzerland), the internal bottom surface of which was coated with poly-L-lysine (500 µg/ml; Sigma, USA) or extracellular matrix proteins (ECM, 1.11 mg/ml; Harbor Bio-Products, Norwood, MA, USA). They were allowed to settle down for approximately 1 hour in medium M199 with Earle’s modified salts, glutamine (Biowest; Nuaille, France), 100 µg/ml Penicillin/Streptomycin and 50 µg/ml Kanamycin (PAA Laboratories, Austria). In addition to the control condition (pure medium), the medium was supplemented with either 5% fetal calf serum (FCS supplemented medium) or 870 nM insulin, 65 nM transferrin and 29 nM Na-selenite (Sigma, USA) (ITS supplemented medium). Myocytes were cultured in an incubator at 37°C with a 5% $CO_2$ atmosphere. After plating the medium was changed at 1 hour, day *in vitro* (DIV) 1, 3 and 6 with warm fresh medium supplemented depending on the particular culture conditions.

For the experiments involving chronic hormonal stimulation, caffeine responses, confocal recordings and viral gene transfer, cells were plated on ECM-coated cover slips, placed in 12-well plates and kept in M199 medium supplemented with ITS unless otherwise stated. Adenovirus-mediated gene transfer was initiated 1 hour after cell plating to allow a fast protein expression. The myocytes were transfected with a multiplicity of infection of 5-20 plaque-forming units/cells. The regime for exchanging the culture medium was as described above.

Continuous electrical stimulation was performed at 37°C. All other experiments were carried out at room temperature (20-22°C).

## 2. Electrical stimulation

For electrical stimulation of entire cell populations, Plexiglas lids were designed and built, that were resistant to heat sterilisation, as shown in fig. 7A. They displayed the following features: (i) two parallel carbon electrodes for electrical field stimulation, (ii) standardised connectors for external electrical pulses and (iii) silicone sealing for taking the culture flask out of the incubator while maintaining sterile internal

conditions. The set-up for stimulation comprised a custom-made high-current pulse amplifier (cp. fig. 7B; Babraham Tech[nix], Cambridge, UK) and custom-made software running under LabView. The software "Cardiac Stimulator" allowed continuous pacing of culture flasks at an adjustable frequency, cp. fig. 7C. I used 0.2 Hz throughout all culture conditions involving pacing of cardiac myocytes.

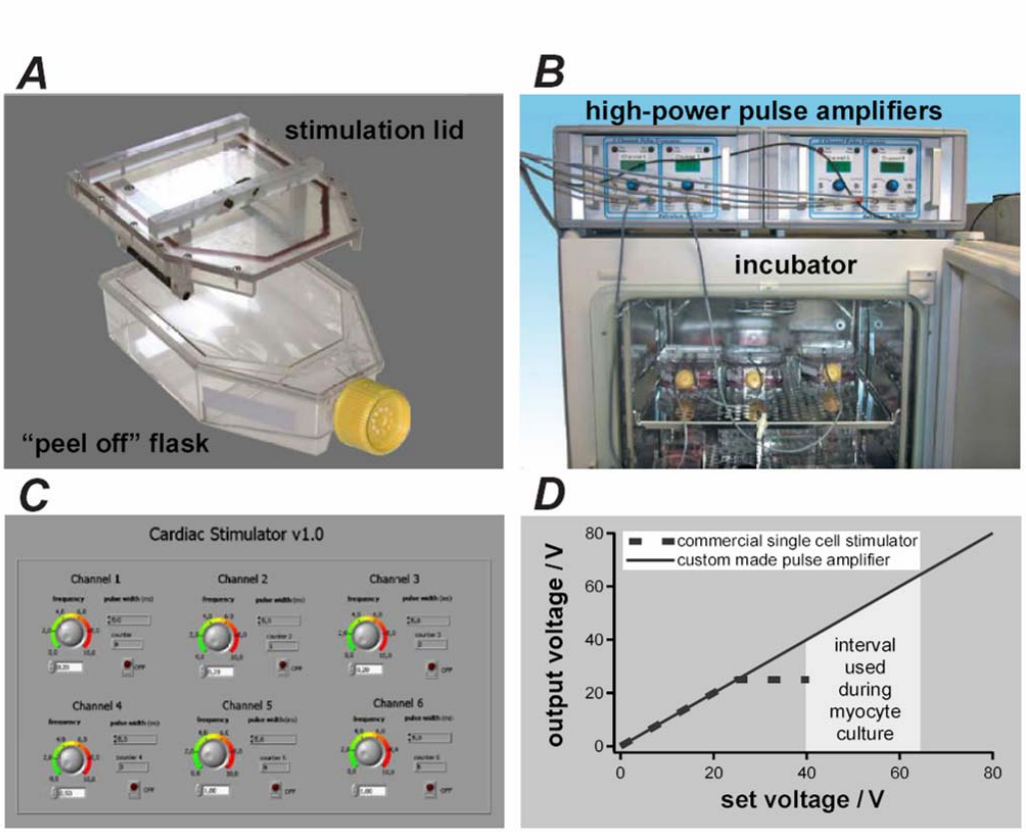


**Fig. 7. Electrical stimulation and prolonged culture of adult cardiomyocytes.**
**Panels A-C illustrate components of the optimised culturing system. A shows the custom-made stimulation lid (top) and "peel-off" flask (bottom), B two high-power amplifiers on top of a standard cell incubator connected to several "peel-off" flasks for electrical stimulation of myocyte populations. Panel C depicts the graphical user interface of the LabView based software "Cardiac stimulator" controlling the electrical pacing of the myocytes in the flasks. Panel D displays the relationship of set voltage (x-axis) and output voltage (y-axis) of a commercial single cell stimulator (marked in red) and the custom made pulse amplifier (marked in black) connected to an individual culture flask filled with medium as shown in panels A and B. The typically required voltages used during myocyte culture are highlighted.**

# 3. Measurements of cell length changes

Using a fast camera, electrical stimulation induced cell-length changes were measured (sampling rate 240 Hz) from cells maintained in the culture flask. For this I removed the flasks from the incubator and quickly transferred those onto the stage of

an inverted microscope (NIKON Eclipse TS100, Japan) equipped with the cell-length acquisition system SoftEdge (IonOptix Corporation, USA). The software measured cell length via real-time contrast analysis of digitised image data. A framegrabber card mounted in the acquisition computer continuously digitised the output of the video camera and displayed it on the computer monitor. I selected separate video lines for both left and right edges of the object being measured. These lines were chosen such that the edge contrast was optimal. These video lines were stripped out of the image and plotted so that I could view the intensity of the edge contrast on a graph. This plot might be conditioned via online smoothing and derivative functions to increase the signal to noise ratio. I then set a threshold value. The computer analysed each video image and considered the surpassing of the threshold value as the edge location. Both the left and right edges of the cell were scanned from the outside in to maximise the possibility of catching the edge properly. This was all performed online and in real-time. The digitised image data were then converted into cell length changes.

The latter were directly put out by the system and further analysed in Igor Pro software (Wavemetrics, USA) with custom-made macros.

# 4. Fluorimetric $Ca^{2+}$ recordings

Global $Ca^{2+}$ transient were measured with either fura-2 (Invitrogen, USA) or the $Ca^{2+}$ sensitive fluorescent protein inverse pericam (Nagai *et al*., 2001). For this, cardiac myocytes were seeded on coated glass cover slips that were placed into culture flasks (for experiments related to $Ca^{2+}$-frequency relationship) or into the wells of a 12-well plate (for caffeine response experiments and for inverse pericam) before seeding. For fluorescence recordings the cover slips were mounted in a custom made chamber on the stage of an inverted microscope (TE2000U, NIKON, Japan) attached to video-imaging hardware. Imaging was carried out through a 20x oil-immersion objective (Planfluor 0.75 NA, NIKON, Japan). The system comprised a video camera (for fura-2: Imago, TILL Photonics, Germany; for inverse pericam: iXon DV887, Andor Inc., Ireland) and a fast monochromator for excitation (Polychrome IV, TILL Photonics, Germany). The video-imaging was operated under the TILL-Vision Software 4 (TILL Photonics, Germany).

For the fura-2 recordings cover slips were loaded with dye (fura-2-AM, 0.4-0.75 µM, from a stock of 1 mM in di-methyl sulfoxide (DMSO) / 20% Pluronic (Invitrogen, USA)) for 20-30 min (depending on the age of the cells in culture) at room temperature. Before recording, the loading solution was exchanged with extracellular solution (ES) composed of (in mM): NaCl 135, KCl 5.4, $MgCl_2$ 1, glucose 10, $CaCl_2$ 2, HEPES 10 adjusted to pH 7.35 with NaOH. Imaging was performed by exciting the cells at the $Ca^{2+}$-dependent wavelength (380 nm). Excitation light was separated from emission by a dichroic filter (FURA, NIKON, Japan) and the fluorescence signal was "cleaned up" by a 440 nm longpass filter. Therefore the fluorescence signal was recorded at wavelenghts >440 nm at an image exposure time of 15 ms. Neutral density filters (Thorlabs, Newton, NJ, USA) with an optical density of 0.2 were also used to reduce the amount of light reaching the recording chamber and then minimise the bleaching effect. The camera CCD-chip was binned 4x4, resulting in an image size of 128x128 pixels. The excitation at 380 nm was interrupted every $50^{th}$ image by recording a single image at the $Ca^{2+}$ independent, isosbestic excitation wavelength of 355 nm (see fig. 14A). For calculating ratiometric data, a linear interpolation was undertaken between the 355 nm-images and the fluorescence values were ratioed against the corresponding 380 nm-image to obtain true $F_{355}/F_{380}$-fura-2 ratio data at a final acquisition frequency of 60 Hz. This ratioing and further semi-automatic peak detection was performed in Igor Pro software running custom made macros after averaging the fluorescence of regions of interest in the imaging software.

Inverse pericam is a chimeric protein resulting from the fusion of a circularly permuted green fluorescent protein and calmodulin (Nagai *et al.*, 2001). Imaging of the inverse pericam fluorescence was performed by exciting the fluorophores at 490 nm, separating excitation from emission light by a dichroic mirror (Fluo LP515 DCLP 490, NIKON, Japan), and recording the fluorescence through a 510 nm long-pass filter (image exposure time 15-20 ms). The final image dimension of 128x128 pixels was obtained by a 4x4 binning on the backthinned CCD-chip. The EM (electron multiplier) gain was set to 70-120. Neutral density filters (Thorlabs, Newton, New Jersey, USA) with an optical density of 0.2 were used for adjusting the intensity of the excitation light. Single fluorescence images were obtained by exporting entire

movies as multi-page TIFF files and processing them in ImageJ (W. Rasband, NIH, USA). For self ratio traces the $F_0/\Delta F$ ratio was calculated since inverse pericam fluorescence decreased with increased $Ca^{2+}$ concentrations, therefore the term "inverse".

# 5. Adenovirus construction

Generation of recombinant adenoviruses was accomplished in the laboratory by Dr. Sandra Ruppenthal (Institute for Molecular Cell Biology, Homburg / Saar, Germany) using the Transpose-Ad™ Adenoviral Vector System (MP Biomedicals, USA) according to the manufacturer's instructions. A pCR259 adenovirus transfer vector encoding for the calcium-sensitive fluorescence protein inverse pericam was transformed in HighQ-1 Transpose-Ad™ 294 competent cells, a bacterial cell line carrying the Transpose-Ad™ 294 plasmid and a plasmid encoding a trans-acting Tn7 transposase. After a Tn7-based transposition, recombinant adenoviral genome was purified from bacteria and transfected into the QBI-HEK 293 cell line using Lipofectamine 2000 (Invitrogen, USA). In this cell line, the recombinant adenoviruses were generated and propagated.

The pcDNA3-inverse pericam vector was kindly provided by Dr. Atsushi Miyawaki (Laboratory for Cell Function and Dynamics, Brain Science Institute, RIKEN, Wako, Saitama, Japan).

# 6. Confocal imaging

Fluorescence changes of the $Ca^{2+}$ indicator fluo-4 (Invitrogen, USA) were analysed by laser scanning confocal microscopy. I used the 2D-array kilobeam scanner (approx. 800 Hz image generation) based $VT_{infinity}$ (VisiTech, UK) equipped with an EM-CCD camera (iXon DV887, Andor Inc., Ireland). The confocal system was mounted to an inverted microscop (TE-2000U, NIKON, Japan) equipped with a 60x oil immersion objective (PlanApo, NA 1.4 DIC H, NIKON, Japan) and controlled by VoxCell Scan software (VisiTech, UK). Fluo-4 requires excitation at the wavelength of 488 nm. Therefore an Argon ion-laser (model 185-F12-NS11266, Spectra Physics,

USA) was coupled to the $VT_{infinity}$. Its excitation energy was adjusted by an AOTF (acousto-optical transmission filter) through the VoxCell Scan software. Laser light was separated from the emission light by a 500 nm dichroic longpass mirror while the emission was "cleaned up" by a 500 nm longpass filter. Series of images were recorded at acquisition speeds ranging from 20 to 100 Hz. For this a 2x2 binning was applied and only part of the CCD-chip was read out to further foster acquisition rates. I set the EM (electron multiplier) gain to 120-150 while the power of the laser was adjusted to 20-40% of the maximal AOTF throughput. All experiments were carried out at room temperature (20-22 °C). The dye (0.4-0.5 µM fluo-4-AM, depending on the age of the cells in culture) was loaded into the cells for 15 min with an additional period of 20 min for de-esterification.

The cell area of cardiac myocytes in culture were assessed by loading the cells with the fluorescent dye Cell Tracker Red (Sigma, USA), recording series of 5 stacks pro myocyte with the confocal microscope $VT_{infinity}$ (VisiTech, UK), doing a Z-projection of the stacks and analysing the average fluorescence level of the stained cells in confocal slices with macros in ImageJ (W. Rasband, NIH, USA) after a series of thresholding and converting the images into 8-bit pictures.

# 7. Data analysis

After storage of the images and movies on DVDs, I analysed the data using ImageJ (W.Rasband, NIH, USA). Region-of-interest fluorescence over time data were transferred into Igor Pro software (Wavemetrics, USA) and further processed for data analysis and display.

With fluorescence values corrected for background, the intracellular concentration of $Ca^{2+}$ ($[Ca^{2+}]_i$) was calculated in accordance to the equation given by Grynkiewicz (Grynkiewicz *et al.*, 1985): $[Ca^{2+}]_i = K_d[(F-F_{min})/(F_{max}-F_{min})]$ where $K_d$ was the constant of dissociation of fluo-4, $F_{min}$ and $F_{max}$ were the minimum and maximum fluorescence intensities and F was the fluorescence intensity at any given time point. The basal $[Ca^{2+}]_i$ was assumed to be at 100 nM (Thomas *et al.*, 2000).

$Ca^{2+}$ spark analysis was performed with an automated algorithm provided by Dr. Daniel Ursu ("CaSparks"; University of Ulm, Germany). This software was

implemented in Delphi 3.0 (Borland International, Scott Valley, CA, USA) and contains five interconnected modules, responsible for different steps of analysis. After a first conversion of the "3D" images (i.e. the confocal slice recording of the entire cell area over time) into line scan images (i.e. a unique "2D" image where the length of the line crossing the cell was plotted *versus* time), the raw image (Fig. 8A) containing the integer data (8 or 16 bit values for each pixel) was converted into a floating-point image. A series of lines "free of sparks" (i.e. with a low standard deviation (SD) value) was then selected automatically in order to estimate (Fig. 8B) and generate (Fig. 8C) the background. The automated detection of background was always performed in low filtered images (pre-filtering type "SMS": 1 smooth, 1 median, 1 smooth). This background image was then used to normalise the pre-filtered image (SMS) into a $\Delta F/F_0$ image (Fig. 8D). Afterwards the normalised image was used for determination of spark parameters and after strong filtering for the spark detection (Fig. 8E). The latter was undertaken by filtering the normalised image 40 times with a 3x3 average smooth filter with a weight of 1. The threshold was calculated as the product of a pre-defined *criterion* (arbitrary value) and the SD of the normalised raw image. The binary image was created *via* the calculated threshold and the sparks were detected as islets (Fig. 8F). Three parameters of detection were determined: amplitude, FWHM and duration (actually full duration at half maximum or FDHM), the values of which were further stored in a database that can be easily transferred into an Excel sheet or into Igor Pro software. The detailed procedure of the spark analysis can be found in the dissertation of Dr. Daniel Ursu (Ursu, 2004).

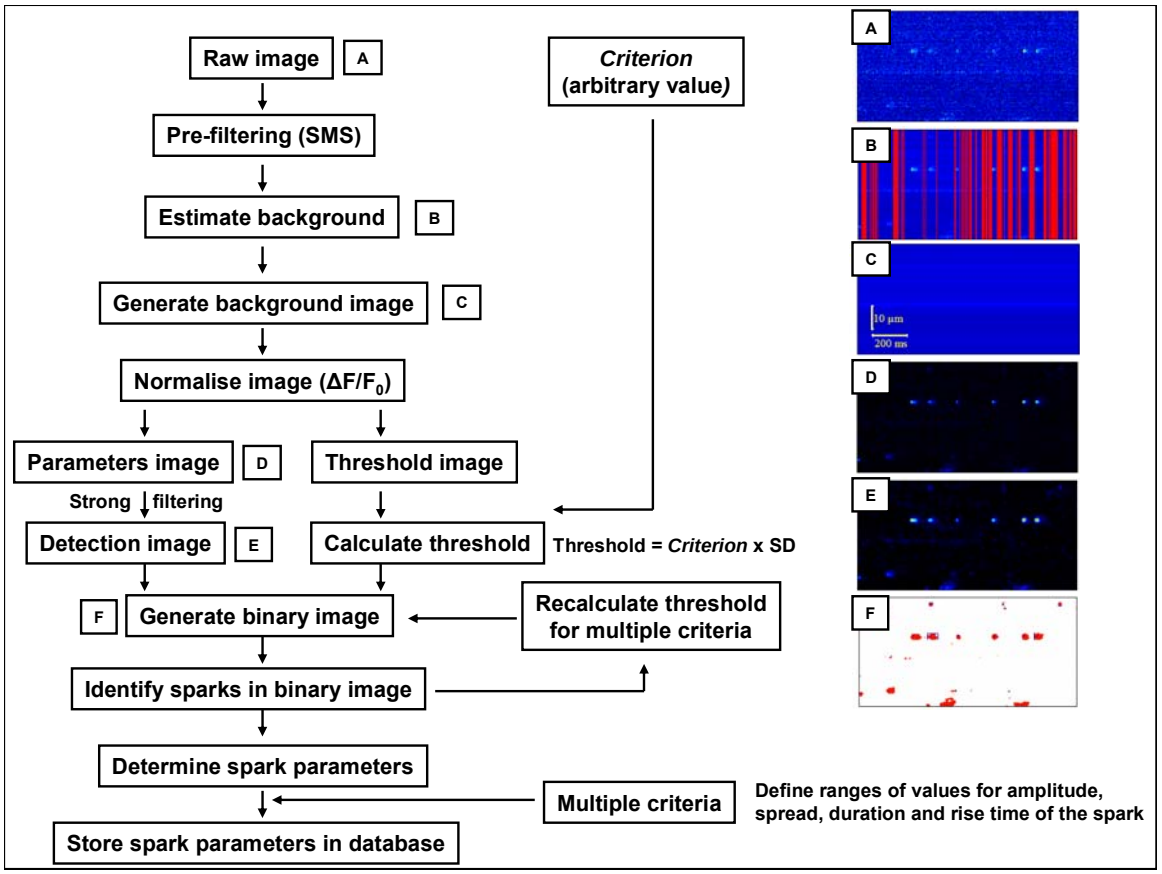


**Fig. 8. Different steps of the $Ca^{2+}$ spark analysis.**
**This panel summarises the procedure of the image processing by the spark analysis algorithm. Intermediate images A-F generated at each stage (on the right-hand side) correspond to the following steps represented on the left-hand side. The automatic background estimation (B) was undertaken from the original fluorescence line scan image (A) by using regions with low SD (showed with red lines) in order to generate the background image (C). (E) Normalised image ($\Delta F/F_0$) obtained from (A) and (C) and strong filtered before applying the threshold value (calculated in parallel to the generation of the detection image (E)) for spark detection. (F) Binary image generated at threshold = 0.4 SD. (D) The detected sparks in (F) were evaluated in low filtered image (filtering type "SMS") for determination of the standard parameters: spark maximum (amplitude), FWHM and FDHM. This figure was adapted from the dissertation of Dr. Daniel Ursu (Eli Lilly, UK) who kindly provided the example images (Ursu, 2004).**

# 8. Hormonal stimulation

After enzymatic isolation, myocytes were allowed to rest for 4 hours. Unless otherwise stated, all hormones were purchased from Sigma-Aldrich (USA). Concentrated stock solutions of PE in distilled water and stock solutions of ET-1 in 5% acetic acid were stored at -20°C. For chronicle hormonal stimulation stock solutions were dissolved directly in the ITS supplemented medium at appropriate concentrations. The ITS medium was exchanged with ITS medium supplemented

with hormones on DIV0, 1, 3 and 6 to assure an effective hormonal concentration in the medium over culturing time.

## 9. Solutions for measurements

All experiments were carried out in a HEPES (Merck, Germany) buffered ES (see 4.). Drugs (Sigma, USA) were dissolved as stock solutions in the appropriate solvents and diluted in the external salt solution at the given concentrations prior to each experiment. Rapid solution switch (exchange time < 300 ms) was achieved by means of a solenoid driven custom-made perfusion system.

Unless otherwise stated, most of the standard chemicals were obtained from Sigma (USA). They were dissolved and conditioned in MilliQ water or in di-methyl sulfoxide (DMSO), or in ethanol, or in acetic acid, or in ES according to the recommendations suggested in the Merck Index-13th edition or recommendations from the suppliers.

## 10. Statistics

Results were analysed using a Mann-Whitney rank sum test (SigmaStat software, USA). Effects were regarded as significant when $p<0.05$ (marked with an asterisk). The results are expressed as mean values $\pm$ SEM.

# Results

## 1. Establishment and exploration of a single-cell model for adult rat cardiomyocytes

### *1.1. Electrical field stimulation of the cardiac myocytes*

In the peel off flask / lid system (see Fig. 7A and section Materials & Methods 2. Electrical stimulation) the field voltage (5 ms pulse duration) was adjusted so that at

least 75% of the isolated myocytes displayed visible contractions (40-60 V). In order to generate these pulses, commercially available pulse generators such as the MyoPacer (IonOptix Corp., USA) were not sufficient, because (i) their voltage output is limited to 40 V and (ii) the electric current necessary for the peel off flask / lid system was higher than the limit of the total output power of the MyoPacer (compare Fig. 7D). This restricted the highest achievable output voltage to 25 V (measured with two independent MyoPacers). It has to be mentioned here that such amplifiers had been designed solely for single cell experiments and my findings might indicate design specific limitations. Thus custom made high power amplifiers were obtained that also allowed fast switching of the voltage (cp. Fig. 7B and section Materials & Methods 2. Electrical stimulation). Such amplifiers delivered enough power to simultaneously drive four of the peel off flasks (per channel) at a maximal voltage of more than 80 V (voltage stability confirmed; voltage change during the pulse <5%). For this the hardware generated an electrical current of approximately 2.1 A (calculation based on a specific electrical resistance of culture medium of approximately 125 Ω cm, an electrode distance of 8 cm and a cylindrical electrode geometry of a length of 7.3 cm and a diameter of 6 mm).

The comparison between a single cell stimulator and the custom made pulse amplifier is depicted in Fig. 7D. For this a single culture flask filled with medium was connected to the amplifier and the actual output voltage was measured for a range of set voltages.

During myocyte culture the voltage was readjusted on a daily bases. With this I ensured to always drive at least 75% of the muscle cells. This was confirmed by visual inspection through a microscope. I observed that the voltage necessary for that increased from about 40 V at DIV0 to approximately 65 V at DIV6. In my studies I applied the pulses (square-shaped; 5 ms in duration) at a constant frequency of 0.2 Hz for the entire culture period.

## *1.2. Long-term culture of cardiomyocytes: whole cell morphology and survival rates*

Isolation of adult rat ventricular myocytes with collagenase type I yielded more than 80% living cells of which more than 70% displayed a rod-shaped morphology

(Fig. 10, black bars on DIV0). Initially, I evaluated various culture conditions based on the light microscopic morphology of the myocytes during a week of culture. Fig. 9A summarises my findings for 5 different culture conditions. Each row of panels depicts the culture conditions while the columns represent successive DIVs.

The first two rows show typical results when culturing adult rat ventricular myocytes in a supplement-free medium (Fig. 9A). Over the time course of 7 days, most of the cells were able to largely retain their elongated phenotype. I found that after a few days the myocytes developed numerous small vesicles or vacuoles, as indicated by the two insets in the first row of images. The development of them was independent of the substrate coating (Fig. 9A 1$^{st}$ and 2$^{nd}$ row).

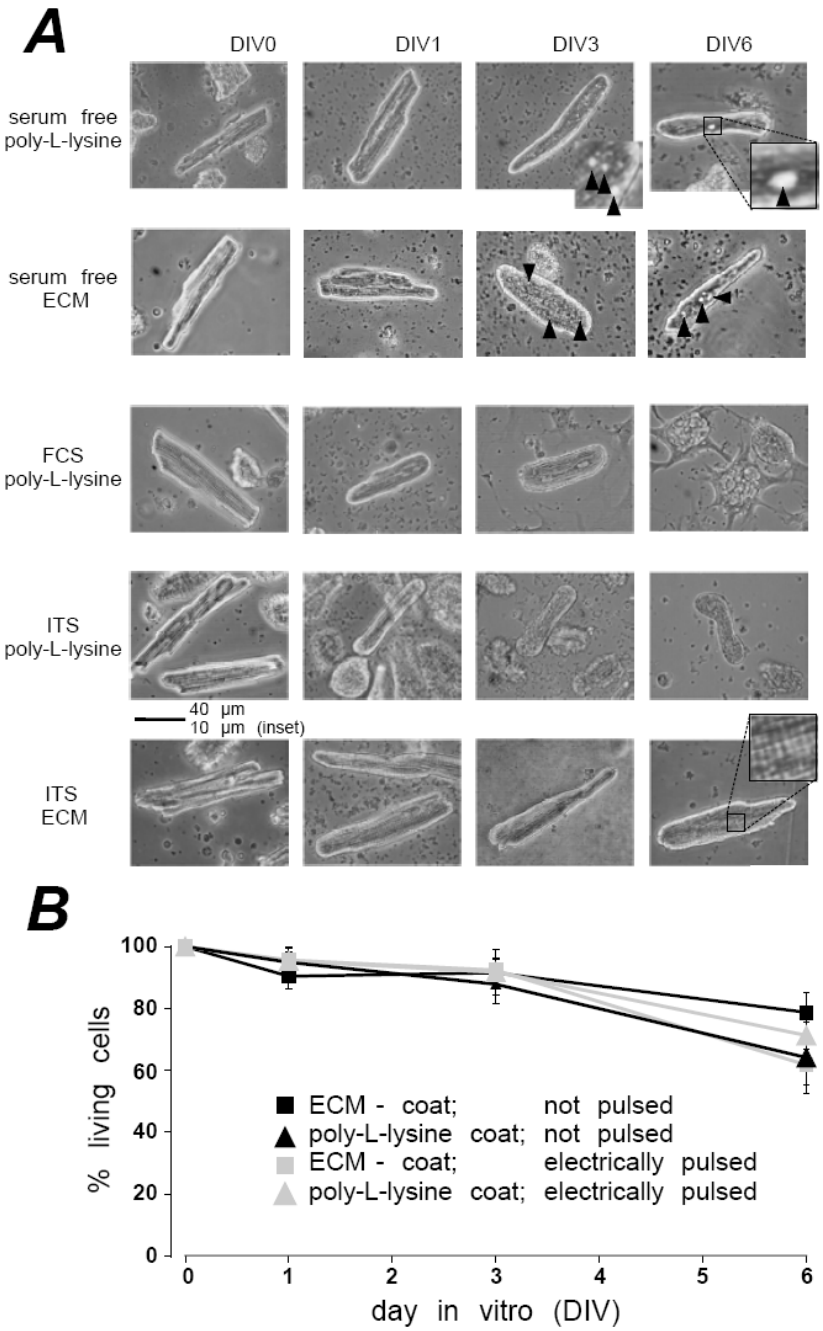


**Fig. 9. Whole cell morphological properties and survival rates of cardiomyocytes in long-term culture.**
**Panel A depicts transmission images of typical adult rat ventricular myocytes under various culturing conditions. The rows represent different culture conditions for the time points shown (columns). For selected combinations part of the cell body has been redrawn in a magnified inset (the same reference length bar indicates 40 µm for the images and 10 µm for the magnified insets). The black arrowheads in the panels of the first two rows highlight the occurrence of numerous vesicles and vacuoles.**
**In panel B, I have plotted the normalised yield of living cells (as percentage of the total number of cells, i.e. living and dead) versus the time of culturing. The data were taken from 4 to 8 different rat heart preparations.**

When cultured in medium supplemented with 5% FCS, the myocytes rapidly dedifferentiated in their morphology (Fig. 9A). This process was so fast that from DIV3 onwards, reliable contraction measurements based on edge detection (c.p. Material & Methods 3) were difficult due to massive changes in the cell geometry, i. e. the majority of cells were rounded up (>65%, see Fig. 10A). Furthermore, at DIV6 most cells started to develop lamellipodia-like structures and a flattened “fried egg” morphology (Fig. 9A, third row, rightmost image). In comparison to serum conditions, for myocytes cultured under serum-free and ITS-supplemented conditions (Fig. 9A, two lower rows) such morphological dedifferentiation was significantly reduced regardless of the culture conditions (poly-L-lysine: Fig. 9A 4$^{th}$ row or ECM-coated substrates: Fig. 9A bottom row). Even after 6 days in culture >32% elongated myocytes were present with the poly-L-lysine coating (Fig. 10C), without any lamellipodia-like structures. The rate of elongated cells on the flasks surfaces coated with ECM was even exceeding those rates (>42%, see Fig. 10D).

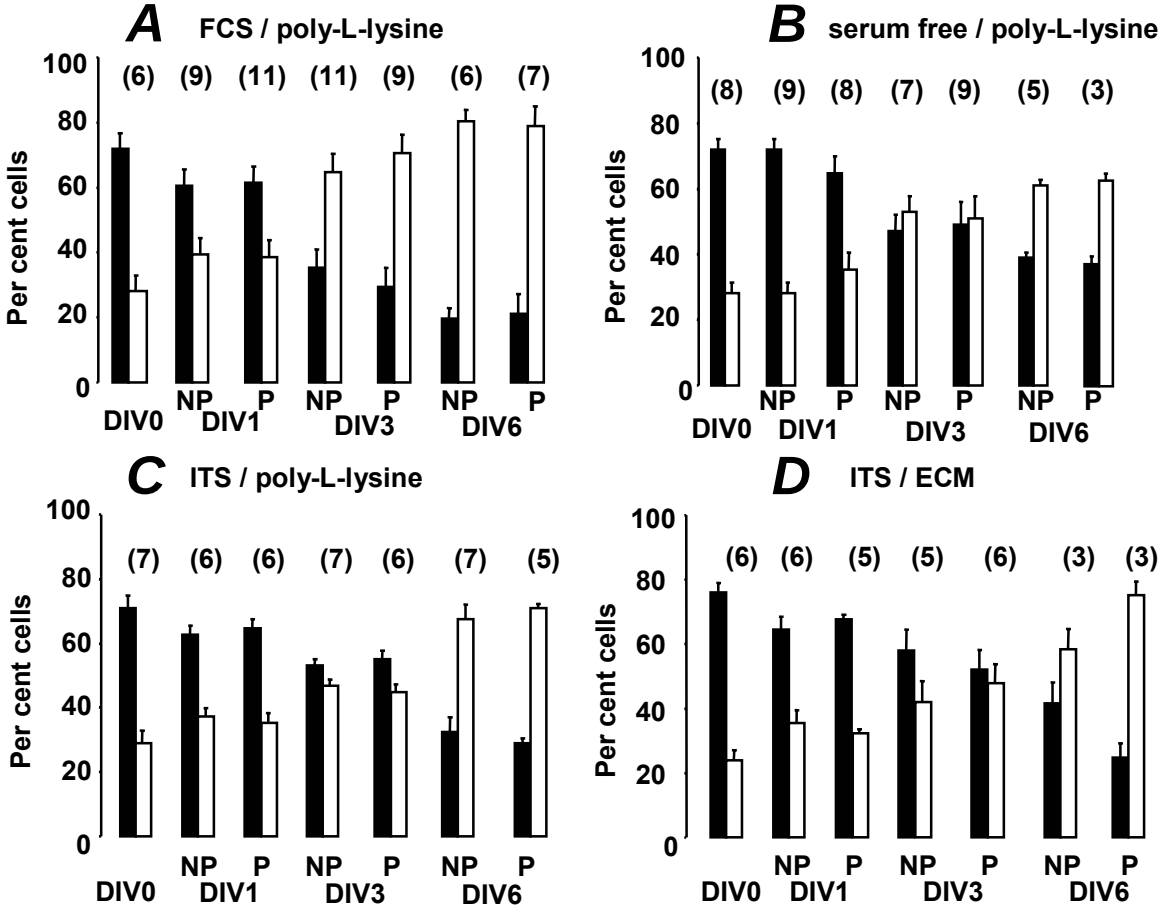

**Fig. 10. Distribution of rod-shaped and round cells in long-term culture of cardiomyocytes. Histograms A-D describe the numbers of myocytes as percentage of the total numbers of living cells over the culturing time (DIV0, 1, 3 and 6) under various conditions: FCS / poly-L-lysine (A), serum free / poly-L-lysine (B), ITS / poly-L-lysine (C) and ITS / ECM (D). The black bars indicate the rod-shaped cells while the white bars indicate the round cells. The values over the bars represent the number of heart preparations used for the study.**

From these results I concluded that the two most favourable culture conditions so far were either without any medium supplements on poly-L-lysine coating or with ITS-supplement on ECM-coated substrates. I thus investigated those two conditions further to identify the superior one with respect to cell survival and conservation of the morphology.

Fig. 9B compares the survival rates of the myocytes under the two most promising culture conditions, i.e. ITS/ECM and no serum/poly-L-lysine for pulsed and non-pulsed cells. From these data it became apparent that the overall survival rates of ITS/ECM cultured cells were not significantly different compared to the non supplemented culture conditions, a finding observed for pulsed and non-pulsed conditions. This obviously indicated that electrical pacing did not exert a detrimental effect on cell survival.

Importantly a higher quantity of cells was found on the ECM-coated surfaces after the isolation and plating steps in comparison to the poly-L-lysine substrate coating, though the cells were seeded with the same density. The value of the ratio R (R= number of cells on ECM over number of cells on poly-L-lysine after the isolation, plating and the first wash on DIV0) was 1,9 ± 0,3 for living myocytes (n=11 heart preparations). In addition, I observed that reliable cell length measurements of myocytes on poly-L-lysine at DIV0 were difficult during the first 4 hours after seeding, because the cells displayed an increased rate of spontaneous activity. Afterwards the interaction between cells and poly-L-lysine was more favourable to consistent recordings, i. e. the cells were quiescent again.

When I analysed the myocytes under both culturing conditions at DIV6 by visual inspection I found that in comparison to the ITS/ECM condition the serum free condition resulted in cells (i) with numerous vesicles and/or vacuoles (see DIV6, first row in Fig. 9A) and (ii) without apparent cross-striation (compare DIV6 first and last row in Fig. 9A).

## *1.3. Long-term culture of cardiomyocytes: analysis of cross-striation*

In order to quantify the presence of cross-striation as an indication for the conservation of the contractile filaments power spectra were calculated from light intensity profiles of elongated adult rat cardiac myocytes under serum free and ITS/ECM conditions (Fig. 11). Intensity profiles were generated (Figs. 11Aa&b) along the longitudinal axis of the myocytes at DIV0 and 6 and power spectra were calculated (Fig. 11B). For cells at DIV0 a peak was consistently found at the spatial frequency of 0.56 ± 0.015 $\mu m^{-1}$ (n=6 cells, translating to a regular structure with a repetition every 1.78 µm) regardless of the particular culture condition. This value for the spatial frequency was very close to the one expected for sarcomeric structures (i.e. 1.8 µm sarcomeric length; Bers, 2001). From that it was concluded that the regular banding visually identified in the myocytes at DIV0 was indeed caused by the typical cross-striation generated by the regular arrangement of the contractile filaments. A similar analysis was performed with cells at DIV6 either in ITS/ECM or in serum free/poly-L-lysine conditions. It was found that the former cells displayed a frequency peak that appeared slightly shifted towards higher frequencies (0.61 ± 0.027 $\mu m^{-1}$ for DIV6 vs. 0.56 ± 0.018 $\mu m^{-1}$ for DIV0, n=6 for each DIV, translating into 1.64 µm for DIV6 vs. 1.78 µm for DIV0). The amplitude in that peak was also reduced to 68.9% ± 10% (n=6). Even for the cells cultured in serum free/poly-L-lysine conditions at DIV6, a spectral frequency peak could be identified in the very same region. Nevertheless, these peaks were shifted towards higher spatial frequencies even further (0.66 ± 0.03 $\mu m^{-1}$, n=5 cells, translating into 1.5 µm). In addition the amplitude in that peak was significantly reduced to 24.5% ± 15% (n=5) when compared to the DIV0 condition.

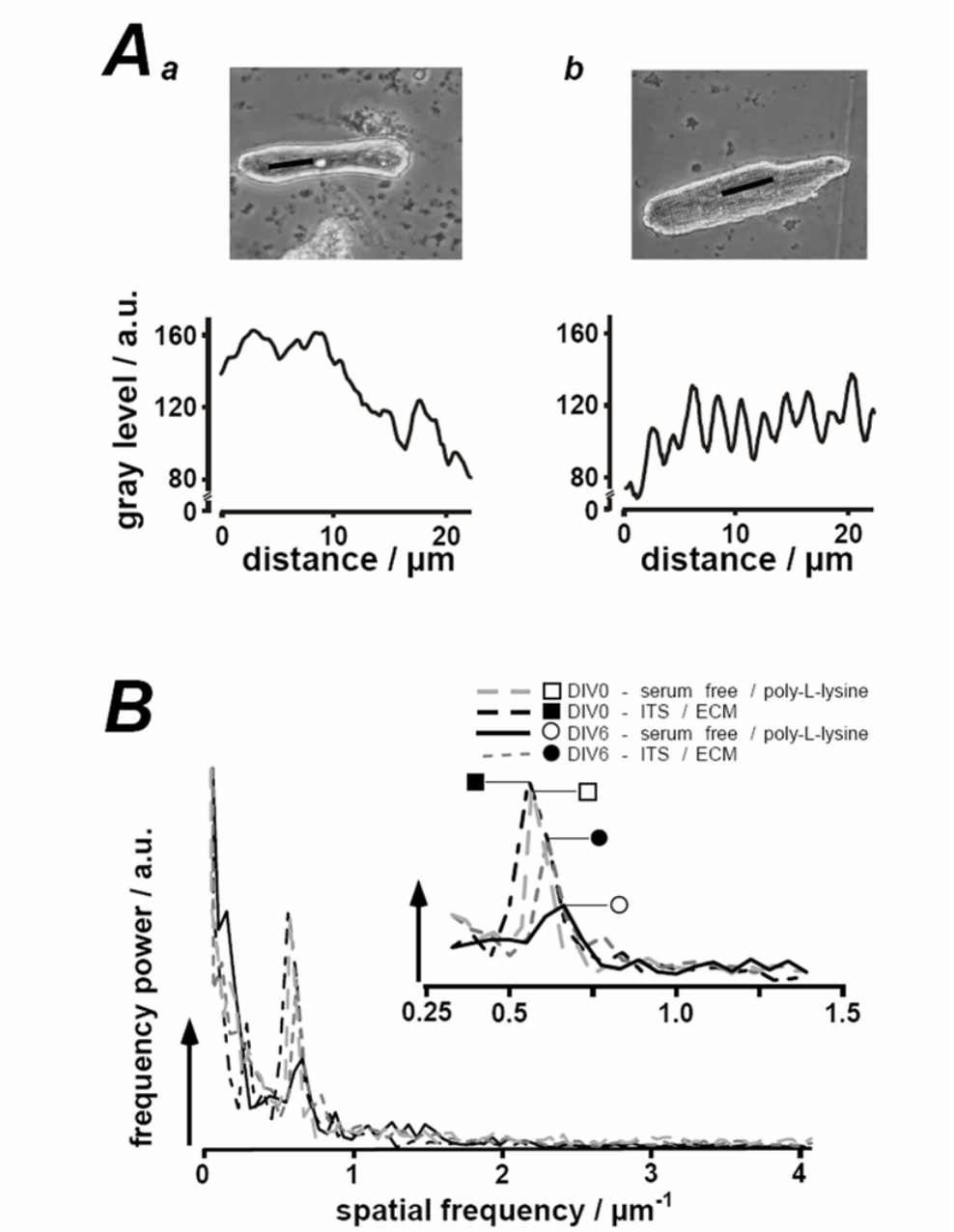


**Fig. 11. Analysis of cross-striation for cardiomyocytes in long-term culture.**
**Panels A-B compare rat ventricular myocytes at DIV0 and DIV6 under various culturing conditions. In order to quantify cross striation intensity profiles were recorded (panel A) of myocyte images taken with a regular phase-contrast transmission microscope along their longitudinal axis. The left image depicts a myocyte at DIV6 cultured in serum free medium on poly-L-lysine (Aa) whilst the right image represents a myocyte at DIV6 cultured in ITS supplemented medium on ECM (Ab). For B a powerspectral analysis of such line profiles were performed, taken from myocytes at DIV0 and DIV6. The inset illustrates a magnified view onto the power peak around spatial frequencies of 0.56 µm$^{-1}$. Symbols highlight the particular peak. Details for the construction of the powerspectra can be found in the Methods section. These results were typical for all cells analysed (n=9 at DIV0 and n=6 for each DIV6 condition; cells were taken from 3 rat hearts)**

After this initial analysis of the culture conditions I set out to comprehensively investigate the physiology of the cultured cells. For this I analysed the frequency dependence of their contractility and $Ca^{2+}$ transients during electrical pacing from DIV0 to DIV6 under various culture conditions.

## *1.4. Cell shortening-electrical stimulation frequency relationship*

Fig. 12A exemplifies the stimulation protocol used for the cell length and for the $Ca^{2+}$ measurements described below. Fig. 12B depicts the time course of cell length changes (0.5 Hz, pulse duration 5 ms) at DIV0. While the first contraction was strong, a typical progressive decay in the contraction amplitude could be observed, a phenomenon termed post-rest potentiation (Bers, 2001). In Figs. 12C&D traces are exemplified for two different culture conditions (left: no medium supplement on poly-L-lysine; right: ITS supplemented medium on ECM coating) at DIV1 (Fig. 12C) and DIV6 (Fig. 12D). While at DIV1 both cells displayed post-rest potentiation, the myocyte cultured without supplement showed a greatly diminished potentiation at DIV6 while the cell with ITS/ECM still revealed post-rest potentiation.

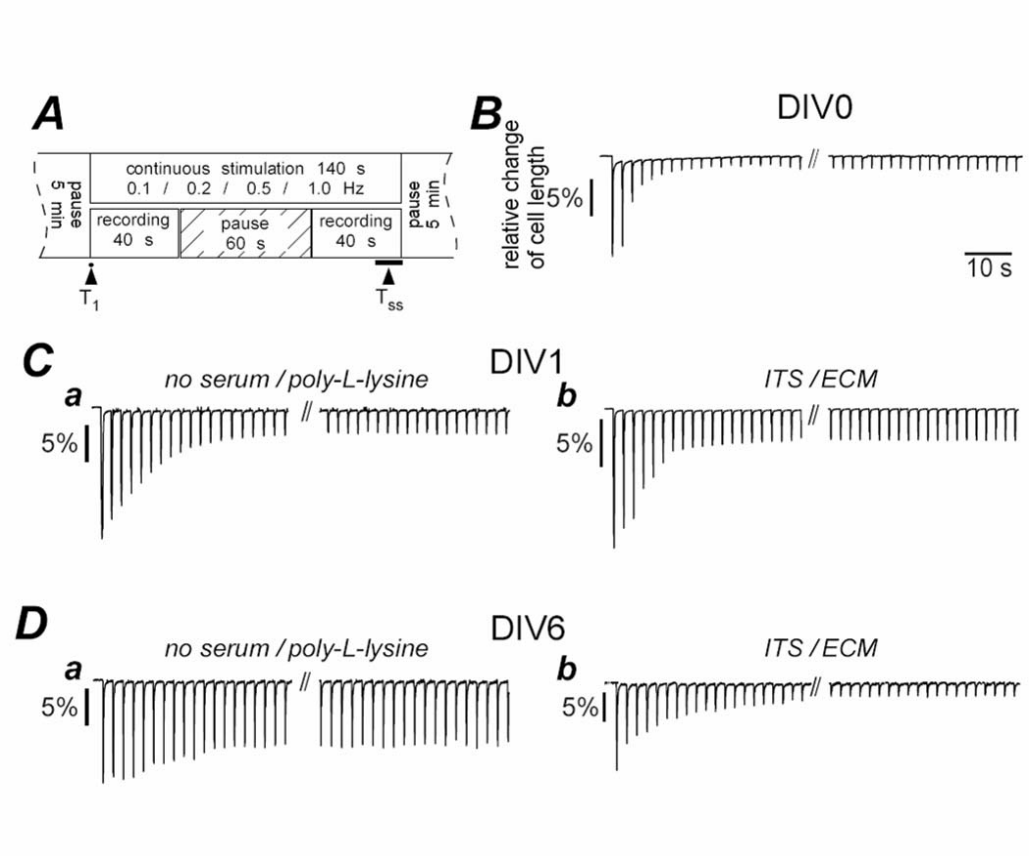


**Fig. 12. Representative traces of contraction-frequency relationship.**
**The stimulation protocol is depicted in panel A. Panel B illustrates the typical time course of cell length changes during such trains of stimulations at DIV (day *in vitro*) 0. In panels C and D cell length changes were plotted for cells at DIV1 (C) and DIV6 (D) that were cultured in serum free/poly-L-lysine (a) or ITS/ECM (b) conditions.**

It is noteworthy that the absolute maximal cell length changes decreased over time in the main from DIV3 onwards in all conditions tested (see Table 1). Most likely this reduction of the absolute amplitudes of cell shortening is attributable to an increase of the interaction between cells and substrates (see details in Discussion section).

***A***

| FCS | Not-pulsed | | | | Pulsed | | | |
|---|---|---|---|---|---|---|---|---|
| | 0.1 Hz | 0.2 Hz | 0.5 Hz | 1 Hz | 0.1 Hz | 0.2 Hz | 0.5 Hz | 1 Hz |
| DIV0 | **13,358** | **11,156** | **7,516** | **5,885** | | | | |
| | 1,351 | 2,330 | 1,180 | 1,177 | | | | |
| DIV1 | **13,851** | **10,409** | **11,026** | **8,956*** | **11,315** | **8,599** | **8,45** | **7,905*** |
| | 1,917 | 1,937 | 2,531 | 1,367 | 1,098 | 0,760 | 0,908 | 0,841 |
| DIV3 | **6,453*** | **5,919*** | **5,133*** | **4,850** | **6,750*** | **4,561*** | **2,879*** | **4,136*** |
| | 0,891 | 0,980 | 1,116 | 0,959 | 1,200 | 0,804 | 0,998 | 1,108 |
| DIV6 | **4,548*** | **3,744*** | **2,710*** | **3,306*** | **4,673*** | **2,947*** | **4,751*** | **4,179*** |
| | 0,933 | 0,840 | 0,467 | 0,925 | 1,953 | 0,647 | 1,799 | 1,321 |

***B***

| Serum free | Not-pulsed | | | | Pulsed | | | |
|---|---|---|---|---|---|---|---|---|
| | 0.1 Hz | 0.2 Hz | 0.5 Hz | 1 Hz | 0.1 Hz | 0.2 Hz | 0.5 Hz | 1 Hz |
| DIV0 | **14,757** | **10,793** | **9,438** | **8,945** | | | | |
| | 1,956 | 1,941 | 1,648 | 1,598 | | | | |
| DIV1 | **13,719** | **8,755** | **6,140*** | **6,246** | **11,430** | **5,283*** | **4,763*** | **5,094*** |
| | 1,101 | 1,296 | 0,935 | 1,137 | 1,454 | 0,951 | 1,126 | 0,930 |
| DIV3 | **7,518*** | **6,600*** | **6,676** | **6,618** | **3,899*** | **2,735*** | **2,439*** | **2,875*** |
| | 1,233 | 1,347 | 1,229 | 1,072 | 0,476 | 0,474 | 0,647 | 0,767 |
| DIV6 | **3,058*** | **2,463*** | **2,020*** | **3,082*** | **1,770*** | **1,971*** | **3,517*** | **3,655*** |
| | 0,644 | 0,4664 | 0,416 | 0,651 | 0,596 | 0,363 | 0,918 | 1,823 |

***C***

| ITS/poly-L-lysine | Not-pulsed | | | | Pulsed | | | |
|---|---|---|---|---|---|---|---|---|
| | 0.1 Hz | 0.2 Hz | 0.5 Hz | 1 Hz | 0.1 Hz | 0.2 Hz | 0.5 Hz | 1 Hz |
| DIV0 | **17,604** | **16,454** | **12,519** | **11,266** | | | | |
| | 1,484 | 1,540 | 1,099 | 1,135 | | | | |
| DIV1 | **16,102** | **12,638*** | **11,392** | **12,707** | **16,676** | **11,141*** | **10,589** | **11,691** |
| | 1,064 | 1,114 | 2,217 | 2,624 | 2,057 | 1,651 | 1,812 | 1,366 |
| DIV3 | **8,123*** | **8,085*** | **5,785*** | **8,047*** | **6,080*** | **3,775*** | **4,291*** | **5,720*** |
| | 2,030 | 2,051 | 1,106 | 1,487 | 0,789 | 0,581 | 1,612 | 1,746 |
| DIV6 | **4,190*** | **4,086*** | **3,913*** | **5,277*** | **2,502*** | **3,845*** | **3,030*** | **2,795*** |
| | 1,406 | 1,665 | 2,019 | 2,488 | 0,674 | 1,410 | 1,189 | 0,832 |

***D***

| ITS/ECM | Not-pulsed | | | | Pulsed | | | |
|---|---|---|---|---|---|---|---|---|
| | 0.1 Hz | 0.2 Hz | 0.5 Hz | 1 Hz | 0.1 Hz | 0.2 Hz | 0.5 Hz | 1 Hz |
| DIV0 | **15,002** | **9,397** | **6,463** | **5,827** | | | | |
| | 2,427 | 1,587 | 1,4667 | 1,200 | | | | |
| DIV1 | **11,375*** | **6,817*** | **5,222** | **6,072** | **12,248** | **6,472*** | **4,504** | **3,613*** |
| | 0,961 | 0,756 | 0,683 | 0,787 | 0,992 | 1,116 | 0,836 | 0,846 |
| DIV3 | **7,227*** | **5,034*** | **4,031*** | **3,426*** | **5,630*** | **5,908** | **4,789** | **4,414** |
| | 1,350 | 0,866 | 0,521 | 0,560 | 1,049 | 3,000 | 2,252 | 2,052 |
| DIV6 | **3,272*** | **2,117*** | **1,023*** | **0,741*** | **3,817*** | **1,865*** | **1,028*** | **0,759*** |
| | 0,541 | 0,534 | 0,180 | 0,164 | 1,001 | 0,167 | 0,253 | 0,328 |

**Table 1. Absolute cell length changes of pulsed and not-pulsed cardiomyocytes.**
**This table displays the absolute values of cell length changes measured in cardiac myocytes cultured under 4 different conditions: FCS/poly-L-lysine (A), serum free/poly-L-lysine (B), ITS/poly-L-lysine (C) and ITS/ECM (D). The myocytes were electrically challenged with different stimulation frequencies (0.1 – 1.0 Hz; random order, 5 ms duration). Mean (bold figures) and SEM (under each mean) values were calculated from data obtained with myocytes that had been continuous pulsed (0.2 Hz, 5 ms duration) or not-pulsed, n=3 to 11 cells (taken from between 2 and 6 rat hearts). Data with a significant difference in comparison to the value for the same stimulation frequency on DIV0 have been marked with an asterisk.**

In order to quantify the degree of post-rest potentiation I calculated the relative change of contractility by ratioing the twitch amplitude under steady-state conditions (last 5 peaks; $T_{SS}$) by the initial contraction amplitude ($T_1$) as depicted in Fig. 12A. Fig. 13 summarises the frequency dependence of that ratio and its relation to the culture conditions. I found that under serum free/poly-L-lysine, FCS/poly-L-lysine and ITS/poly-L-lysine conditions, the negative frequency dependence of the $T_{SS}/T_1$ ratio was lost between DIV3 and DIV6. In contrast, myocytes cultured in ITS-supplemented medium on ECM-coated substrates largely retained the negative frequency dependence (Figs. 13Ad, Bd, Cd, Dd for DIV6 data). I observed a particular dramatic change for cells cultured in FCS-supplemented medium. The negative frequency dependence turned into a positive relationship termed post-rest decay (Fig. 13Bd, closed symbols).

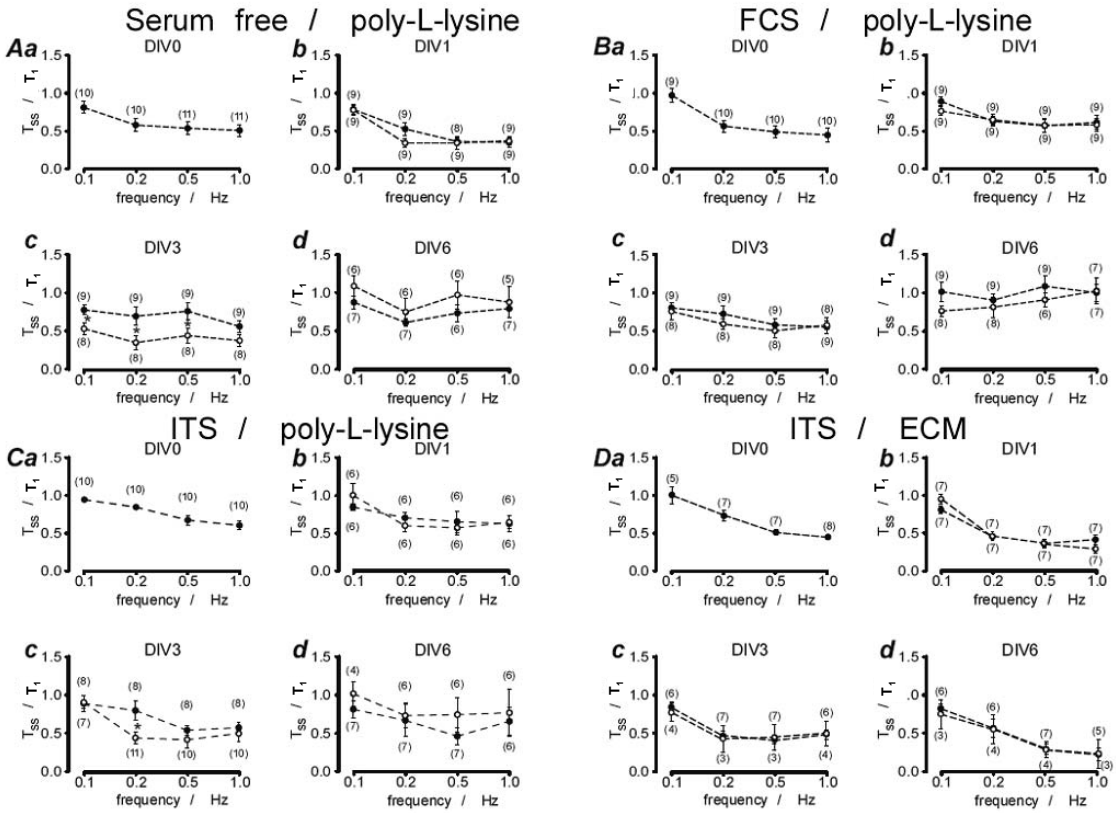


**Fig. 13. Summarised data of the shortening-frequency relationship.**
**For panels A-D populations of cells (taken from between 2 and 6 rat hearts) have been analysed and their post-rest behaviour has been quantified as $T_{ss}/T_1$ ratios (see fig. 2A and text for explanation). The ratio has been plotted against the stimulation frequencies (0.1 – 1.0 Hz; random order, 5 ms duration). Open and closed symbols represent data from myocytes that had been continuous pulsed (0.2 Hz, 5 ms duration) or not-pulsed, respectively. The numbers**

**adjacent to each point gives the number of myocytes observed. Data pairs with a significant difference have been marked with an asterisk.**

When I compared data from cells not stimulated during the culture period with those derived from pulsed cell populations (Fig. 13 open symbols) I found no major changes in the contractile behaviour of the myocytes regardless of their other culture conditions. Nevertheless, I observed a significant change at DIV3 at 0.2 Hz for cells cultured in ITS supplemented medium with a poly-L-lysine coating (Fig. 13Cc, marked with an asterisk), i. e. a 45% decrease of the $T_{SS}/T_1$ ratio in pulsed myocytes (non-pulsed cells, n=8; pulsed cells, n=11). Furthermore, significant differences between paced and non-paced cells were apparent for myocytes cultured under serum free/poly-L-lysine conditions for DIV3 (Fig. 13Ac). Nevertheless, the rather flat frequency dependency was still preserved during pacing.

From these data I concluded that the contractile behaviour at DIV0 was best preserved in a culture medium supplemented with ITS when cells were grown on ECM-coated substrates regardless of whether they were paced or not. In the following a similar series of experiments were conducted analysing global $Ca^{2+}$ transients with the $Ca^{2+}$ sensitive fluorescent probe fura-2.

## *1.5. $Ca^{2+}$ transient-electrical stimulation frequency relationship*

Figs. 14 and 15 summarise experiments performed under similar experimental conditions as for Figs. 12 and 13 using cells from the same preparations in order to be able to correlate the data with each other. Fig. 14A illustrates the method of fura-2 imaging that was used. Similar to the twitch data presented in Fig. 12A, the global $Ca^{2+}$ transients also displayed post-rest potentiation when measured in freshly isolated rat ventricular myocytes (Fig. 14B for DIV0). A comparison of the time course of the $Ca^{2+}$ transient amplitude was made under conditions of serum free medium and poly-L-lysine coating with the time course with ITS supplemented medium and ECM coating (Figs. 14C, D, a and b, respectively). As a result a loss of post-rest potentiation was also found only in the former condition while the ITS/ECM condition resulted in a conserved post-rest potentiation. At DIV6 in the absence of serum the initial post-rest potentiation even turned into a strong post-rest decay (Fig. 14Da).

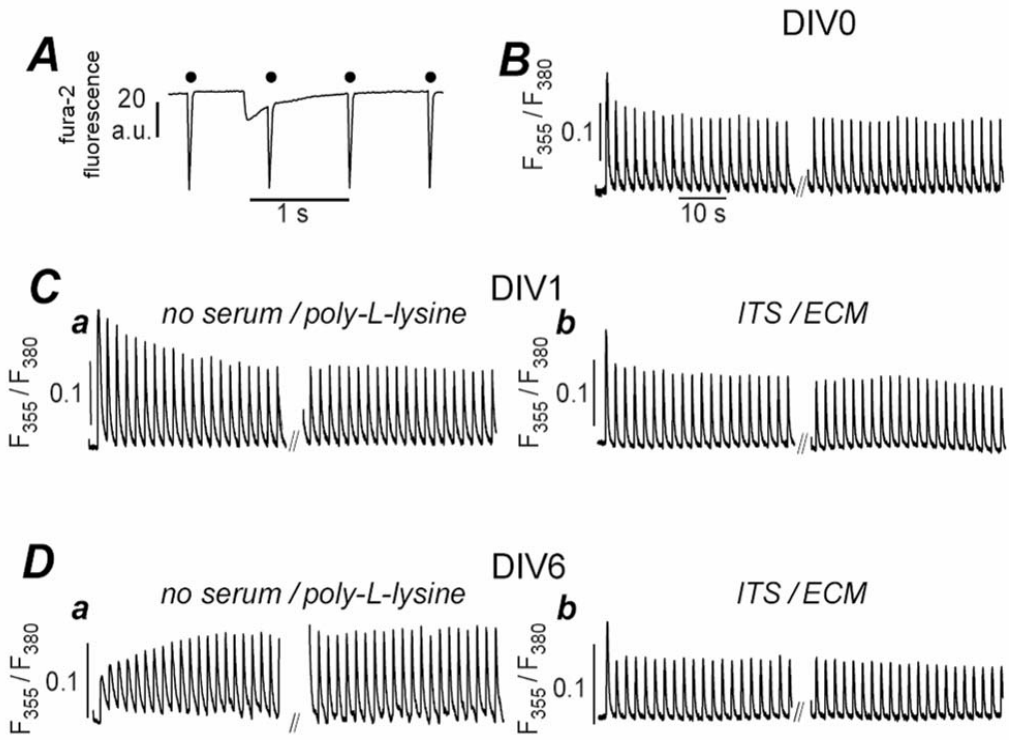


**Fig. 14. Representative traces of the fura-2 ratio transient-frequency relationship.**
**Panel A depicts the mode of recording the fura-2 fluorescence (downward deflections marked by a filled circle correspond to the 355 nm excitation images). The typical time course of ratio transients during such trains of stimulations at DIV0 is depicted in panel B. For the stimulation regime see figure 2A. In panels C and D fura-2 ratio transients were plotted for cells at DIV1 (C) and DIV6 (D) that were cultured in serum free/poly-L-lysine (a) or ITS/ECM (b) conditions.**

Since in almost 50% of all cells tested at DIV0 the $Ca^{2+}$ transients fused together (relaxation was not complete between the transients leading to a gradual diastolic build-up of the $Ca^{2+}$ concentration) when stimulation frequencies exceeded 0.5-0.7 Hz the 1 Hz data were omitted in the further analysis. All other conditions were similar to those described in Fig. 13. In contrast to the relationships of the twitch amplitude the height of the $Ca^{2+}$ transients only displayed a modest post-rest potentiation with basically flat frequency dependence at DIV0 (Fig. 15Aa). This flat amplitude-frequency relationship was preserved for all DIVs and for all culture conditions with the exception of a sole set of conditions. Here, the myocytes at DIV6 that were paced continuously in the absence of any medium supplement on poly-L-lysine displayed a dramatic shift from modest post-rest potentiation at 0.1 Hz to a significant post-rest decay at 0.5 Hz (open symbols in Fig. 15Ad). Similarly to the

results I obtained for the twitch measurements (Fig. 13) continuous pacing did not make any difference to the frequency relationships at any DIV nor under any culture conditions apart from the ITS/poly-L-lysine combination at DIV3 (Fig. 15Cc).

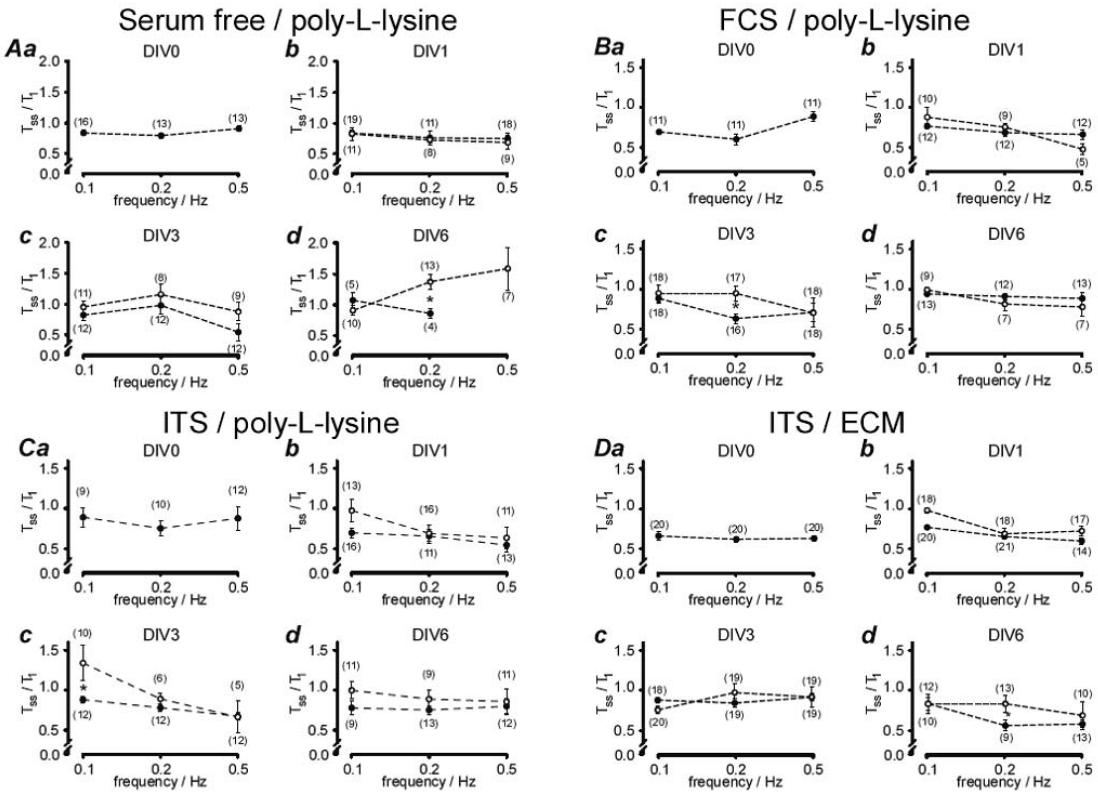


**Fig. 15. Summarised data of the fura-2 ratio transient-frequency relationship.**
**For panels A-D a population of cells (taken from 5 rat hearts) have been analysed and the amplitude ratios $T_{ss}/T_1$ have been plotted against the stimulation frequencies (0.1 – 0.5 Hz, random order, 5 ms duration) for various culture conditions as depicted in each panel. Open and closed symbols display mean values for the continuously pulsed and non-pulsed myocytes respectively (0.2 Hz, 5 ms pulse length). The numbers adjacent to each value give the number of myocytes. Data pairs with a significant difference have been marked with an asterisk.**

Thus, myocytes cultured in ITS-supplemented medium on ECM-coated substrates most closely retained their morphology, contractility and $Ca^{2+}$ handling when compared to DIV0.

I thus conducted the final series of experiments to investigate whether cardiomyocytes cultured under ITS/ECM conditions were a good system to perform long-term expression of exogenous proteins. From the fura-2 data I knew that under

my culture conditions, $Ca^{2+}$ handling was largely conserved through the one-week period of culturing. I thus tested expression of a genetically coded $Ca^{2+}$ indicator by adenoviral gene transfer (inverse pericam as originally described by Nagai and co-workers (Nagai *et al*., 2001)).

## *1.6. Inverse pericam expression and $Ca^{2+}$ measurements*

The freshly isolated ventricular myocytes were infected with the virus 1 h after plating and fluorescence could already be recorded within 24 hours. Typically experiments were started 18 hours after transfection. Already at that early stage, more than 95% of all viable myocytes displayed sufficient levels of fluorescence for recording $Ca^{2+}$-dependent fluorescence changes. Fig. 16A exemplifies such changes as recorded in response to electrical stimulations. In all cells analysed at DIV1 a maximal fluorescence change of 25% $\pm$ 3.1% (n=65) could be recorded. Since excitation of inverse pericams does not require the application of UV light it was possible to test and perform long-term recordings as depicted in Fig. 16B. An electrical stimulation regime was designed employing constant pulsing at 0.1 Hz and optical recording for 40 s periods separated by 6 min without light excitation. For the recordings in Fig. 16B this stimulation regime continued for a total of 90 min without a detectable loss in pericam self-ratio amplitude or signal quality. During the same time period the absolute inverse pericam fluorescence was decreased by less then 15%, most probably due to bleaching. In some experiments recordings lasted for more than 2 hours with a similar experimental regime without a noticeable decrease in signal quality.

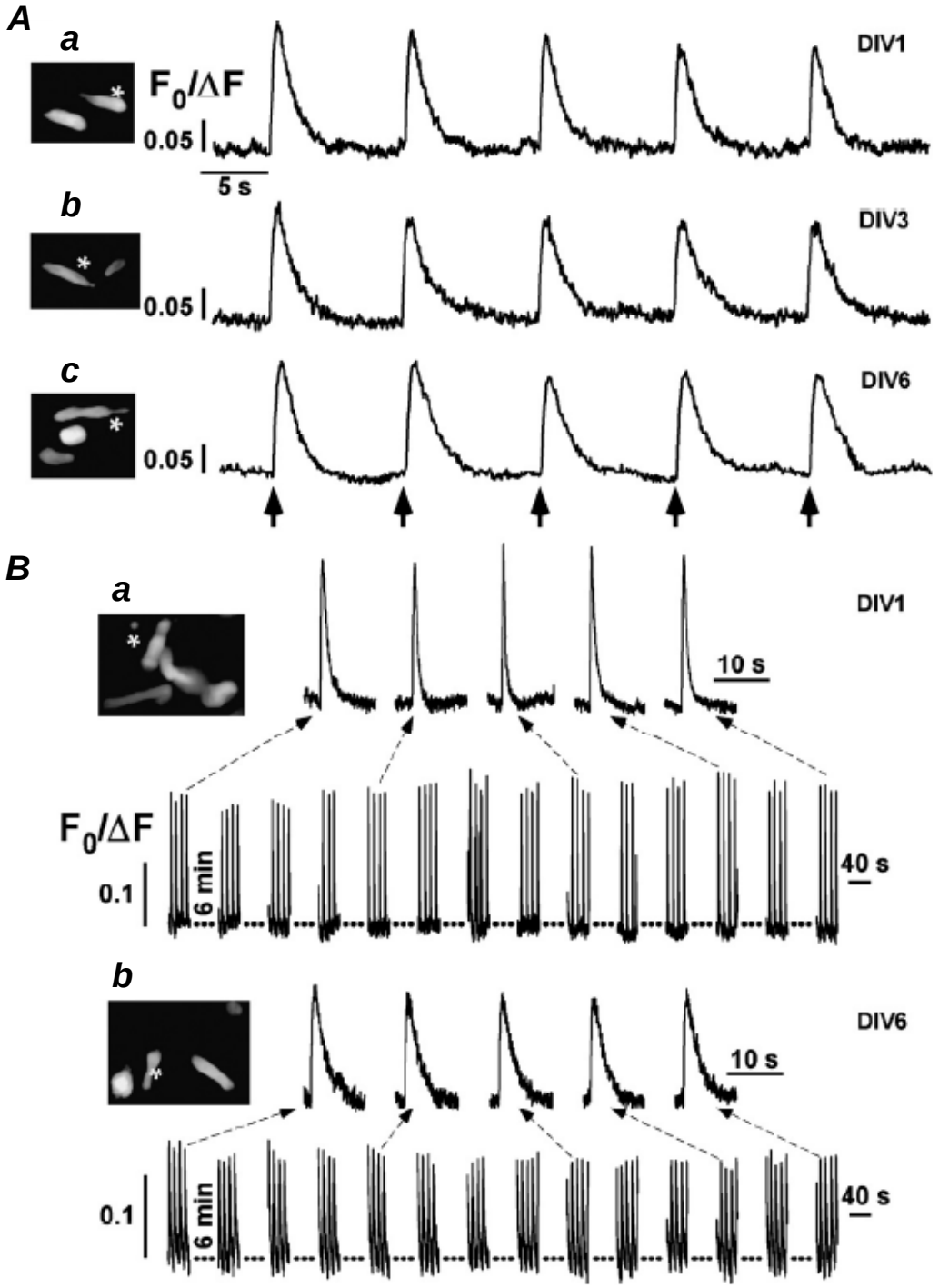


**Fig. 16. Inverse pericam fluorescence in cultured rat ventricular myocytes after adenoviral gene transfer.**

**Panel A depicts typical self-ratio traces of the inverse pericam fluorescence recorded from cultured myocytes at the time points given. Panel Ac illustrates the stimulation regime used (black arrows indicate electrical impulses, 5 ms duration). Cell images are added for each example and the cell used for calculation of the ratio traces has been marked with a white asterisk. Panel B shows ratio traces of adult ventricular myocytes 1 day (Ba) and 6 days (Bb) after virus infection. Dashed arrows depict recording periods for which exemplified individual ratio transients have been replotted. In the fluorescence images an asterisk marks the myocyte from which the ratio was calculated. Traces shown here were typical for all cells analysed under these experimental conditions (n>60 from 3 rat hearts).**

## *1.7. The loading state of internal $Ca^{2+}$ stores*

After studying the characteristics of important physiological properties over time i.e. cell length change and intracellular global $Ca^{2+}$ transients during electrical stimulation, I assessed the loading state of internal $Ca^{2+}$ stores with brief caffeine applications (10 mM, 5 s) directly onto the cells and after a 5 min resting period. As a potent agonist of the RyRs (Wang *et al*., 2003), caffeine causes the internal $Ca^{2+}$ stores to deplete. Similar approaches have been used numerously in many reports to assess the SR loading state (e.g. Díaz *et al.*, 2004). A typical caffeine response of fura-2 loaded cardiac myocytes (Fig. 17A) displayed three major phases: (i) a rapid upstroke, (ii) a partial recovery in the presence of caffeine and (iii) a final relaxation upon washout of the caffeine. After the enzymatic isolation, on DIV0 (Fig. 17B), the elevation of the fluorescence level due to caffeine was 20% (n=21 elongated cells) in comparison to the basal level and the absolute ratio change was reduced by 19% on DIV1 ($p<0.02$, n=36 elongated cells) in comparison to DIV0. The amplitude of caffeine responses were only 11% (n=28 elongated cells) of elevation of the fluorescence in comparison to the basal level after 3 days of culturing, 12% (n=24 elongated cells) after 6 days and 11% (n=10 elongated cells) after 8 days. Therefore, on DIV3 and 6, the reduced twitch amplitudes responses were accompanied by significantly decreased amplitudes of caffeine-induced $Ca^{2+}$ transients (Fig.17B): 42% decrease of the absolute ratio change on DIV3 (n=28; $p<0.001$) and 39% decrease on DIV6 (n=24; $p<0.001$). Decreased caffeine responses were maintained on DIV8 (n=10; $p<0.001$). Nevertheless no significant difference was found between DIV3, DIV6 and DIV8 in elongated myocytes.

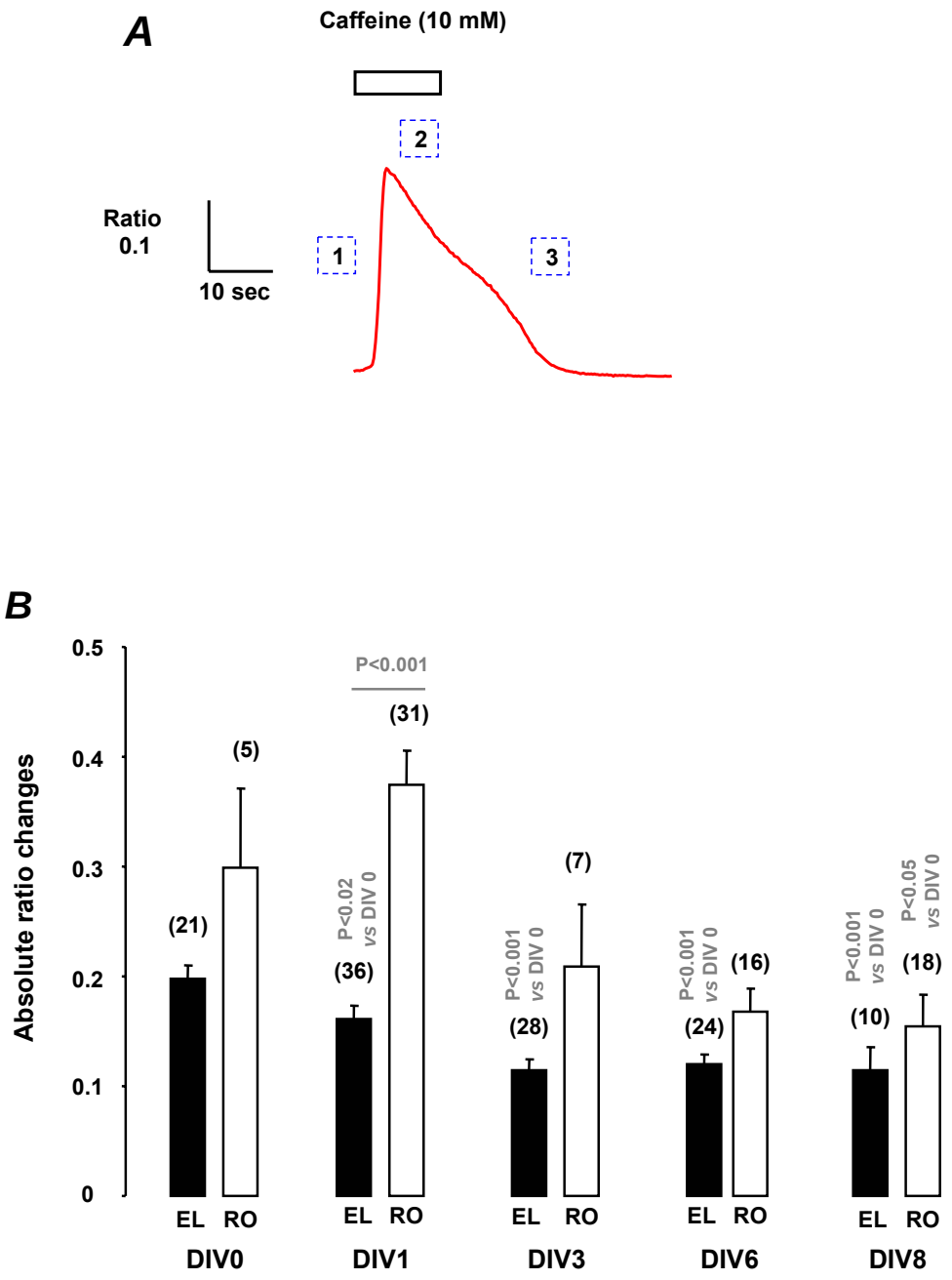


**Fig. 17. Assessment of the loading state of internal $Ca^{2+}$ stores in unstimulated cultured cardiac myocytes.**
**(A) The trace depicts an exemplified fura-2 ratio change response to the application of 10 mM caffeine with its three phases: (1) a rapid upstroke, (2) a partial recovery during caffeine application and (3) a final relaxation during the washout of caffeine.**
**(B) The histogram shows the responses to caffeine (10 mM, 5 s) expressed as absolute changes of the basal fura-2 ratio. Elongated (EL; black bars) and round cells (RO; white bars) were acutely challenged with caffeine over 8 days of culturing. The numbers adjacent to each value give the number of myocytes tested. Data with a significant difference in comparison to the value on DIV0, elongated and round myocytes respectively, or in comparison between EL and RO cells on the same day, have been marked with the corresponding "p" value. When no significant difference was found (either in comparison to the respective value on DIV0, or in comparison between EL and RO cells on the same day), no "p" value was stated. The data were taken from 2 to 5 rat hearts.**

Moreover, the round myocytes followed a similar but delayed pattern of responses with an elevation of the fluorescence level of 30% (n=5) under caffeine stimulation on DIV0 and decreased amplitudes of the responses over time: 15% of elevation of the fluorescence level in comparison to the basal level on DIV8 (49% decrease of the absolute ratio change in comparison to DIV0; n=18; $p<0.05$). It is noteworthy that there was one single significant difference between elongated and round cells at DIV1 ($p<0.001$, n=36 elongated cells and n=31 round cells) with round cells having a larger amplitude. Therefore, I considered that the pattern of responses for elongated and round cells were somewhat comparable in terms of behaviour over time but since these cells displayed differences, they could not be pooled and were regarded as two independent types of cardiac myocytes with reference to the loading state of the SR during culturing.

## *1.8. Spontaneous $Ca^{2+}$ waves*

In addition to the previous characterisation of responses to electrical stimulation and caffeine application in cultured cardiac myocytes, spatially resolved $Ca^{2+}$ imaging (realtime confocal microscopy) was undertaken at a maximal frame rate of 20 to 100 frames per second to describe the spatio-temporal features of spontaneous $Ca^{2+}$ release events. This study will further characterise the myocytes in culture in more detail. In cardiac myocytes spontaneous $Ca^{2+}$ transients can occur as (i) $Ca^{2+}$ waves that propagate through the entire cell as a “band” of elevated $Ca^{2+}$, (ii) homogeneous $Ca^{2+}$ increases induced by spontaneous APs (these are usually very rare) and (iii) spatially restricted $Ca^{2+}$ release signals, the $Ca^{2+}$ sparks.

Firstly I was interested in spontaneous $Ca^{2+}$ waves, which could be identified based on the $Ca^{2+}$ wavefront propagation. Furthermore they displayed different shapes (spirals, circular waves, propagating across the whole cell). In this study, I characterised the occurrence of $Ca^{2+}$ waves (wave frequency) rather than their properties (propagation velocity or steepness for instance).

As defined above (see Introduction section 2.3 and Results section 1.2), cultures of adult ventricular myocytes exhibit a fraction of myocytes that are round (that’s why they are called myoballs) and highly spontaneously active. Interestlingly round

myocytes displayed a 2-fold higher frequency of waves after the isolation ($p<0.05$; n=18 elongated cells and n=10 round cells at DIV 0), at DIV1 ($p<0.05$; n=11 elongated cells and n=5 round cells) and at DIV 3 ($p=0.002$; n=9 elongated cells and n=8 round cells), in comparison to elongated cells (Fig. 18).

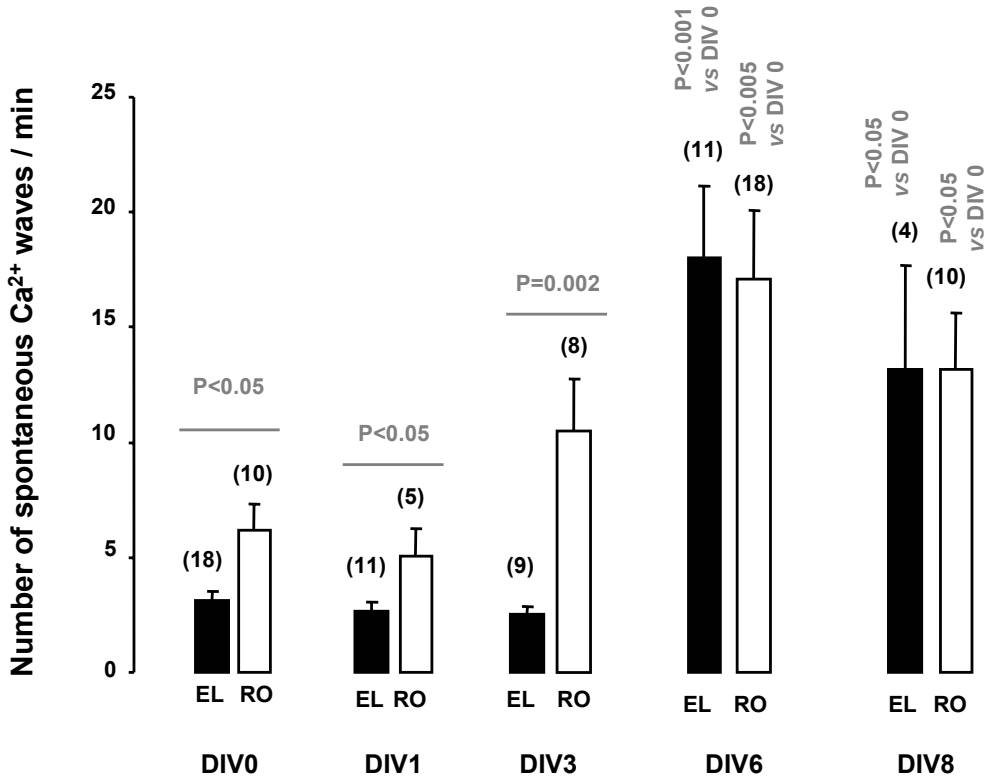


**Fig. 18. Spontaneous activity of cardiomyocytes in culture: analysis of the frequency of $Ca^{2+}$ waves.**
**The number of spontaneous $Ca^{2+}$ waves per cell in one minute was plotted against the different stages of culturing. Elongated (EL; black bars) and round cells (RO; white bars) were loaded with fluo-4 and changes of fluorescence were recorded with confocal microscopy. The numbers adjacent to each value give the number of myocytes tested. Data with a significant difference in comparison to the value on DIV 0 for each type of cells or in comparison between EL and RO cells on the same day have been marked with the corresponding "p" value. When no significant difference was found (either in comparison to the respective value on DIV 0, or in comparison between EL and RO cells on the same day), no "p" value was stated. The data were taken from 2 to 5 rat heart preparations.**

Surprisingly despite a lack of $Ca^{2+}$ increase in the internal stores (see Results section 1.7 and Fig. 17B), the frequency of spontaneous waves in elongated myocytes was dramatically augmented by 6-fold from DIV6 onwards ($p<0.001$; n=11 for DIV6, n=18 for DIV0). A similar obervation was made for round cells where I found a 3-fold

increase ($p<0.005$; n=18 for DIV6, n=10 for DIV0). This increase was maintained for both types of cells on DIV8 (Fig. 18).

These data seem to imply that despite similar levels of SR $Ca^{2+}$ load elongated cells and round cells displayed a vastly different rate of spontaneous $Ca^{2+}$ waves possibly indicating additional differences in the intracellular $Ca^{2+}$ homeostasis.

## *1.9. Spatially restricted $Ca^{2+}$ signals: sparks*

Spatially resolved $Ca^{2+}$ imaging (realtime confocal microscopy; $VT_{infinity}$, VisiTech, UK) was performed at a maximal frame rate of 20 to 100 frames per second to characterise the spatio-temporal features of spontaneous $Ca^{2+}$ sparks.

Indeed another way of assessing the $Ca^{2+}$ handling is to study the spatially restricted $Ca^{2+}$ transients, so-called $Ca^{2+}$ sparks. For this I chose elongated myocytes randomly and recorded the spontaneous activity in a single cell for 5 different days of culture. I performed 3 to 5 runs of 10 to 60s each for one single myocyte so that series of 500 to 1000 pictures over time were recorded per run. Each series of pictures over time was then converted into a pseudo linescan by the software "CaSparks" (see Methods section 7 and Fig. 8). Depending on the size of the cell, 3 to 5 pseudo linescans per run for one single cell were analysed by "CaSparks" (see Methods section 7 and Fig. 8). The software identified sparks and analysed the following parameters: amplitude, width and duration of the spark. A comparison between the results of the analysis and the observed sparks in the initial recording was undertaken in order to discard "false positives". I calculated mean values for each parameter and the number of sparks in one cell per minute was plotted (spark frequency). Eventhough the amplitude of caffeine-evoked $Ca^{2+}$ transients declined (see Results section 1.7) over the culturing time, no significant change was observed in terms of amplitude (Fig. 19A) and frequency (Fig. 19D) of local events. Though one can note a slight tendency to an increase of the frequency on DIV1, the diversity in the activity of the myocytes (reflected by the large SEM values) rendered the difference not significant. Noteworthy is that $E_m$ also selectively increased on DIV1 from -70 to -60 mV and then returned to its basal value from DIV3 onwards

(unpublished results; Dr. Martin Oberhofer, Institute for Molecular Cell Biology, Homburg / Saar, Germany).

Nevertheless, when I analysed the spatial spread of the $Ca^{2+}$ sparks I found a 24% ($p<0.001$, n=733 events taken from 11 cells out of 6 hearts), 33% ($p<0.001$, n=331 events taken from 8 cells out of 2 hearts), and 21% ($p<0.01$, n=68 events taken from 3 cells out of 3 hearts) increase in the spatial spread (Fig. 19B) on DIV1, DIV6 and DIV8 respectively in comparison to DIV0 (n=309 events, taken from 6 cells out of 3 hearts). The return to the basal values on DIV3 was probably due to the large decrease of the SR content at this stage (see Results section 1.7), which seemed to be compensated for on DIV6 and DIV8, since spark width augmented despite a lower SR content. Moreover also selectively on DIV1 the duration of the events (Fig. 19C) was significantly higher (+21%, $p<0.001$, n=309 and 773 events for DIV0 and 1 respectively). This shows an adaptation to the culture system that remained transitory probably due to the large decrease of SR content from DIV3 onwards.

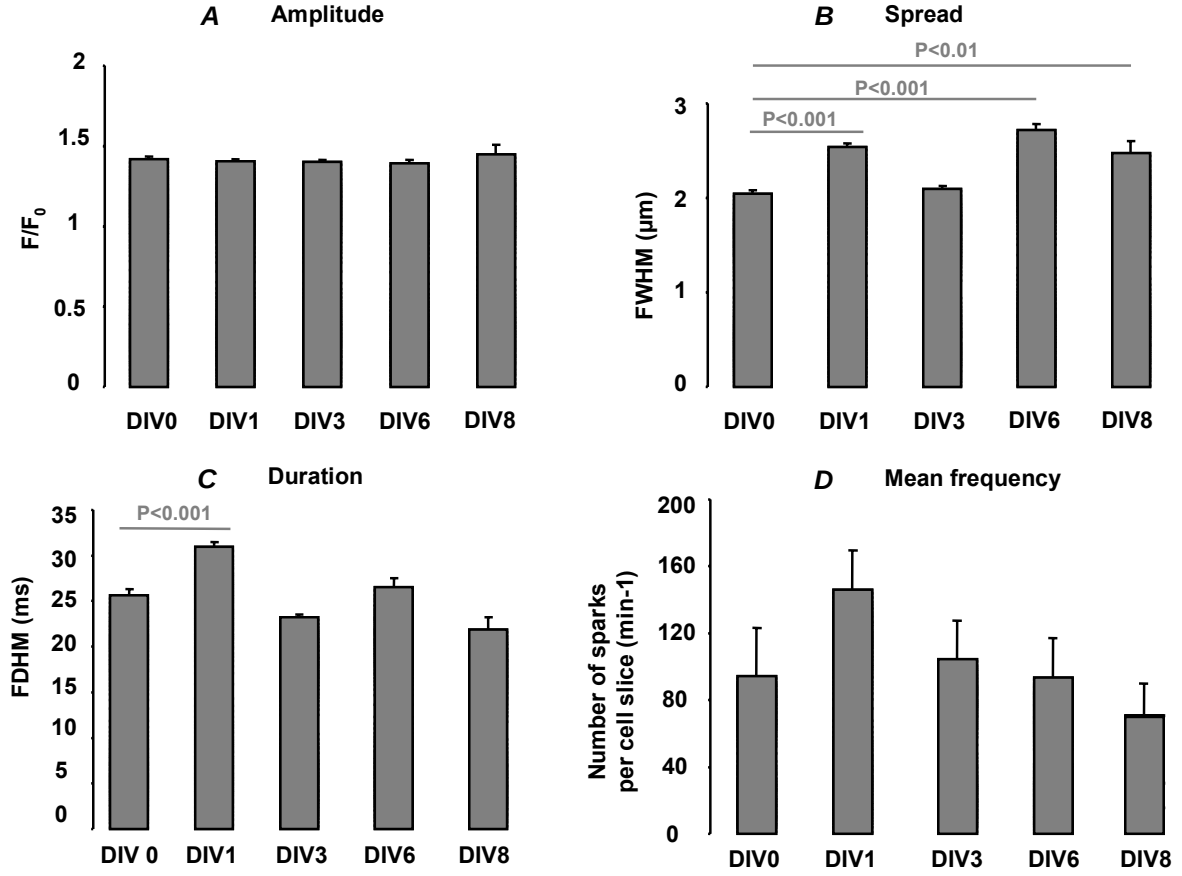


**Fig. 19. Spontaneous activity of cardiomyocytes in culture: analysis of $Ca^{2+}$ sparks.**
**The bar diagrams exhibits the study of four parameters ((A) amplitude of the changes of fluo-4 fluorescence, (B) spread of spark as full width at half maximum of the fluorescence peak,**

**(C) duration of spark as full duration at half maximum of the fluorescence peak and (D) averaged frequency of sparks for one cell confocal slice in one minute) describing the activity of spontaneous sparks over culturing time (DIV0, 1, 3, 6 and 8). Data with a significant difference in comparison to the value on DIV0 have been marked with the corresponding "p" value. The mean values were calculated from 309 sparks (6 cells out of 3 hearts) on DIV0, 733 sparks (11 cells out of 6 hearts) on DIV1, 505 sparks (10 cells out of 6 hearts) on DIV3, 331 sparks (8 cells out of 2 hearts) on DIV6, and 68 sparks (3 cells out of 3 hearts) on DIV8.**

Furthermore, I investigated the subcellular distribution of the active $Ca^{2+}$ spark sites by constructing histograms for the distance between spark site and the closest cell edge. Figure 20 summarises that analysis. In order to compensate for individual differences in cell width I normalised the spark position with the individual cell width. The black circles mark the distribution of active spark sites at DIV0. Surprisingly I did not find a homogeneous distribution but instead a broad band of occurrence with a significant gathering of active sites at around $1/5^{th}$ of the cell width. Interestingly, after an initial broadening at DIV1 and DIV3 (blue triangles and green squares, respectively), cells at DIV6 displayed a very sharp peak occurrence at around $1/10^{th}$ of the cell width (red diamonds). For each distribution analysis I characterised more than 200 active spark sites from 15 to 24 cells (3 to 6 hearts). This alteration of the site distribution was not due to systematic changes in the cell width. While from DIV0 to DIV6 the cell length and cell area progressively decrased by approximatively 17% ($p=0.001$, n=15 myocytes) and 38% ($p<0.001$, n=18 myocytes) on DIV6 respectively in comparison to DIV 0 (n=50 cells for mean length and 18 cells for mean area), the cell width remained stable over the same time period (see Table 2).

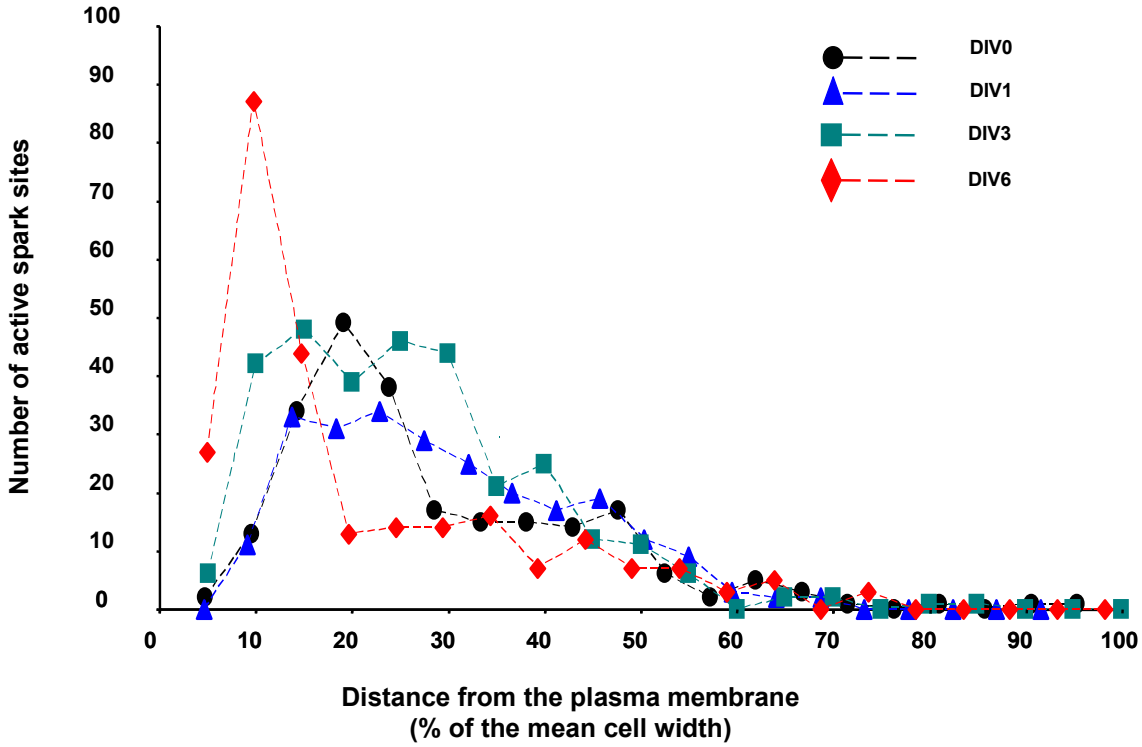


**Figure 20. Spontaneous activity of cardiomyocytes in culture: spatial distribution of active $Ca^{2+}$ spark sites.**
**The distance between active spark sites and the respective closest plasma membrane was measured and the ratio distance over averaged width of the cell for each day of culture was plotted to show the evolution of the repartition of the majority of the sites over culturing time. The spark data were obtained from 234 to 306 events (15 to 24 cells out of 3 to 6 heart preparations). Black circles, blue triangles, green squares and red lozenges represent myocytes at DIV0, 1, 3 and 6 respectively.**

| DIVs | Cell size (µm) | Cell area (%) | Cell width (%) |
|---|---|---|---|
| 0 | 125,550 ± 2,817<br>*n=50* | 100 ± 5,852<br>*n=18* | 100 ± 5,555<br>*n=15* |
| 1 | 117,125 ± 4,451<br>*n=20* | 86,301 ± 6,127<br>*n=17* | 104,146 ± 7,162<br>*n=18* |
| 3 | 121,25 ± 4,255<br>*n=20* | 93,753 ± 6,382<br>*n=18* | 95,411 ± 4,636<br>*n=24* |
| 6 | 104,000 ± 6,870*<br>*n=15* | 61,791 ± 3,968*<br>*n=18* | 97,087 ± 4,160<br>*n=17* |

**Table 2. Evaluation of cell size, cell area and cell width for cardiomyocytes in long-term culture.**
**I measured the longitudinal length, the cell area and the width of elongated cardiac myocytes cultured with ITS supplemented medium and a coating of ECM proteins. Investigations were**

**carried out on DIVs 0, 1, 3 and 6. Data with a significant difference in comparison to the value on DIV0 have been marked with an asterisk. The sample size (myocytes measured) is directly given in the table. The averaged values were obtained from 2 to 6 heart preparations.**

Hence, together with a preserved general myocyte morphology and physiology, $Ca^{2+}$ sparks displayed a dynamic profile in long-term culture in terms of size of the RyR cluster involved, duration and distribution over the cell. We propose that these changes accompany the adaptation of the SR content to the culturing system over time.

# 2. Induction of cardiac remodelling in long-term cultured adult rat cardiomyocytes

The aim of this study was to investigate the possible responses of isolated cardiac myocytes in culture when chronically challenged with hormones acting through the $G_q$-coupled signalling pathway, such as ET-1 and PE. A plethora of works has reported that the chronic application of these hormones to neonatal cardiac myocytes induces hypertrophic responses (O'Donnell *et al.*, 2001; Kawaguchi-Manabe *et al.*, 2007). For this chapter I aimed to investigate the action of these hormones on adult rat ventricular myocytes.

## *2.1. Chronic $G_q$-coupled receptor stimulation: morphological study*

After enzymatic isolation of the myocytes with Liberase (see Methods section 1) the yield of living cells was usually >90% with 81% elongated and 19% round cells (n=5 heart preparations). After 3 days in culture, 62% of the living cells were elongated and 38% round (n=4 heart preparations). Even over one week of culturing (DIV6-8), the percentage of rod-shaped cells was still >42% while the rate of round cells was <58% (n=3 heart preparations). This baseline behaviour changed significantly in the chronic presence of 100 µM of PE. Here the proportion of round cells at DIV3 was already exceeding 50%. At DIV6-8 the cell population lacked any elongated cells; they were either of the round type (60%) or already displayed massive dedifferentiation with the adoption of a flattened "fried egg" morphology (40%) and numerous lamellipodia-like extensions (Fig. 21, rightmost central images). Under visual inspection spontaneous beatings were found for the flattened cells. In myocyte populations chronically stimulated with 100 nM ET-1 (Fig. 21, lowest row of images),

the cell responses with respect to their morphology was somewhat in between the control and the PE stimulation. Even at DIV8 more than 20% of all cells were of an elongated morphology. It is noteworthy that 10 µM of PE was also tested and gave similar results then the 100 µM but with a delayed onset of 72 hours. Despite significant effects of the hormonal stimulation on the cell morphology (see Fig. 21), the survival rate (measured as cell density over culturing time) was unaffected by the hormonal challenges.

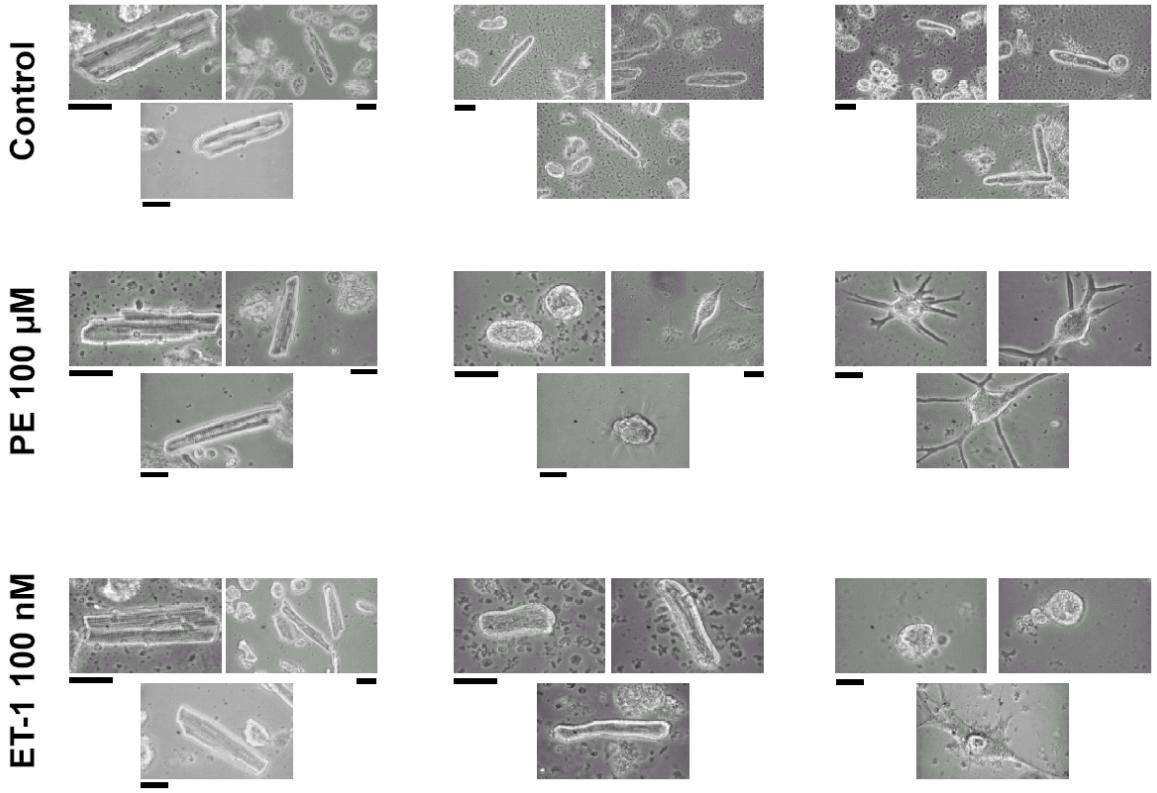


**Fig. 21. Morphological properties of cardiomyocytes after long-term treatment with neurohormones.**
**This panel depicts transmission images of typical adult rat ventricular myocytes (ITS/ECM conditions) under chronic stimulation with PE (100 µM) or ET-1 (100 nM) on DIV0, 3 and 8. The black rectangle below each picture or assigned to a group of 3 pictures indicates the scale bar (= 40 µm).**

Thus, both hormones induced cardiac myocyte remodelling in the cell culture model but with largely different time courses and extents. In the following I thought of investigating changes of the $Ca^{2+}$ homeostasis in myocyte populations chronically treated with such hormones.

## 2.2. Electrical pacing-induced $Ca^{2+}$ transients in hormone-stimulated myocytes

The myocytes treated with the hormones were probed with trains of electrical stimulations similar to the approach described in section 1.5. The post-rest behaviour of the cells was studied at a stimulation frequency of 0.5 Hz, which was the highest that still allowed reliable recordings of fura-2 ratio in long-term cultured myocytes (see paragraph 1.5). Figure 22 summarises the findings of this series of experiments. For this I plotted the amplitude ratio $T_{ss}/T_1$ (i.e. steady-state amplitude over the amplitude of the first $Ca^{2+}$ transient) for 5 different days in culture in the presence of PE (red bars), ET-1 (blue bars) or under control conditions (black bars). Neither PE (100 µM) nor ET-1 (100 nM) significantly changed the mean value of this ratio in comparison to control cells (Fig. 22). From this it became apparent that the myocytes were able to preserve their post-rest behaviour under all challenges applied. In an attempt to further characterise possible changes in $Ca^{2+}$ handling that might have been missed by simply analysing transient amplitudes and/or post-rest behaviour, I characterised electrically-evoked $Ca^{2+}$ transients in greater depth, i.e. the decay time constant. For this the relaxation phases of the $Ca^{2+}$ transients were fitted with mono-exponential time courses and the decay time constant was derived from such fits. Figure 23 shows the results of such an analysis with the same colour coding as for Fig. 22. Interestingly, under control conditions (black bars) the time constant displayed a sudden and significant increase (from around 500 ms at DIV0 to approximatively 1000 ms at DIV3) that reverses back to its initial value at DIV8. Surprisingly, both hormonal stimulation, ET-1 and PE, seemed to partially (PE, red bars), or totally (ET-1, blue bars), suppress that increase in the decay time constant. Thus, under control conditions, culture-evoked remodelling of the $Ca^{2+}$ homeostasis in the rat myocytes occurs but this remodelling could be compensated for by chronic stimulation of the myocytes with ET-1 and PE.

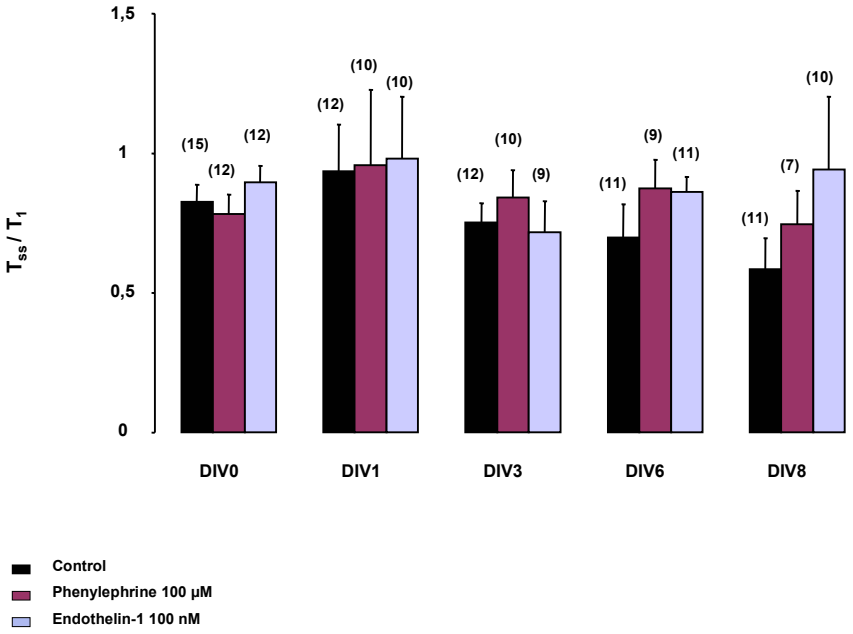


**Fig. 22. Post-rest potentiation of $Ca^{2+}$ transients in hormone-stimulated myocytes.**
**Trains of stimulations were electrically (0.5 Hz, 4-15 V according to the age of the cells in culture, 5 ms pulse) induced after rest (5 min) in myocytes cultured in ITS/ECM conditions supplemented with the neurohormones PE (100 µM, red bars) and ET-1 (100 nM, blue bars), or not (black bars). The resulting fura-2 ratio transients were analysed as amplitude ratios $T_{ss}/T_1$ that were plotted against the culturing time (from DIV0 up to DIV8). The numbers adjacent to each value give the number of myocytes. Data pairs without a "p" value indicate no significant difference. The data were taken from 2 to 3 rat heart preparations.**

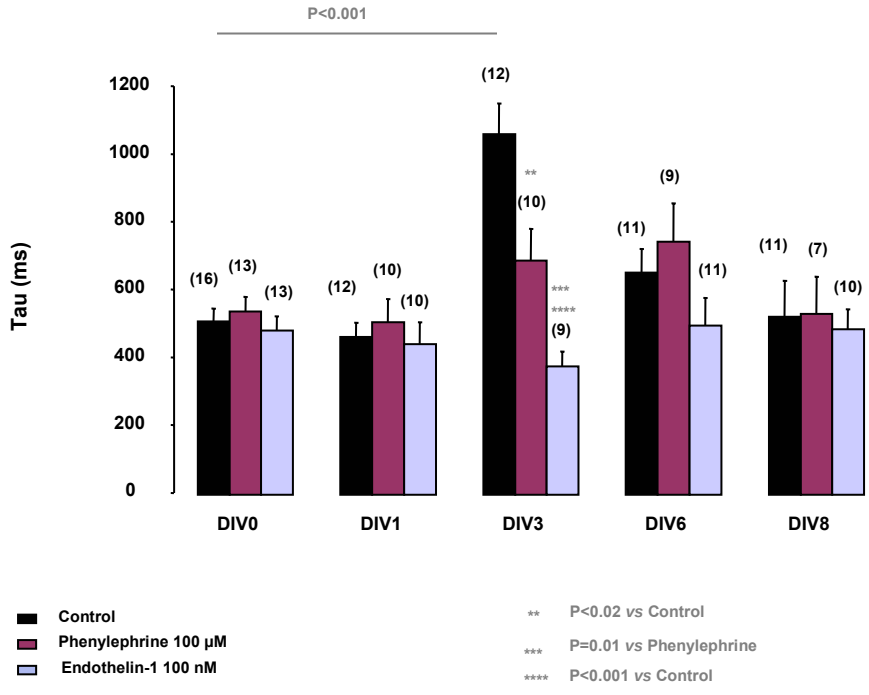


**Fig. 23. Kinetic of $Ca^{2+}$ transients in hormone-stimulated myocytes.**
**The ratios of the electrical stimulation-induced fura-2 transients were analysed with an exponential fitting in order to determine the "tau" values of the decay phases. Trains of**

**stimulations were electrically (0.5 Hz, 4-15 V according to the age of the cells in culture, 5 ms pulse) induced after rest (5 min) in myocytes cultured in ITS/ECM conditions supplemented with the neurohormones PE (100 µM, red bars) and ET-1 (100 nM, blue bars), or not (black bars). Data pairs with a significant difference have been marked with a "p" value. The data were taken from 2 to 3 rat heart preparations.**

To better understand the relationship between electrical stimulation and $Ca^{2+}$ transients in hormone-treated myocytes I studied responses of the myocytes to acute electrical stimulation. For this I selected and plotted six representative time courses of fura-2 transients in Figure 24. The topmost traces represent cells treated with PE and while the first one displayed a behaviour of post-rest potentiation (Fig. 24Aa), the second one (Fig. 24Ab) exhibited a post-rest decay (note that the cell failed to return to the baseline after the first transient and that the amplitude of the following transients increased). In Fig. 24B the ET-1 cell failed to return to the baseline for 25 s and extra $Ca^{2+}$ transients (marked with a red arrowhead) occurred during this phase. The PE myocyte in Fig. 24C displayed a higher rate of fura-2 transients, together with an increase of the basal level of intracellular $Ca^{2+}$. The ET-1 cell in Fig. 24D did not react to the first electrical pulse (note the absence of transients for 5 s after the start of the stimulation marked with an orange arrowhead) and did not show regular peaks at 0.5 Hz, or peaks in phase with electrical pulses. This myocyte seemed to spontaneously release $Ca^{2+}$ independently of the train of stimulation. Figure 24E shows a PE cell trying to follow the imposed frequency of stimulation but in vain. Though the peaks were in phase with the electrical pulses, the myocyte did not manage to reach the frequency of 0.5 Hz and the amplitude of the $Ca^{2+}$ transients remained heterogeneous.

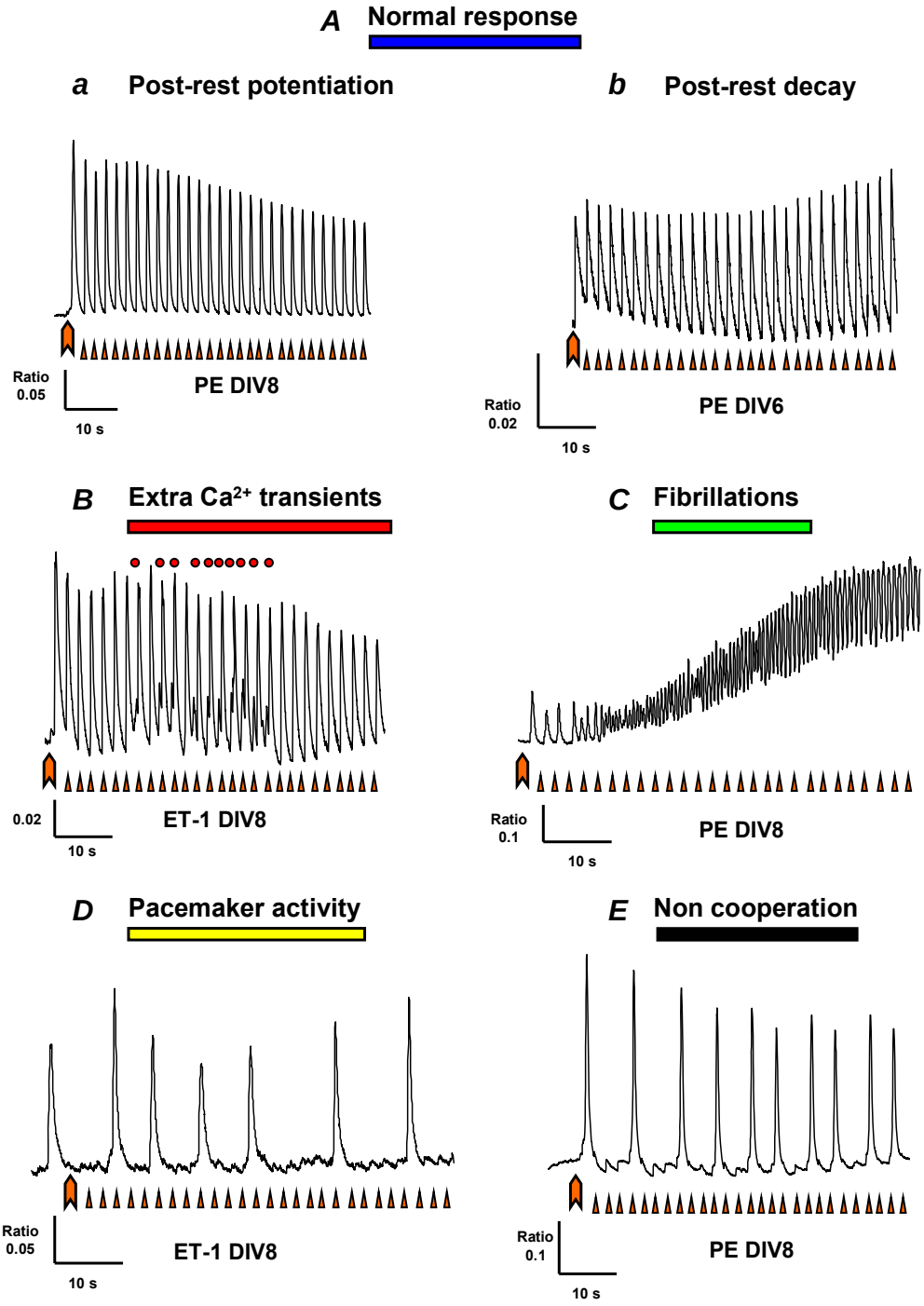


**Fig. 24. Exemplified traces of the response to a train of electrical stimulation.**
**Six representative time courses of fura-2 transients were plotted to show the different types of response to a train of electrical stimulation (0.5 Hz, 60 s) in 6 different PE or ET-1 chronically treated myocytes at DIVs 6 and 8. The large orange arrowhead indicates the start of the electrical stimulation, while the small orange arrowheads show the series of impulses. Panel Aa depicts a "normal" behaviour of post-rest potentiation, whereas panel Ab exhibits a post-rest decay. In panel B the cell displayed a phase of occurrence of extra $Ca^{2+}$ transients (marked with red circles). The myocyte in panel C was a typical example of cellular "fibrillations". The cell in panel D spontaneously released $Ca^{2+}$ independently of the train of stimulation; this phenomenon referred to as "pacemaker" activity. Panel E shows a cell trying in vain to follow the imposed frequency of stimulation (non cooperation). The same colour coding will be used in Fig. 25.**

Five categories of responses were thus determined: (i) “normal” responses (post-rest decay and post-rest potentiation), (ii) occurence of extra $Ca^{2+}$ transients (at least 2 per run of 60 s), (iii) cellular “pacemaker” activity defined as the presence of independent spontaneous global $Ca^{2+}$ rises, (iv) cellular “fibrillations” defined as $Ca^{2+}$ signals with high frequency that fuse (Mackenzie *et al.*, 2002), and (v) myocytes not following the imposed frequency of stimulation whatever the voltage applied.

Summarised data expressed as percentages were plotted in Fig. 25 where the same colour coding as Fig. 24 was used. From this I concluded that more myocytes displayed extra $Ca^{2+}$ transients, “pacemaker” activity and cellular “fibrillations” when chronically stimulated with PE and ET-1 in comparison to unstimulated myocytes from DIV3 onwards (Fig. 25). Moreover the number of cells exhibiting post-rest decay (Fig. 24Ab), defined as the first transient after rest being smaller in amplitude in comparison to the steady-state (Bers, 2001), was increased in hormone-stimulated cells when I pooled the different stages: 23% of control cells presenting post-rest decay (out of 62 control myocytes with “normal” responses), 31% for PE cells (out of 49 PE-stimulated myocytes with “normal” responses) and 28% for ET-1 cells (out of 53 ET-1-treated myocytes with “normal” responses).

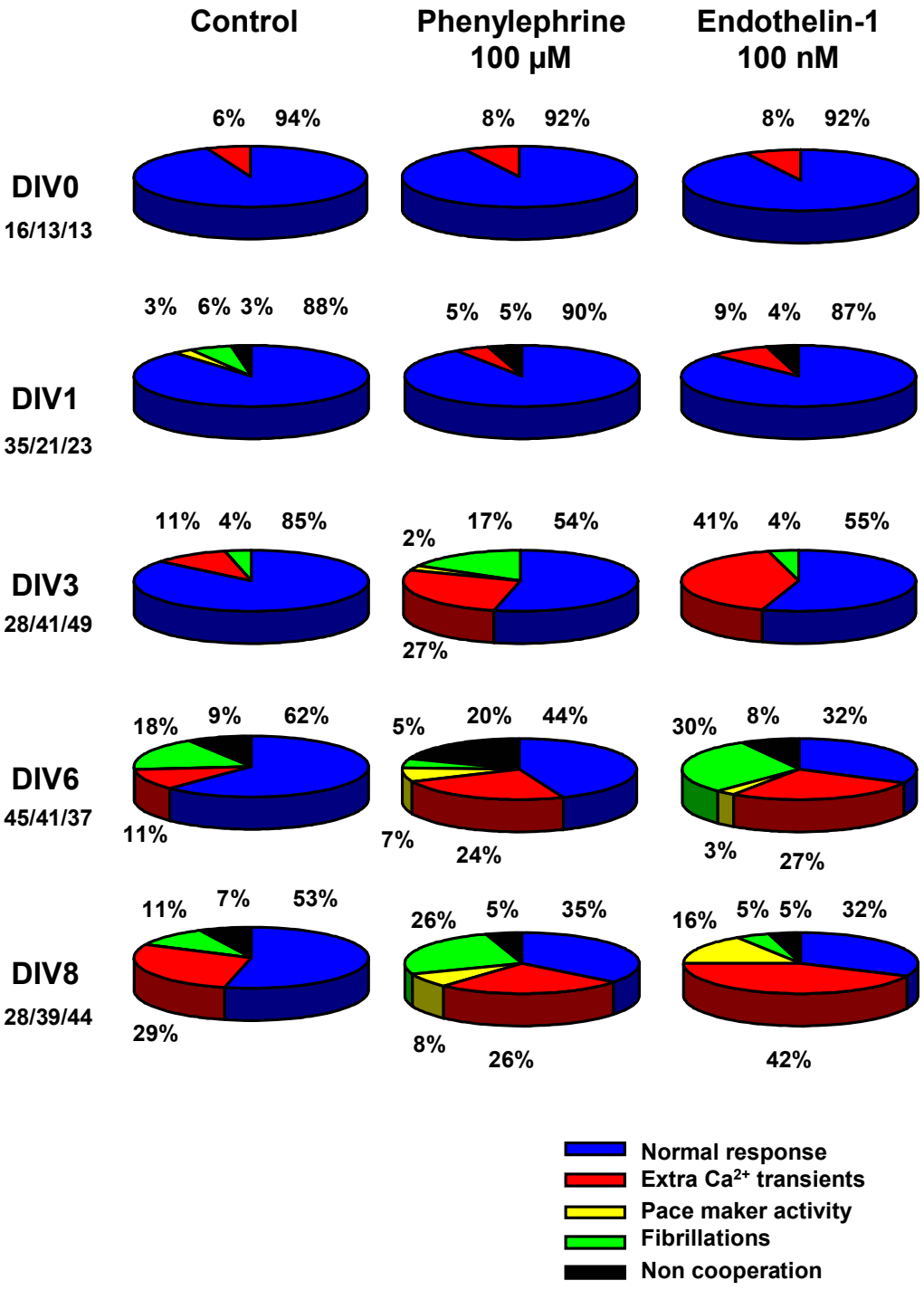


**Fig. 25. Types of responses to a train of electrical stimulation.**
**The protocol of electrical stimulation described in Figs. 22&23 was carried out and different categories of responses were identified: standard and regular fura-2 transients (in blue), presence of extra $Ca^{2+}$ transients (in red), independent spontaneous global $Ca^{2+}$ increases (in yellow), cellular "fibrillations" determined as $Ca^{2+}$ transients with high frequency and $Ca^{2+}$ signals fusing together (in green), and cells not following the imposed frequency of stimulation (in black). The numbers adjacent to the culturing stages indicate the number of cells tested for each condition: control myocytes, PE and ET-1-stimulated cells. The data were taken from 2 to 6 rat heart preparations.**

In spite of more conserved kinetics of the $Ca^{2+}$ transients in hormone-treated myocytes, it seemed that the chronically stimulated cells also exhibited more spontaneous activity than control cells during electrical stimulation, which might be an indication for a remodelling of $Ca^{2+}$ handling.

## *2.3. The loading state of internal $Ca^{2+}$ stores during chronic neurohormonal stimulation*

To investigate the activity of the SR and to estimate its content under long-term hormonal challenge, I performed brief caffeine applications (10 mM, 5 s) on ventricular myocytes as described above (see Results section 1.7). Only elongated cells were measured from DIV0 to DIV3, since elongated and round cells displayed different caffeine responses and spontaneous events in control conditions (see 1.7 and 1.8). Indeed, it seemed to me rather problematic to interpret the action of hormonal substances on round cells that exhibited an altered $Ca^{2+}$ handling from DIV0 to DIV3 in comparison to preserved elongated myocytes. Afterwards, the different types of cells were pooled: elongated, round and dedifferentiated myocytes. At DIV3, dedifferentiated and round cells were taken into account in PE conditions since they were predominantly present (see 2.1). Interestingly, the chronic stimulation with PE (red bars in Fig. 26B) led to the maintenance of caffeine responses with conserved amplitudes of 0.23 to 0.29 of fluorescence change from DIV1 to DIV8 (n=8 to 20 cells). Moreover caffeine responses increased on DIV3 and DIV6 in comparison to DIV0 ($p<0.01$ and $p<0.02$ respectively, n=8 cells on both stages). Hence, caffeine responses were significantly higher in PE cells in comparison to elongated control cells on DIV8 ($p=0.002$, n=20 PE cells and n=10 control cells, see Fig. 17B). I obtained similar results with the ET-1 (blue bars in Fig. 26B) treatment on DIV6 and DIV8. However, ET-1 myocytes firstly exhibited smaller amplitudes on DIV3 in comparison to DIV0 ($p<0.001$, n=10 cells) and in comparison to PE cells at the same stage ($p<0.001$, n=8 PE cells and n=10 ET-1 cells), which was very comparable to what was observed in control cells on the same stage.

**A**

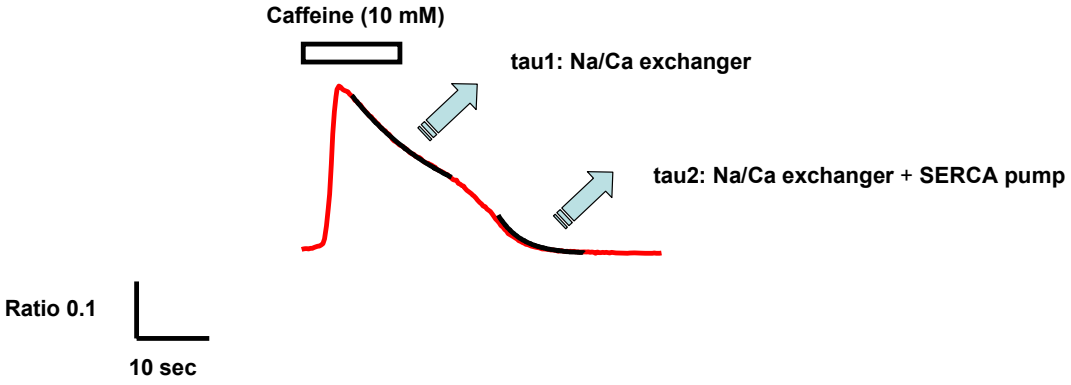


$$f(x) = y0+A*\exp(-(x-x0)/tau)$$

**B**

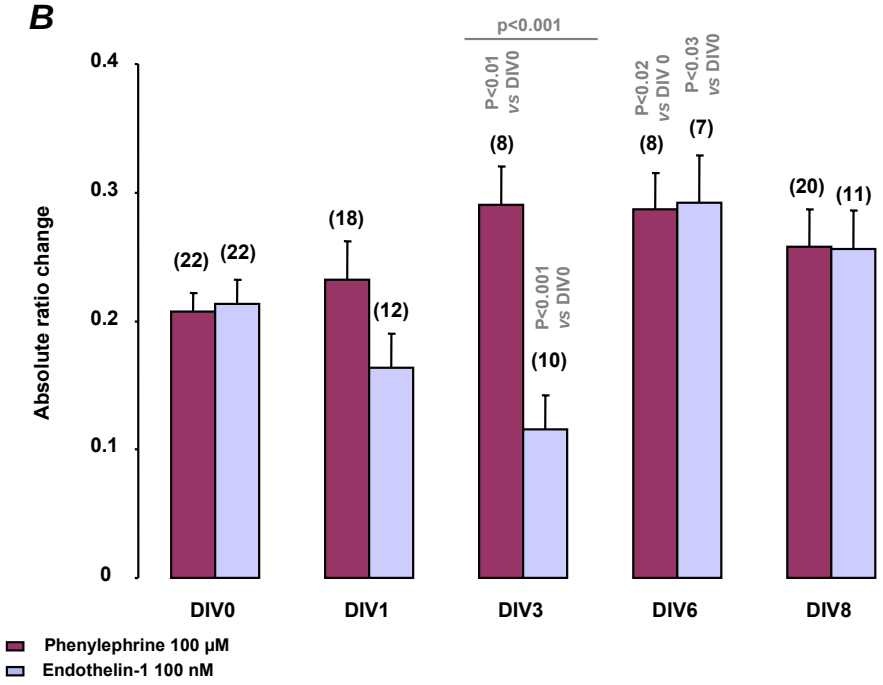

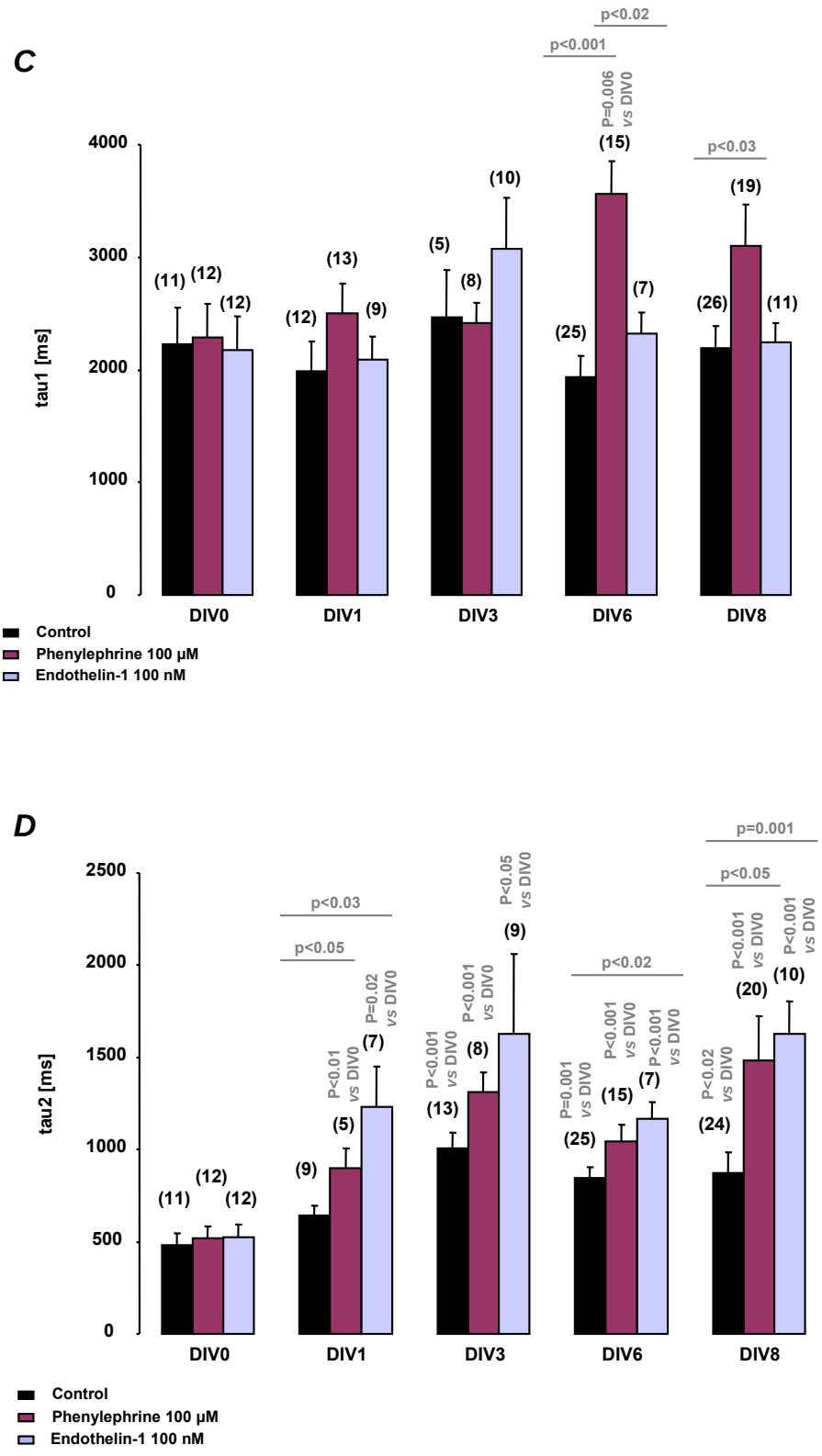


**Fig. 26. Study of caffeine-induced $[Ca^{2+}]_i$ responses in cultured ventricular myocytes during chronic $G_q$-coupled stimulation.**
**(A) Typical response of ventricular myocytes to caffeine (10 mM) showing the two relaxation phases that can be fitted to an exponential curve with the equation indicated below the trace. (B) Amplitude changes in response to caffeine in PE (100 µM, red bars) and ET-1 (100 nM, blue bars) treated cells. (C) Kinetic analysis of the slow decay in PE and ET-1 treated cells. (D) Kinetic analysis of the rapid decay in PE and ET-1 treated cells. The numbers adjacent to**

**each value give the number of myocytes tested. Data with a significant difference in comparison to the value on DIV0 for each type of cells or in comparison between PE and ET-1 cells on the same day have been marked with the corresponding "p" value. When no significant difference was found (either in comparison to the respective value on DIV0, or in comparison between PE and ET-1 cells on the same day), no "p" value was stated. The data were taken from 1 to 5 rat heart preparations.**

As it is shown in Fig. 26A, responses to a fast application of caffeine directly onto the cells exhibited two decay phases, a slow one followed by a rapid one. To characterise their kinetics, the relaxation phases of the caffeine responses were fitted with mono-exponential time courses and the decay time constants "tau1" (slow decay) and "tau2" (rapid decay) were derived from such fits. In my hands, none of the conditions tested (control, PE or ET-1) significantly modified the value of "tau1" over time (Fig. 26C) which was 2231 ms at DIV0 (n=11 control myocytes), except for a single increase with PE on DIV6 ($p=0.006$, n=15 myocytes). Nevertheless PE cells displayed a slower decay (i. e. higher "tau1" value) on DIV6 in comparison to control and ET-1 conditions ($p<0.001$ and $p<0.02$ respectively, n=25, 15 and 7 control, PE and ET cells) and on DIV8 in comparison to control myocytes ($p<0.03$, n=26 control cells and n=19 PE cells). In contrast, long-term culturing significantly increased the values of "tau2" from DIV3 onwards by 2-fold ($p<0.001$, n=13 control cells) in comparison to DIV0 (Fig. 26D). Moreover, hormonal treatment augmented the values of "tau2" by 3-fold on DIV8 ($p<0.001$ for both hormones, n=20 PE cells, n=10 ET-1 cells) in comparison to DIV0 and this increase could be measured from DIV1 onwards. No difference was found between PE and ET-1 treated myocytes over time. However, the rapid decay was much slower (i. e. higher "tau2" value) in chronically stimulated cells in comparison to untreated cells especially on DIV8 ($p<0.05$, n=20 PE cells; $p=0.001$, n=10 ET-1 cells).

Hence, changes in the responses of the SR to caffeine applications accompanied the morphological modifications observed in chronic hormonal stimulated myocytes: (i) the amplitude of caffeine responses were conserved and (ii) treated myocytes displayed slower decay phases after 8 days of culture. To further explore $Ca^{2+}$ remodelling in hormone-stimulated myocytes, I investigated spontaneous $Ca^{2+}$ signals.

## *2.4. Spontaneous $Ca^{2+}$ waves*

Similarly to what has been described for unstimulated myocytes over culturing time, spatially resolved $Ca^{2+}$ imaging (realtime confocal microscopy) was undertaken to describe the occurrence of spontaneous $Ca^{2+}$ waves (number of spontaneous $Ca^{2+}$ waves in one cell per minute) in myocytes treated with 100 µM of PE and 100 nM of ET-1. Since round cells differed in the frequency of waves in control conditions (see paragraph 1.8), I focussed my interest on elongated treated cells on DIV0 and DIV1. Then, waves were measured in elongated ET-1-treated cells on DIV3 and on dedifferentiated cells as soon as they appeared during chronic stimulation (see paragraph 2.1), i. e. for PE on DIV3 and both hormones on DIV6 and DIV8.

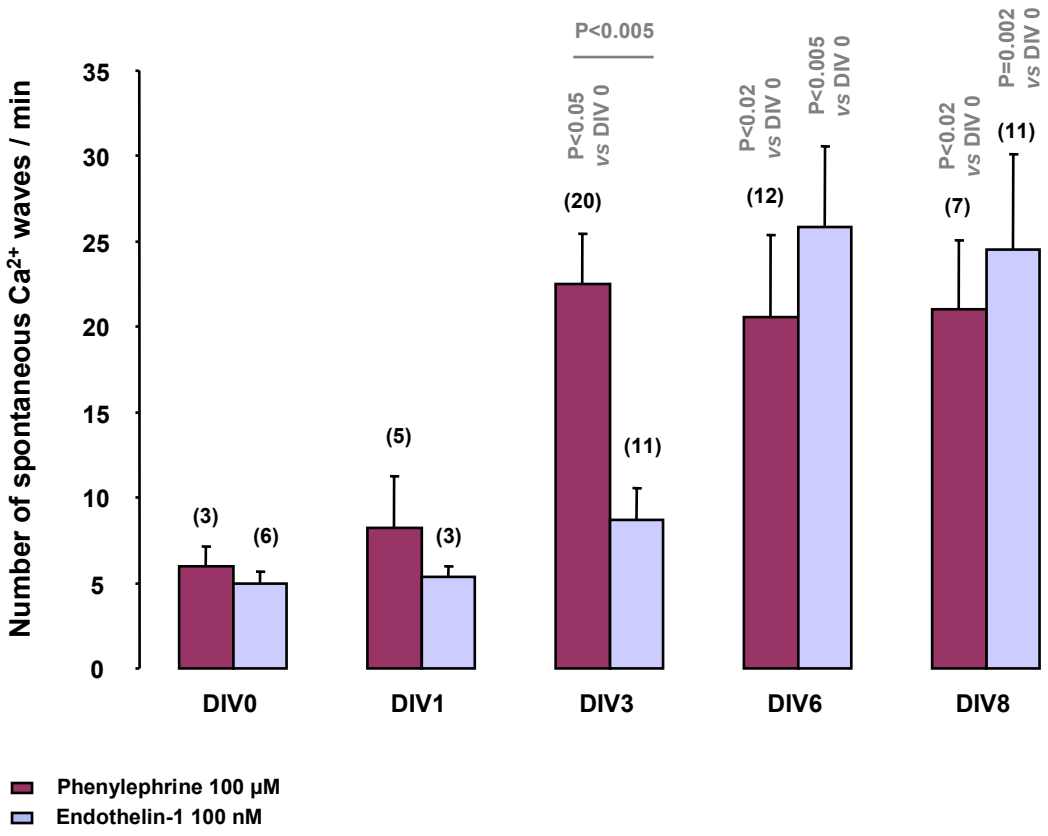


**Fig. 27. Spontaneous activity of hormone-stimulated cardiac myocytes: analysis of the frequency of $Ca^{2+}$ waves.**
**The number of spontaneous $Ca^{2+}$ waves per cell in one minute was plotted against the different stages of culturing. PE (red bars) and ET-1 cells (blue bars) were loaded with fluo-4 and changes of fluorescence were recorded with confocal microscopy. The numbers adjacent to each value give the number of myocytes tested. Data with a significant difference in comparison to the value on DIV0 for each type of cells or in comparison between phenylephrine and endothelin-1 cells on the same day have been marked with the corresponding "p" value. When no significant difference was found (either in comparison to**

**the respective value on DIV0, or in comparison between phenylephrine and endothelin-1 cells on the same day), no "p" value was stated. The data were taken from 1 to 3 rat heart preparations.**

Hormone-stimulated cells presented frequency values over culturing time very comparable to what has been observed in round myocytes in control conditions (compare Fig. 18 for unstimulated cells and Fig. 27 for treated cells). However, the mean frequency of 6 ± 1.2 waves pro minute (n=3 myocytes) on DIV0 for PE increased by almost 4-fold ($p<0.05$, n=20 cells for PE) on DIV3 (Fig. 27, red bars). Then PE cells maintained their high frequency of waves from DIV6 onwards similar to control (elongated and round) cells and ET-1-treated myocytes did without any significantly different values between the three groups at DIV6 and DIV8 (Fig. 18 and Fig. 27, blue bars for ET-1). The only significant difference between PE and ET-1 occurred on DIV3: PE cells presented a 3-fold higher frequency than ET-1 cells ($p<0.005$, n=20 for PE and n=11 for ET-1). Indeed, ET-1 cells increased their number of waves from DIV6 onwards as elongated and round cells did in control conditions.

Thus there seemed to be a correlation between the early (on DIV3) appearance of dedifferentiated myocytes when chronically stimulated with PE and the early increase of the frequency of spontaneous $Ca^{2+}$ waves. Further investigations of the spontaneous $Ca^{2+}$ events were necessary to decipher the links between $G_q$ stimulation and $Ca^{2+}$ remodelling.

## *2.5. Spatially restricted $Ca^{2+}$ signals: sparks*

Since $Ca^{2+}$ handling seemed to be changed upon chronic hormonal stimulation as described above, I was interested to investigate the elementary $Ca^{2+}$ events that underlie the occurrence of global $Ca^{2+}$ transients.

I used the approach detailed in Results section 1.9. Elongated cells alone on DIV0 and DIV1 as well as round and dedifferentiated myocytes from DIV3 onwards were recorded under conditions of chronic PE (100 µM) and ET-1 (100 nM) stimulation. Figure 28 exemplifies two confocal recordings converted into pseudo linescans showing the spontaneous spark activity in one control myocyte at DIV3 (Fig. 28A) and the changes induced by chronic PE treatment on the spark activity of a cell at the same stage (Fig. 28B).

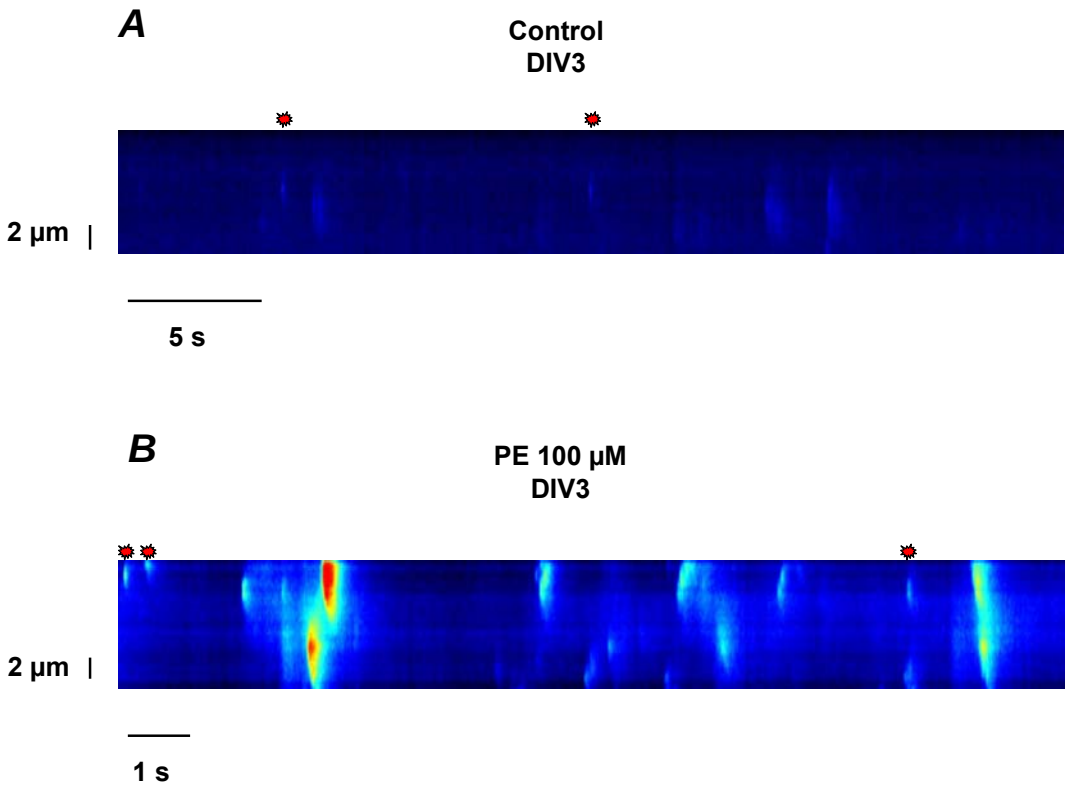


**Fig. 28. Influence of hormonal treatment on the spontaneous $Ca^{2+}$ spark activity.**
**This panel depicts two typical pseudo linescans recorded in two different myocytes at DIV3: control cell (A) and PE-stimulated cell (B). The increase of fluorescence intensity (i. e. increase of cytosolic $Ca^{2+}$) is shown by the warm colours. The red stars above the scans indicate the occurrence of representative $Ca^{2+}$ sparks.**

The summarised data for both hormones and all DIVs tested are depicted in Figure 29. While neither PE nor ET-1 treatment altered the spark characteristics on DIV0 (compare with control cells in Fig.19) whatever the parameter tested (amplitude, width, duration, frequency), significant differences occured over the culturing time, except for the mean frequency (Fig. 29D). While PE (red bars) increased the amplitude of the sparks from DIV3 onwards ($p<0.001$, n=6 cells; Fig. 29A) and then displayed higher values than ET-1 (blue bars), myocytes treated with ET-1 initially decreased their amplitude on DIV3 and DIV6, before increasing it on DIV8 ($p<0.02$, n=3 cells). Furthermore the spark amplitudes in PE-treated cells were also higher than those in control cells from DIV3 onwards ($p<0.001$, n=6 PE-treated cells and n=10 control cells, see Fig. 19A) whereas ET-1 cells exhibited one single difference on DIV6 in comparison to control cells where the amplitude was decreased ($p=0.002$, n=6 ET-1 cells and 6 control cells).

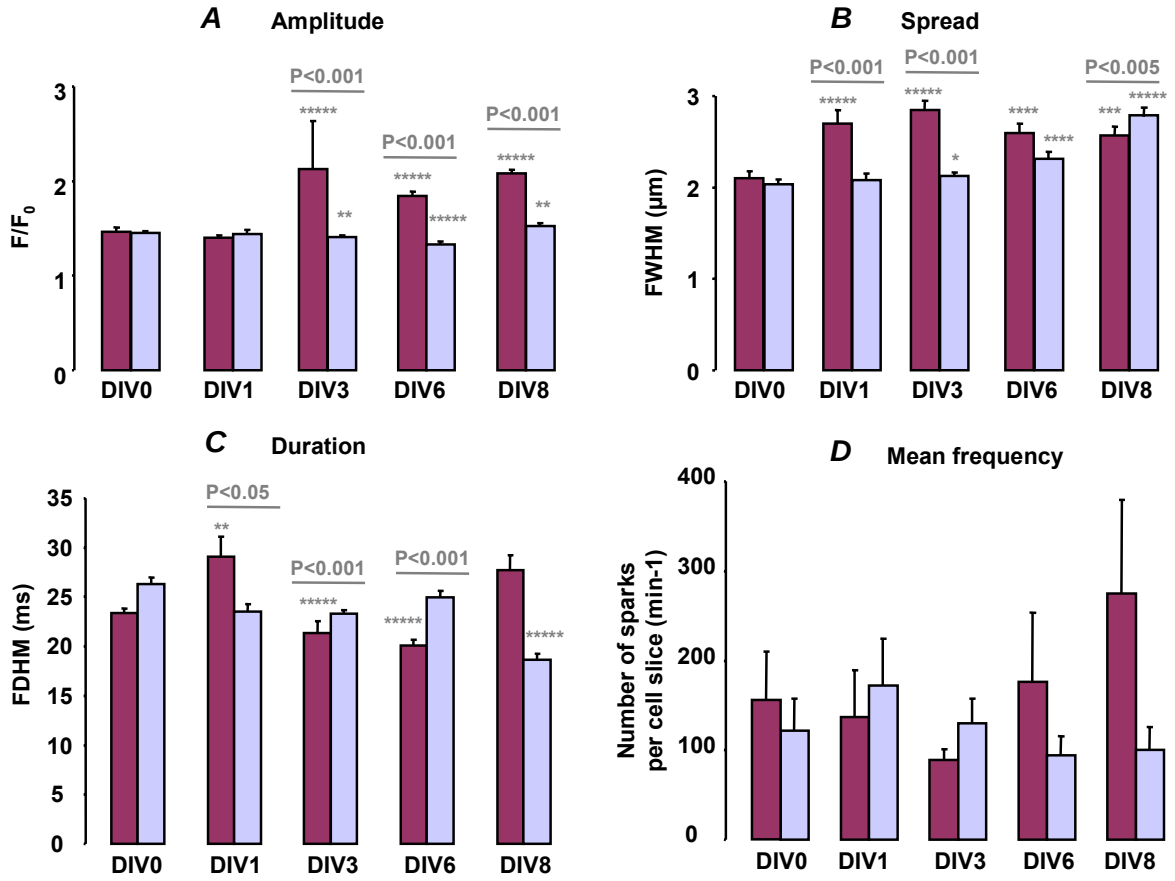


**Fig. 29. Analysis of $Ca^{2+}$ sparks during chronic hormonal stimulation.**
**Pooled spark data for PE (red bars) and ET-1-treated cells (blue bars) are plotted in this figure. The bar diagrams exhibits the study of four parameters ((A) amplitude of the changes of fluo-4 fluorescence, (B) spread of spark as full width at half maximum of the fluorescence peak, (C) duration of spark as full duration at half maximum of the fluorescence peak and (D) averaged frequency of sparks for one cell confocal slice in one minute) describing the activity of spontaneous sparks over culturing time (DIV= days *in vitro* 0, 1, 3, 6 and 8). Data with a significant difference between PE and ET-1 cells on the same day have been marked with the corresponding "p" value. Data with a significant difference in comparison to the value on DIV0 for PE or ET-1 respectively have been marked with asterisks: * p<0.05, ** p<0.02, *** p<0.01, **** p=0.002, ***** p<0.001. The mean values for PE were calculated from 201 sparks (5 cells out of 3 hearts) on DIV0, 134 sparks (3 cells out of 1 heart) on DIV1, 140 sparks (6 cells out of 1 heart) on DIV3, 181 sparks (5 cells out of 2 hearts) on DIV6, and 204 sparks (3 cells out of 1 heart) on DIV8. The mean values for ET were calculated from 262 sparks (4 cells out of 2 hearts) on DIV0, 109 sparks (3 cells out of 1 heart) on DIV1, 441 sparks (7 cells out of 4 hearts) on DIV3, 119 sparks (6 cells out of 2 hearts) on DIV6, and 90 sparks (3 cells out of 2 hearts) on DIV8.**

Moreover, similarly to control cells I found an increase of the spark width from DIV1 onwards in PE-stimulated cells (p<0.001, n=3 cells, Fig. 29B). Interestingly this increase was also preserved on DIV3, which was not the case in control conditions (p<0.001, n=6 PE-treated cells and n=10 control cells, Fig.19B). In contrast ET-1-treated myocytes started to present wider sparks from DIV3 onwards (p<0.05, n=7 cells) and they even seemed to display higher spatial spread in comparison to PE-treated cells on DIV8 (p<0.005, n=3 cells for both hormones). Nevertheless ET-1-

treated cells used to exhibit smaller spreads on DIV1 and DIV3 than PE-treated cells, the latter having values and an overall behaviour that were comparable to those found in control cells (see Fig. 19B). Furthermore, the FWHM values were significantly higher in control cells than in ET-1-stimulated myocytes on DIV1 ($p<0.001$, n=3 cells for ET-1 and n=11 control cells) and DIV6 ($p<0.001$, n=6 cells for ET-1 and n=8 control cells).

The mean duration of the sparks was also affected by the hormonal treatment (Fig. 29C). Cells stimulated with PE showed longer events on DIV1 ($p<0.05$, n=3 myocytes) identically to the pattern of responses in control cells (see Fig. 19C). However, FDHM values decreased on DIV3 and DIV6 in PE-treated cells, which was not the case in control cells. Moreover the events in PE-treated cells seemed to be shorter than in control cells on DIV3 ($p<0.001$, n=6 PE cells and n=10 control cells) and DIV6 ($p<0.001$, n=5 PE cells and n=8 control cells). Surprisingly the ET-1 stimulation induced only one single reduction of the spark duration on DIV8 ($p<0.001$, n=3 myocytes). In addition, ET-1-treated cells displayed shorter events than PE-stimulated myocytes on DIV1, 3 and 6 (see Fig. 29C) and than control cells (see Fig. 19C) on DIV1 ($p<0.001$, n=3 ET cells and n=11 control cells) and DIV8 ($p=0.003$, n=3 cells for both conditions).

Hence, it became apparent that the pattern of spatially restricted signal responses was rather dynamic upon chronic hormonal stimulation, meaning $G_q$-coupled stimulation altered the elementary $Ca^{2+}$ handling: $Ca^{2+}$ sparks tended to become (i) larger in amplitude, (ii) wider and (iii) of shorter duration, which was accompanied by an increased SR content (Fig. 26B).

## *2.6. Nuclear $Ca^{2+}$ signals during spontaneous activity*

The exploration of confocal recordings of fluo-4 loaded myocytes led to the observation of spontaneous global elevations of the intracellular $Ca^{2+}$ concentration reaching the entire cell at the same time, which was easily distinguishable from $Ca^{2+}$ waves. These events of high fluorescence amplitude occurred in fully dedifferentiated myocytes from DIV6 onwards and displayed oscillations with a mean frequency of 0.3 Hz (n=13 treated cells) that were more frequent in hormonal treated cells than in

control cells. The linescans in Fig. 30B show two examples of these $Ca^{2+}$ events in PE (on the left hand) and ET-1 (on the right hand) treated cells. Surprisingly, the region of the scan passing through the nucleus exhibited a prolongation of the fluorescence increase when compared to the cytosolic region. When I calculated the intracellular concentration of free $Ca^{2+}$ (Fig. 30C) with the equation of Grynkiewicz (Grynkiewicz *et al.*, 1985), I used the values of $K_d$ in the cytosol and nucleus previously given by Thomas and colleagues since they differ from each other (Thomas *et al.*, 2000). Considering the ratio of the $[Ca^{2+}]_i$ increase amplitudes (nucleus over cytosol), I noted no significant difference between the different treatments and the control conditions when the dedifferentiated myocytes from DIV6 to DIV10 were pooled. The ratio values were: 0.767 ± 0.088 (n=5 control cells), 0.659 ± 0.081 (n=7 PE cells) and 0.63 ± 0.241 (n=4 ET-1 cells). On the contrary, the ratio of the transient duration in the nucleus over the duration in the cytosol was increased by 33% with PE ($p<0.005$, n=5 control cells, n=8 treated cells) and by 22% with ET-1 ($p<0.05$, n=5 control cells, n=5 treated cells) over one week of culturing (Fig. 30D). Hence, it became apparent that $Ca^{2+}$ remodelling due to neuroendocrine challenge also affected the nuclear signals.

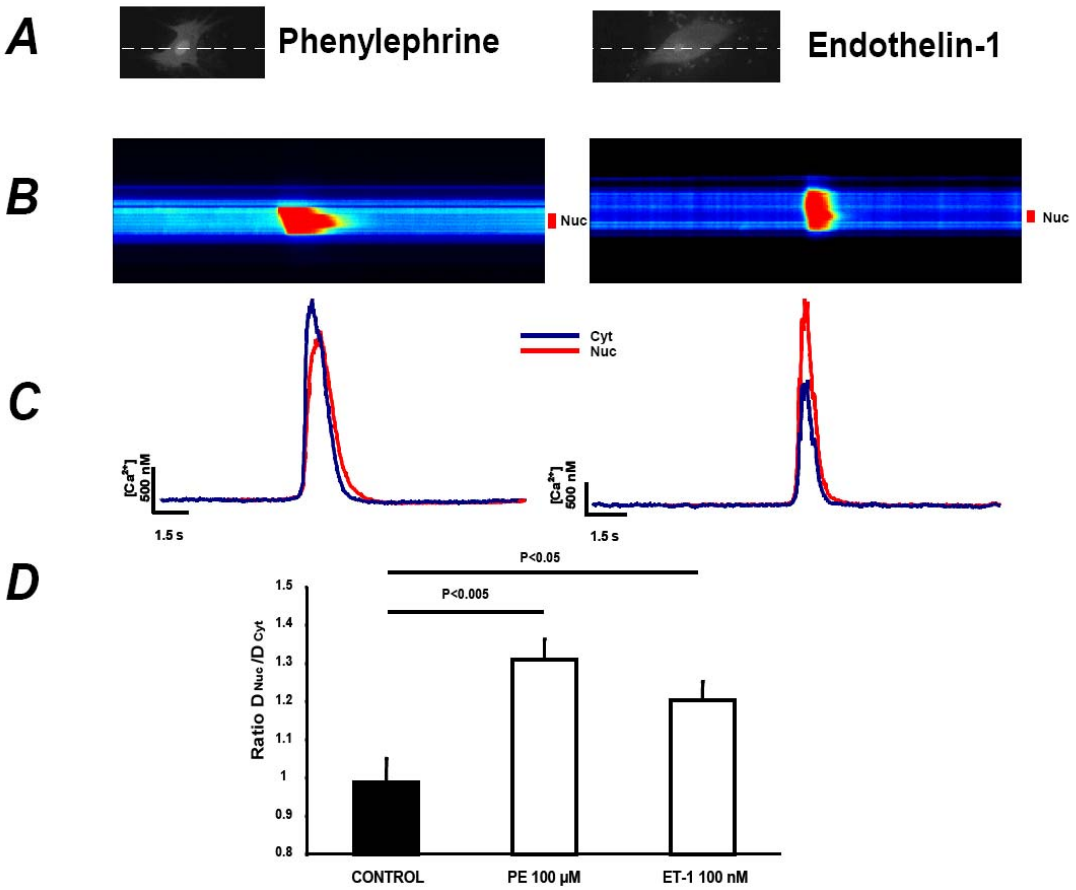


**Fig. 30. Prolonged nuclear $Ca^{2+}$ signals in chronically $G_q$-stimulated cardiomyocytes.**
**Panel A depicts confocal sections of typical fluo-4-loaded myocytes following chronic hormonal stimulation over one week. The white dashed lines indicate the scan line across the cell used to produce the linescan images (B). The nuclear region is marked "Nuc" and the cytosol region is marked "Cyt". Panel C depicts the time courses of local $Ca^{2+}$ concentrations. The ratio of the peak durations is plotted in panel D. Myocytes from DIV6 to DIV10 were pooled for each condition since they presented no significant difference. n=5 to 8 cells (taken from 3 hearts).**

# Discussion

## 1. Long-term culture of adult cardiomyocytes

The aim of this study was to develop and explore an adult rat cardiac myocyte culture system and procedures that allow extended experimental manipulation of these cells under conditions of diminished dedifferentiation. To achieve this I setup an experimental system for a long-term culture of adult cardiac myocytes that largely suppressed dedifferentiation, best maintained the morphological and physiological

properties of freshly isolated cells and allowed long-term expression of a genetically encoded $Ca^{2+}$ indicator for the first time.

One of the major problems with long term cultures of adult cardiac myocytes is the rapid occurrence of morphological and physiological dedifferentiation. The structural changes appearing during longer culturing time of rat ventricular myocytes was studied extensively (e.g. Eppenberger *et al.*, 1995; Nag *et al.*, 1996). In parallel there were numerous attempts to modulate culture conditions towards minimizing dedifferentiation. Such approaches included omitting or substituting the medium supplement FCS (e.g. Mitcheson *et al.*, 1996) and electrical pacing of the adult cells (e.g. Berger *et al.*, 1994). All of those approaches have provided progress towards extended time periods of reduced dedifferentiation of the adult cells.

I omitted serum from the medium and substituted it by an ITS mixture. In addition, I coated the substrates (plastic and glass) with ECM. Both steps revealed major improvements in both the number of viable cells (i. e. the loss of viable cells was greatly reduced between DIV0 and DIV6) and the preservation of cell morphology, subcellular microarchitecture (contractile filaments) and physiology (contractility and $Ca^{2+}$ handling) of the cells over the time course of culturing.

As described above, in my hands too, the presence of serum in the culture medium appeared to promote dedifferentiation resulting in a flattened morphology. Interestingly, similar shapes are “normal” for cardiac cell lines such as the H9C2 cell line (e.g. Kimes & Brandt, 1976). I found that simply omitting the serum supplement is slowing down the dedifferentiation process (see also Mitcheson *et al.*, 1996 for rabbit cardiomyocytes) and more cells survive the culture period with an elongated cell body. Unfortunately, rat cells cultured under these conditions displayed a progressively increasing number of subcellular vacuoles and/or vesicles, a gradual loss of cross-striation, reduced maximal cell length changes and modifications of the post-rest behaviour. From such findings I deducted that this culture condition was in fact sub-optimal. On the contrary, ITS-supplemented medium greatly improved the conservation of the cellular properties found at DIV0, whether the cells were seeded on poly-L-lysine or on ECM-coated substrates, whereas the latter condition provided even better results.

In the vast majority of conditions, there was neither a beneficial nor a detrimental effect of electrical pacing, in contrast to the findings of Berger and co-workers (Berger *et al.*, 1994). This held true for both physiological parameters that I analysed – the contractile performance and $Ca^{2+}$ transients in response to electrical stimulation – and the stimulation frequency dependence of both parameters. Nevertheless, this does not exclude the possibility that certain culture conditions combined with particular stimulation protocols might increase or decrease survival of the cells or their morphological/physiological state. Interestingly, other studies described hypertrophic responses of myocytes when pacing frequencies were raised to higher stimulation frequencies in adult myocyte cultures (3 Hz; Kaye *et al.*, 1996). This is puzzling considering that these stimulation rates are rather physiological for rodent hearts (3-10 Hz) but might be attributed to my finding that such high stimulation frequencies might not be followed by the myocytes since in culture they will perform unloaded contractions. Mechanical relaxation of individual myocytes in the intact cardiac tissue is mainly performed by the elastic properties of the surrondoung tissue rather then by the myocyte itself.

I found that the maximal absolute cell length change in response to electrical stimulation was progressively decreasing over the culturing time (see table 1). This reduced contractility of the ventricular myocytes could represent a mechanical phenomenon, especially considering the increasing strength of the adhesion of the myocytes to the substrates during the culturing period. It has indeed been reported recently, that cardiomyocytes modulate their own synthesis of ECM molecules (Gupta *et al.*, 2006). Hence, it is conceivable that this production participates to the increase of interaction between the cells and their substrate over culturing time and thus to a decrease of absolute maximal shortening. Therefore I used the post-rest behaviour and the stimulation frequency to characterise the myocytes. The post-rest contractile behaviour of isolated myocytes indicates the ability of the myocyte machinery to adjust $Ca^{2+}$ handling to changes (frequency, rest) of the excitation-contraction coupling (Bers, 2001). The rational behind this protocol was indeed (i) to work with reliable relative shortening changes in order to avoid individual differences and (ii) to compare whole frequency dependence relationships instead of selective electrical stimulation frequencies.

Genetic manipulation of adult cardiac myocytes has been limited to short term procedures and/or to the generation of genetically modified donor animals. While the latter is a very elegant way of introducing proteins to or knocking proteins out from cardiac myocytes, the generation of these animals is expensive and tissue specific, inducible genetic manipulation is not an easy routine work. Thus, genetic manipulation of isolated cardiac myocytes might be a feasible intermediate step towards genetically modified animals. Traditionally, genetic manipulation of cardiac myocytes has been performed on neonatal ventricular cells from the rat (e.g. Bauer *et al.*, 2005). Neonatal cells can be transfected with traditional means (i. e. commercially available transfectant; Heiser, 2003), but in adult cells the yield is usually <10%. Better expression or knock-out rates can be achieved with viral gene transfer systems, e. g. adenovirus. Unfortunately, results obtained from neonatal systems are often difficult to transfer to the adult situation, due to developmental changes. Therefore, it is desirable to perform such experiments on adult cardiac myocytes. Indeed, there are some examples where genetic manipulation – e. g. with an adenoviral system – has been applied successfully (e.g. Rinne *et al.*, 2006). Mostly, such approaches have been limited to short-term expression (1-2 DIV) and have thus avoided unwanted dedifferentiation of the cells. Nevertheless, longer expression would be highly desirable, given that many effects of genetic manipulations and/or stimulation regimes will require longer culture periods.

As far as I know, this work contains the first description ever of the expression of a genetically encoded $Ca^{2+}$ sensor (inverse pericam) in cultured adult rat ventricular myocytes for extended periods of time. In my hands, the myocytes cultured under ITS/ECM conditions were not negatively affected by the gene transfer through an adenovirus. Expression levels were already high enough for fluorescence recording less than 24 hours after infection. Throughout the culture period of 7 days expression levels were steadily increasing. This will certainly require additional investigation and titration of the best multiplicity of infection for rapid onset of fluorescence and stable expression levels. In less than 24 hours, expression levels allowed extended recording regimes of $Ca^{2+}$ transients without detrimental effects in the signal to noise ratio. In some experiments it was possible to record for more than 2 hours on the single cell level and the recording was not limited by bleaching or a decrease in the

cell quality. Moreover, data acquisition frequency was not reduced in favour of a prolonged recording time; I collected images at a rate of 50-60 frames/second that allowed e. g. the recording of $Ca^{2+}$ waves (see Results section 1.8). Thus extended expression of genetically encoded $Ca^{2+}$ sensors is a promising approach for long-term, continuous observation of $Ca^{2+}$ handling in isolated cardiac myocytes, especially when working on species for which an appropriate transgene does not exist. A potentially interesting transgenic mouse expressing a $Ca^{2+}$ indicator was introduced recently (Tallini *et al.*, 2006).

# 2. $G_q$-induced $Ca^{2+}$ remodelling

As discussed above, cell culturing is a usefull complementary approach to *in vivo* studies because it enables the investigator to work with a stable, controllable system and to study biological mechanisms at the cellular level, but also at the subcellular level, mainly when using single-cell models, where the cells are isolated from each others. To date, *in vitro* studies of the influence of $G_q$ stimulation on cardiac function and remodelling were almost exclusively restricted to neonatal cardiac myocytes (e. g. O'Donnell *et al.*, 2001) or to adult cells in short-term culture (48 hours maximally, e. g. Anwar *et al*., 2005). Indeed, the loss of the differentiated phenotype during conventional long-term culturing rendered the interpretation of the results extremely difficult. Furthermore, while neonatal or embryonic myocytes provided a reliable and very easy-to-handle model, they did not represent adult cardiac myocyte physiology well enough. In addition, it is most likely that important physiological phenomena induce "slow-onset" cellular responses, based on long-term gene expression for instance, that entail long-term culturing of the myocytes.

In the current study, I introduced the novel culturing system that allowed chronic stimulation with minimised dedifferentiation of the myocytes. Over culturing time, unstimulated cells preserved their morphology and functionality and underwent obvious reproducible changes that I characterised in order to define the base-line necessary for the study of the influence of chronic neurohormonal stimulation on adult ventricular myocytes.

Chronic neuroendocrine stimulation accelerated the dedifferentiation into myoballs and then into spreading complexes, even exhibiting a high rate of spontaneous and regular beatings. This finding is very similar to what was previously shown in chronically (10 days) hormonally stimulated adult ventricular cells (Volz *et al.*, 1991) and to what can be obtained when the adult myocytes are cultured with medium supplemented with serum, fetal calf serum for instance (Poindexter *et al.*, 2001). In my hands, long-term hormone-stimulated isolated adult rat cardiomyocytes rapidly changed from a rod-shaped structure towards a more stellated shape which is very close to a neonatal cell structure (Poindexter *et al.*, 2001), as if the stimulated adult cells did endure a reprogramming towards a "younger" phenotype. It is noteworthy that these morphological changes were observed for PE at 10 and 100 µM and ET-1 at 100 nM.

In addition, stimulated cells preserved their post-rest behaviour and the kinetics of electrically-induced $Ca^{2+}$ transients. Therefore it seemed that a conserved low "tau" value enabled rapid decay phases in hormone-stimulated myocytes – this was especially true for endothelin-treated cells – and thus maintained a short refractoriness period allowing the occurrence of extra $Ca^{2+}$ signals massively already on DIV3. In contrast, control cells had a higher decay time constant on DIV3 which could presumably decrease the likelihood of emergence of extra $Ca^{2+}$ transients.

The study of spontaneous $Ca^{2+}$ waves showed no difference in the behaviour of unstimulated and stimulated myocytes over time. However, elongated and round cells displayed spontaneous $Ca^{2+}$ events in short-term culture differently; round cells exhibiting more waves, probably indicating that these cells did not regulate the $Ca^{2+}$ release and/or uptake as efficiently as elongated myocytes did. Secondly the increase of waves in both types of cells from DIV6 onwards most likely puts the stress on the adaptation of the myocytes to the long-term culturing; the cells seemed to lose their functions of control on global $Ca^{2+}$ signals.

I also investigated another important type of spontaneous signals, namely the $Ca^{2+}$ sparks. It appeared that their average amplitude values after cell isolation were lower than described previously (Cheng *et al.*, 1993). As shown in Fig. 31, it seems that the filtering of the algorithm employed led to a spatial smoothing of the fluorescence

changes and consequently to reductions of the amplitudes. Nevertheless, as I was interested in the relative changes of the amplitude over culturing time, this smoothing did not play any role in the interpretation of the results.

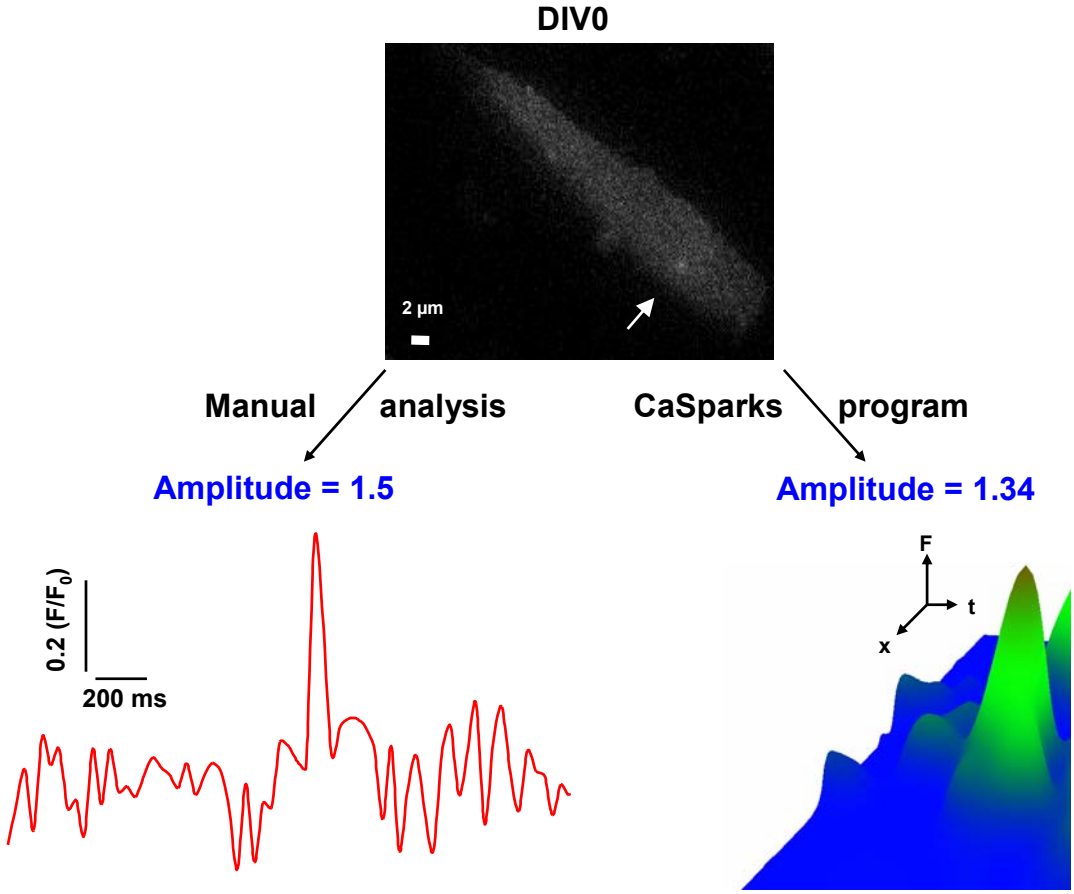


**Fig. 31. Comparison of the amplitude calculation between "CaSparks" software and manual analysis.**
**Realtime confocal microscopy was performed at a maximal rate of 33.2 frames per second to monitor the fluorescence changes in this representative cardiac myocyte on DIV0. The white arrowhead indicates the spark chosen for analysis. While a value of 1.5 (corresponding to the increase of fluorescence $F/F_0$ from the basis of the peak to the maximum) was found for the amplitude by manual analysis, "CaSparks" software showed a value of 1.34. The plot on the right hand side is a 3D surface representation of the pseudo linescan used by the software with arbitrary unit values (F: fluorescence ratio, t: time, x: space) but conform to the units used by the program to determine the amplitude value. The pseudo linescan was constructed according to the following parameters: pixel time= 30,121 ms and pixel size= 0.1896 µm.**

While most of the spark characteristics were maintained over the culturing time in normal conditions, the spread of the sparks tended to become broader. Furthermore, my results on the spark distribution pointed out a reorganisation of the active spark sites towards a sub-plasma membrane localisation on DIV6 in untreated cells. Despite a conservation of the cross striations in culture, this redistribution might corroborate the changes in the structure of the T-tubules network previously

described during culturing (Brette & Orchard, 2007). Karin Hammer (Institute for Molecular Cell Biology, Germany) showed that the transversal cytosolic organisation indeed tended to faint, while T-tubules remained present mostly under the plasma membrane (unpublished results), which seems to be similar to the native SR network displayed by the atrial myocytes (MacKenzie *et al.*, 2002).

In contrast, hormonally stimulated cells drastically changed their morphology and lost their cross striations. No reliable study of the spark distribution was possible since the treated myocytes exhibited different types of irregular shapes. Moreover, their sparks became larger in amplitude, broader and had a shorter duration over time. Hence, $G_q$-related $Ca^{2+}$ remodelling took place at the elementary level, and since the recruitment of sparks are said to trigger global $Ca^{2+}$ signals (Thomas *et al.*, 1998) these changes might account for the modifications of the large $Ca^{2+}$ transients, especially the increase of the spontaneous activity during chronic stimulation.

In comparison to untreated cells, hormonally stimulated cells maintained caffeine responses of high amplitude, most likely indicating that these cells were able to retain their $Ca^{2+}$ content. Another less plausible explanation could be that their RyRs on the SR membrane preserved their sensitivity, open probability or number on the SR surface. To measure the accurate loading of the internal $Ca^{2+}$ stores and confirm the maintenance the SR content in hormonal stimulated cells, a reliable method was described by Trafford and his colleagues (Trafford *et al.*, 1997) and was based on ionic flux recordings in caffeine stimulated myocytes. Nevertheless, the technique that I use gives indications of the SR content and enables me to consider that the SR preserved its functionality in hormonal stimulated cells, which probably underlied the increase of the spark amplitude over time.

Moreover, the value of “tau2” was largely increased, indicating a reduced activity of the SERCA pump. It is widely accepted and demonstrated that the first and slow decay phase of caffeine-induced $Ca^{2+}$ increases is to a large extent (75%) due to the activity of the $Na^+/Ca^{2+}$ exchanger on the plasma membrane in its forward mode (i. e. $Ca^{2+}$-extrusion, Bers, 2001). Thus it is highly conceivable that the second and rapid decay phase observed (after caffeine withdrawal) is due to the reactivation of the SERCA pumps (Bers, 2001). Hence, the slower activity of the SERCA pumps in the

one week cultured and hormonally stimulated myocytes might account (at least in part) for an altered $Ca^{2+}$ clearance in the cytosol and thus probably for the increase in the frequency of spontaneous $Ca^{2+}$ waves. Indeed, if the internal $Ca^{2+}$ concentration remains high for too long, then the likelihood that the activation propagates from a RyR cluster to another is higher, which leads to the creation of waves. Slower SERCA pumps might also explain the increase in the size of the spark spread: the SERCA pumps in the vicinity of RyR clusters would be less efficient and several neighbour clusters could be then activated at the same time. While chronic hormone-stimulated myocytes seemed to display a much slower activity of the SERCA pumps than control cells, it became apparent that PE induced in addition a higher value of “tau1” in comparison to ET-1, most likely indicating a more reduced activity of $Na^{+}/Ca^{2+}$ exchangers in PE-treated cells. This certainly might have played a role in the impairment of $Ca^{2+}$ extrusion on DIV6 and DIV8, leading to a more predominant presence of $Ca^{2+}$ in the cells, which was probably involved in the drastic dedifferentiation process that took place rapidly under PE stimulation.

Besides the activity of the SERCA pumps, one has to take into account that the expression and the functionality of sarcoplasmic and cytosolic $Ca^{2+}$ buffers (Bers, 2001) could also be altered, which might allow too for the increase in the frequency of spontaneous $Ca^{2+}$ waves and the increase in the size of the spark spread in one week cultured cells.

In addition, spontaneous nuclear $Ca^{2+}$ events were prolonged in chronic neuroendocrine-stimulated cells. An increasing number of recent data sheds some light on the existence and the role of $Ca^{2+}$ in the nucleus. Particularly and as discussed previously, it seems that the $G_q$-$InsP_3$ pathway plays a central role in the occurrence of specific nuclear $Ca^{2+}$ events. Roderick and collaborators recently furnished pieces of evidence concerning the induction of $Ca^{2+}$ waves in the nuclear region of neonatal cardiomyocytes under ET-1 stimulation that were sustained by $InsP_3$ receptors (Fearnley *et al.*, 2007).

Intracellular $Ca^{2+}$ signals correspond to a cellular language; the parameters of which (amplitude, frequency, kinetic, spread) can be decoded and interpreted by specific

proteins that consist of $Ca^{2+}$ binding domains and lead to the modulation of kinase activities and to phosphorylation. For instance, the ubiquitous transcription factor CREB is the target for two $Ca^{2+}$-related signalling pathways: MAPK (see Fig. 6A&B) and $Ca^{2+}$-calmoduline cascades (Hardingham *et al.*, 2001). Therefore, it seems highly conceivable that this prolonged presence of $Ca^{2+}$ in the nucleus could be necessary to activate gene expression processes required for the remodelling induced by $G_q$-coupled receptors stimulation. The maintained SR content in treated myocytes played most likely a pivotal role in order to reach the threshold of activation of these extended nuclear $Ca^{2+}$ signals.

Neuroendocrine stimulation might be an important part of cardiac remodelling *in vivo* that can be mimicked and studied (at least in part) in an *in vitro* model of adult myocytes. My single-cell model thus provides a new advance towards high-content screening of these highly specialised cells.

# Conclusion and outlook

In my thesis dissertation I have introduced a potentially important approach for a cardiac myocyte single cell model combined with expression of exogenous proteins for extended periods of time and with chronic hormonal stimulation-induced cardiac remodelling. Such an approach will allow further explorations of *in vitro* models for studying long term signal transduction in cardiac myocytes allowing quasi-continuous supervision of physiological and morphological parameters such as contractility and $Ca^{2+}$ handling. I envisage my report to be a foundation for the further development of high-content screening systems (Lipp & Kaestner, 2006) employing adult cardiac myocytes, because the application of adenoviral gene transfer allows the application of genetically encoded reporters, such as $Ca^{2+}$ sensors, but also sensors of other signal transduction processes (e.g. phosphorylation) in cardiac myocytes.